Electronic Supplementary Material (ESI) to:

Syntheses, Structures, Modification, and Optical Properties of *meso*-Tetraphenyl-2,3-dimethoxychlorin and Two Isomeric *meso*-Tetraaryl-2,3,12,13-tetrahydroxybacteriochlorins

Lalith P. Samankumara, Matthias Zeller, Jeanette A. Krause, and Christian Brückner*

**Corresponding Author: Department of Chemistry, University of Connecticut, Unit 3060, Storrs, CT 06269-3060, U.S.A.*

Fax: +860-486-2981; Tel: +860-486-2743; E-mail: c.bruckner@uconn.edu

ESI Table of Contents:

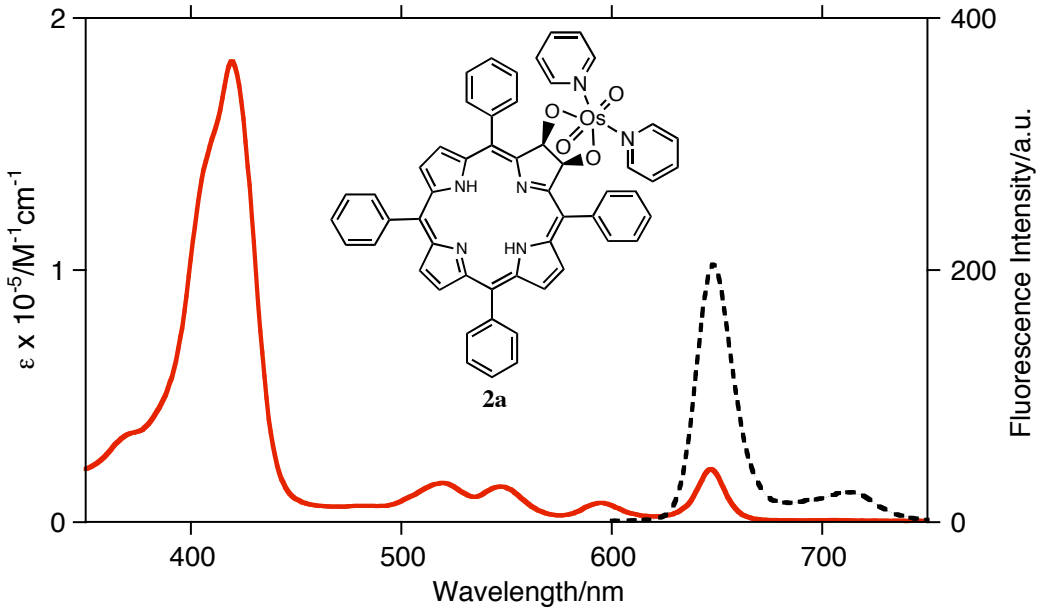

Figure ESI-1. UV-vis (solid red trace) and fluorescence (broken black trace) spectra of **2a** in CH_2Cl_2

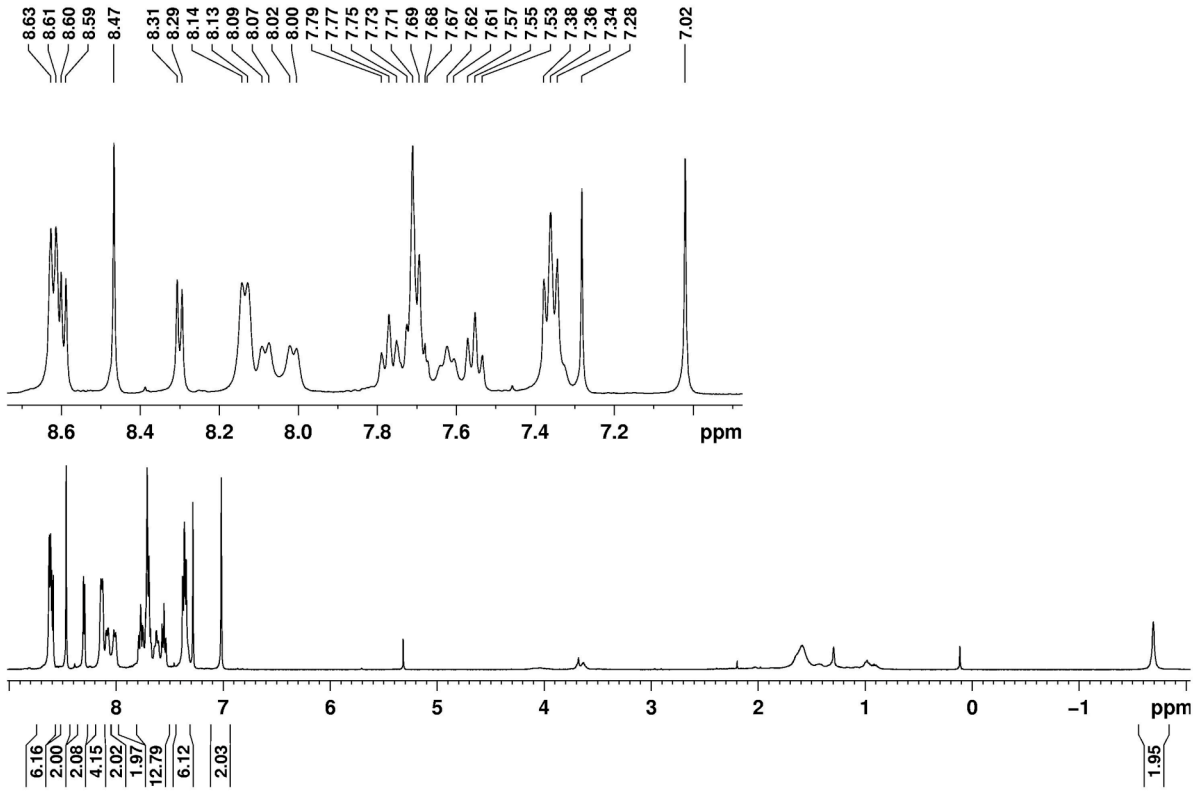

Figure ESI-2. ^{1}H NMR spectrum (400 MHz, $CDCl_3$) of **2a**

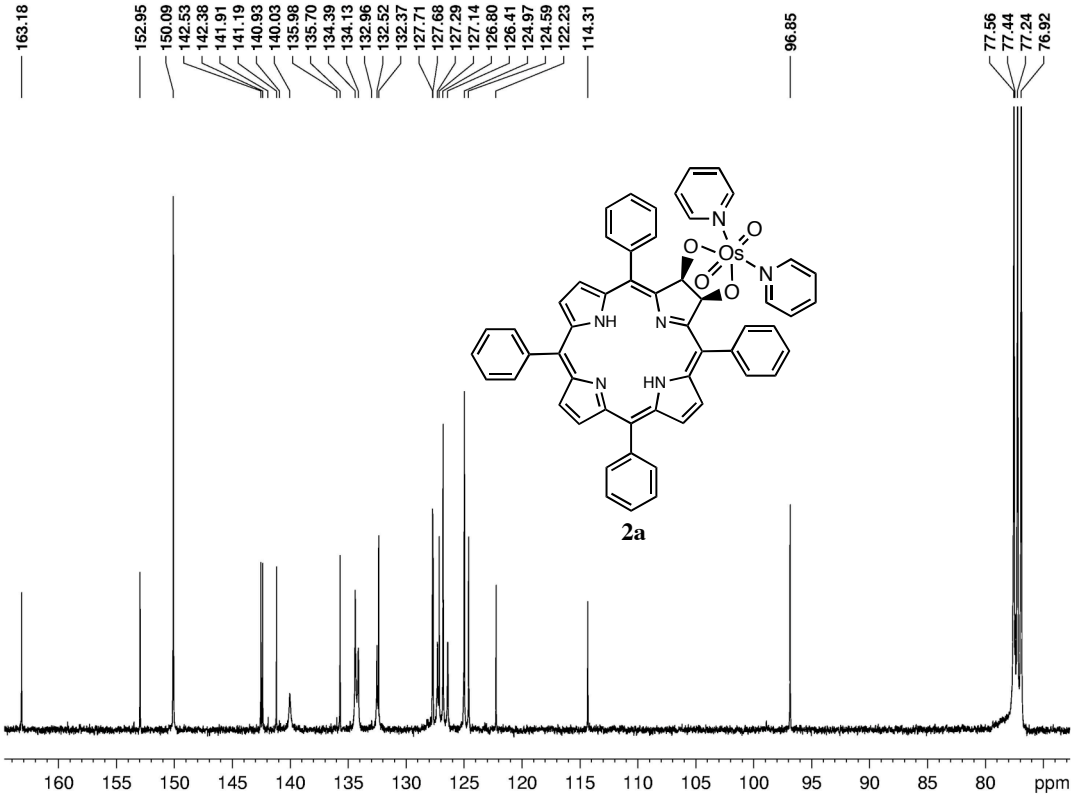

Figure ESI-3. ^{13}C NMR spectrum (100 MHz, $CDCl_3$) of **2a**

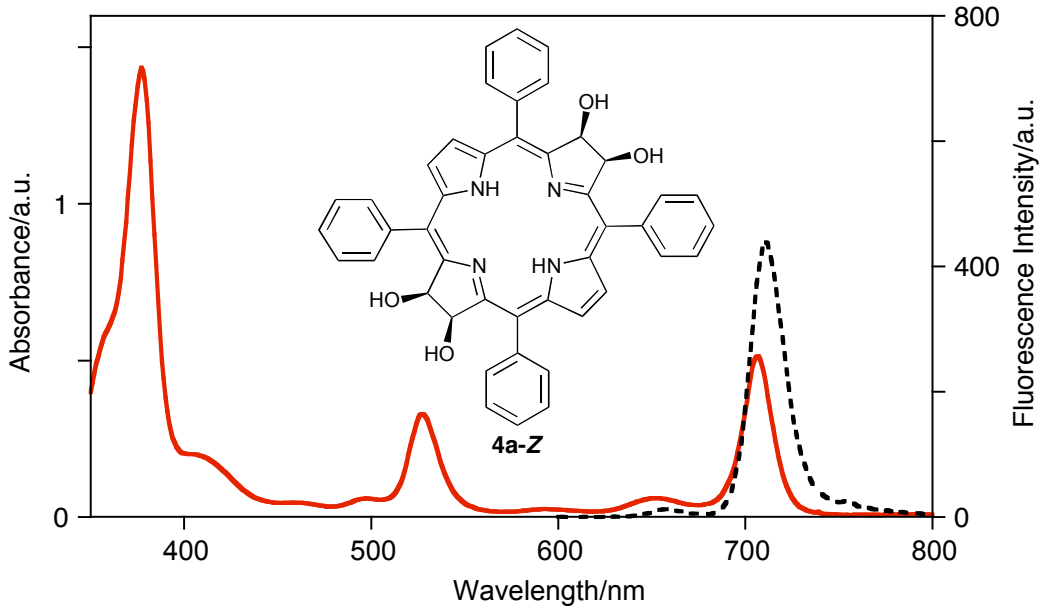

Figure ESI-4. UV-vis (solid red trace) and fluorescence (broken black trace) spectra of **4a-*Z*** in CH_2Cl_2

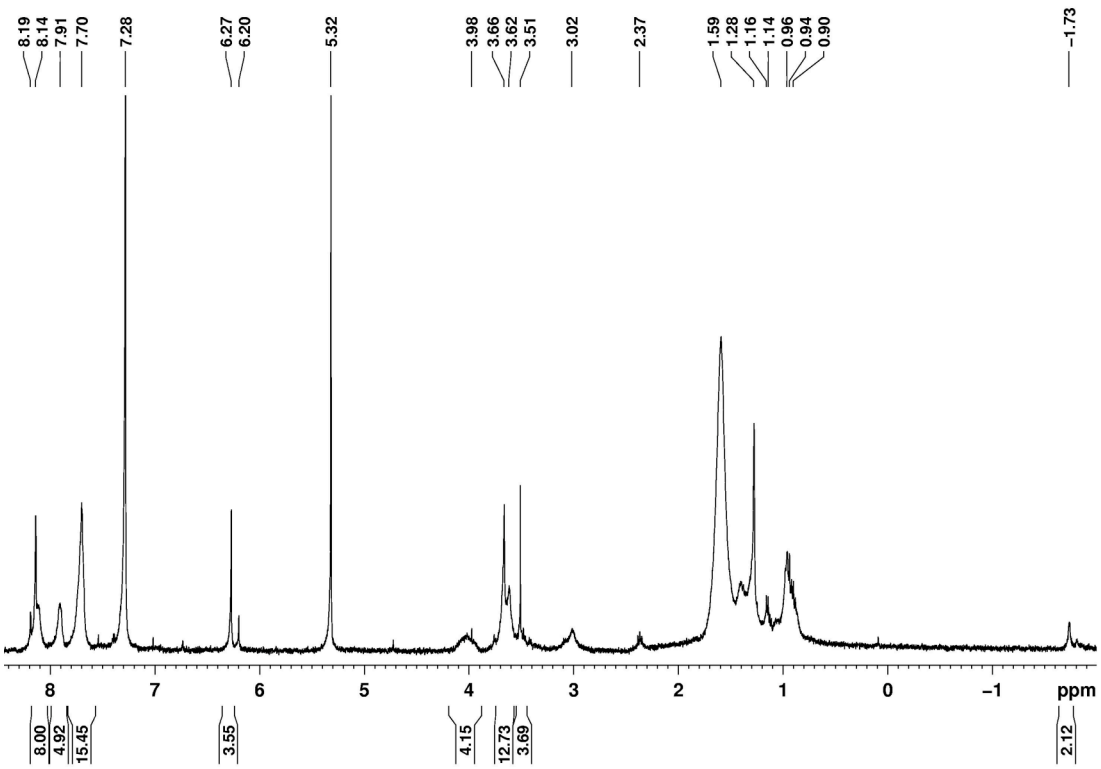

Figure ESI-5. ^{1}H NMR spectrum (400 MHz, CDCl3) of **4a-*Z***. The compound is of limited solubility in this solvent.

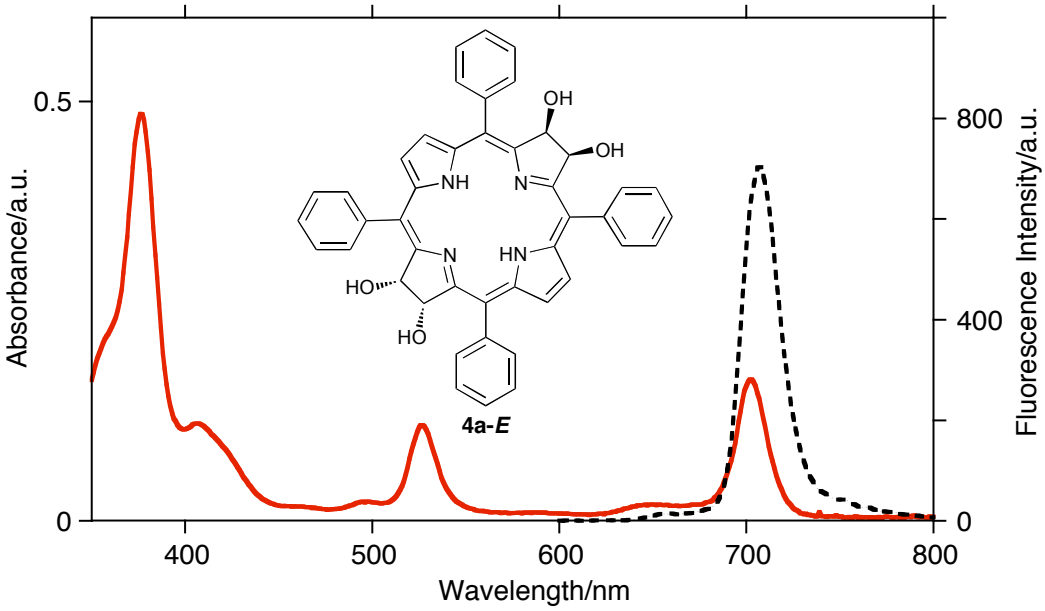

Figure ESI-6. UV-vis (solid red trace) and fluorescence (broken black trace) spectra of **4a-*E*** in CH_2Cl_2

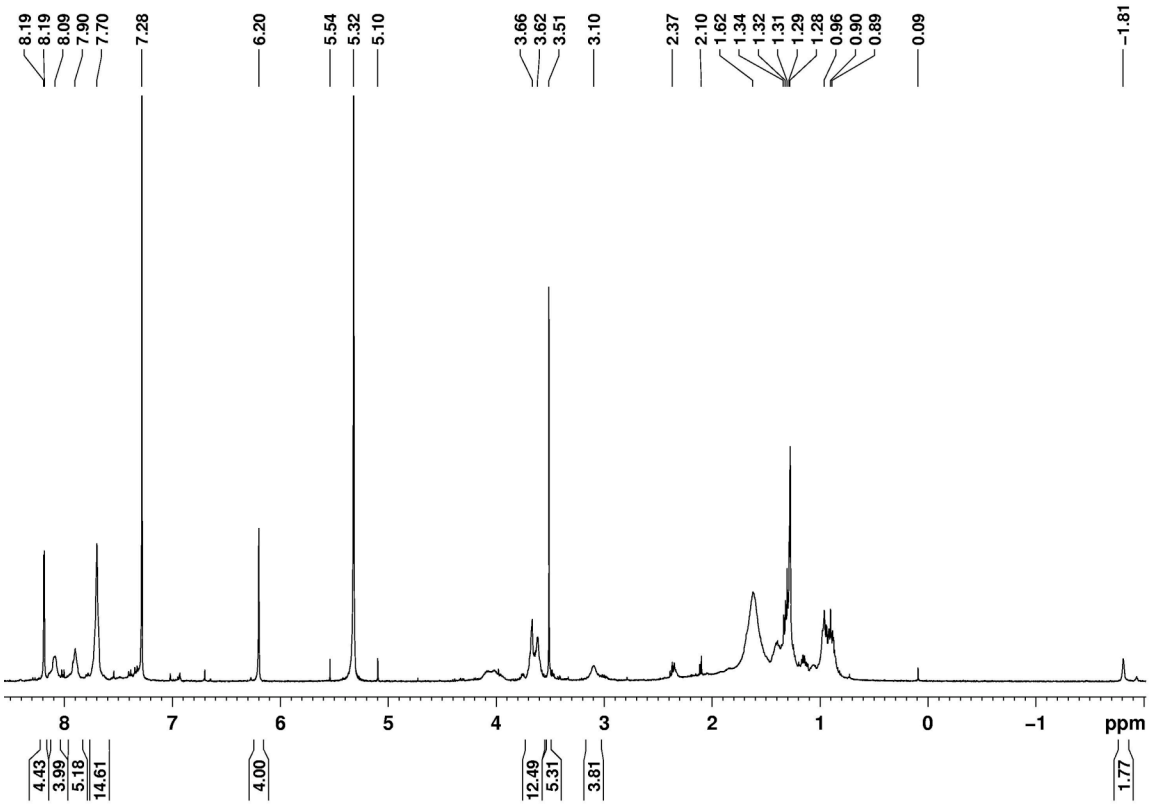

Figure ESI-7. ^{1}H NMR spectrum (400 MHz, $CDCl_3$) of **4a-*E***

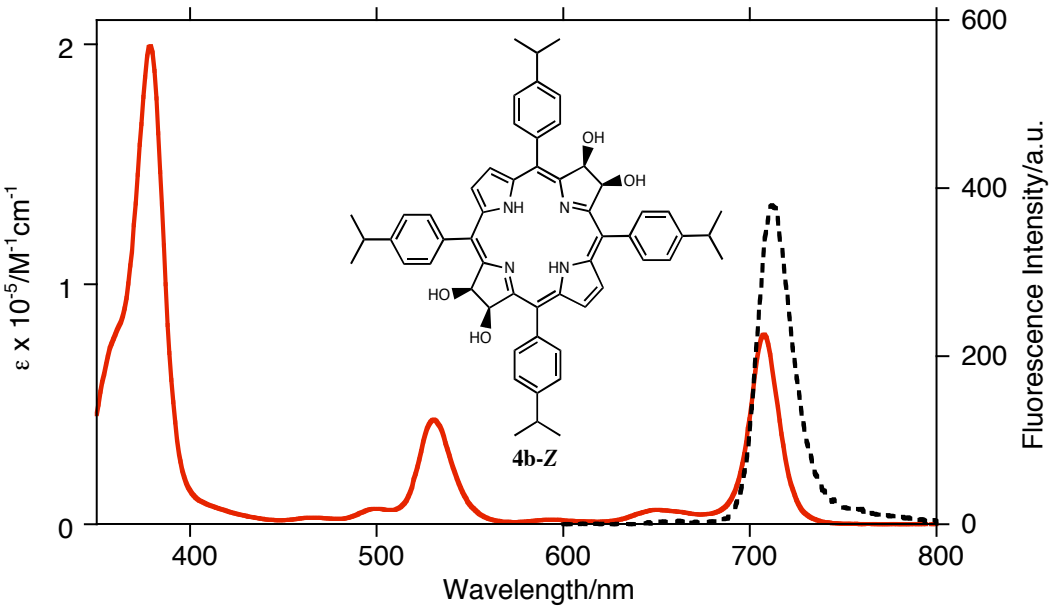

Figure ESI-8. UV-vis (solid red trace) and fluorescence (broken black trace) spectra of **4b-*Z*** in CH_2Cl_2

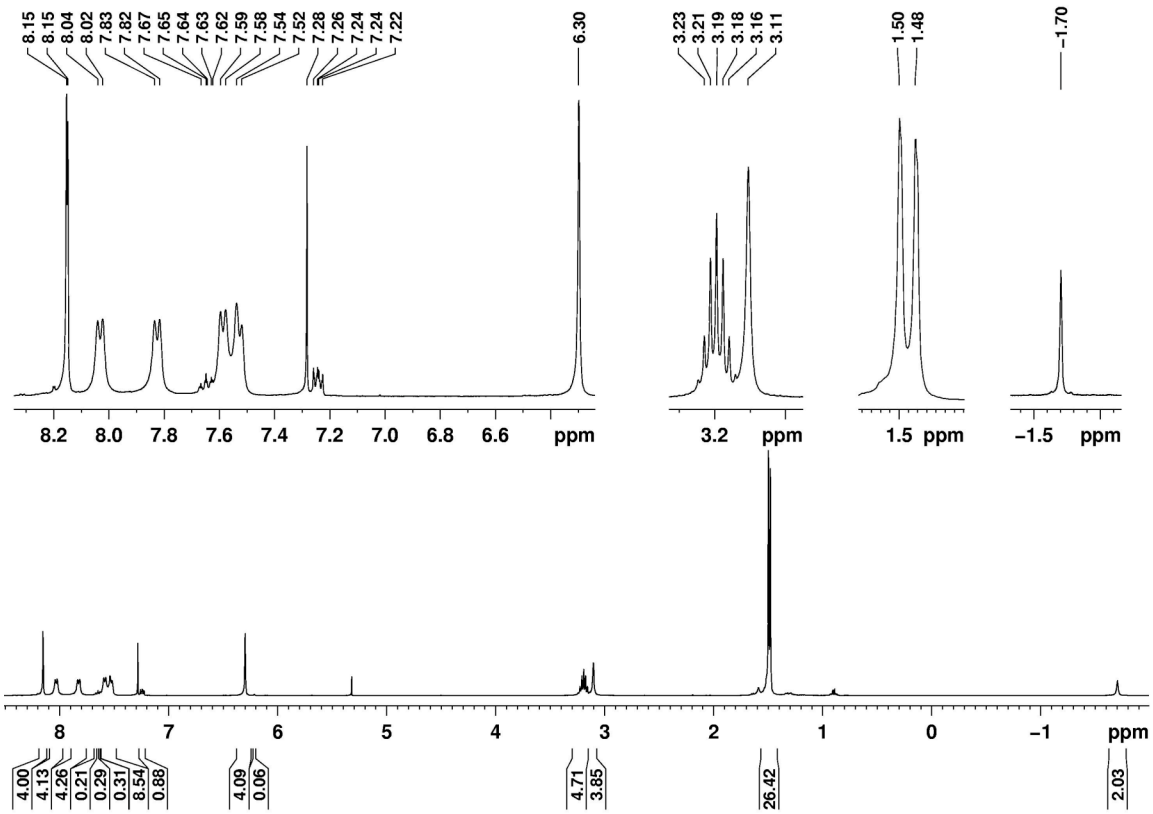

Figure ESI-9. ^{1}H NMR spectrum (400 MHz, $CDCl_3$) of **4b-*Z***

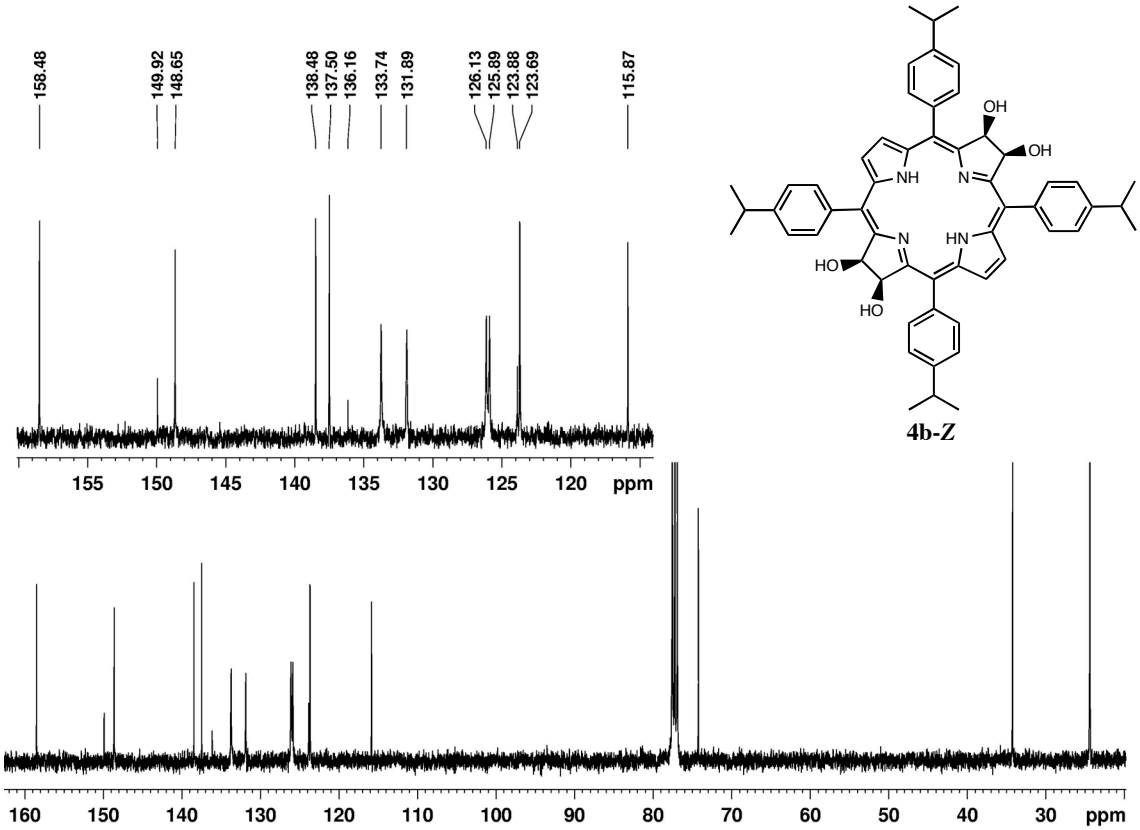

Figure ESI-10. ^{13}C NMR spectrum (100 MHz, $CDCl_3$) of **4b-*Z***

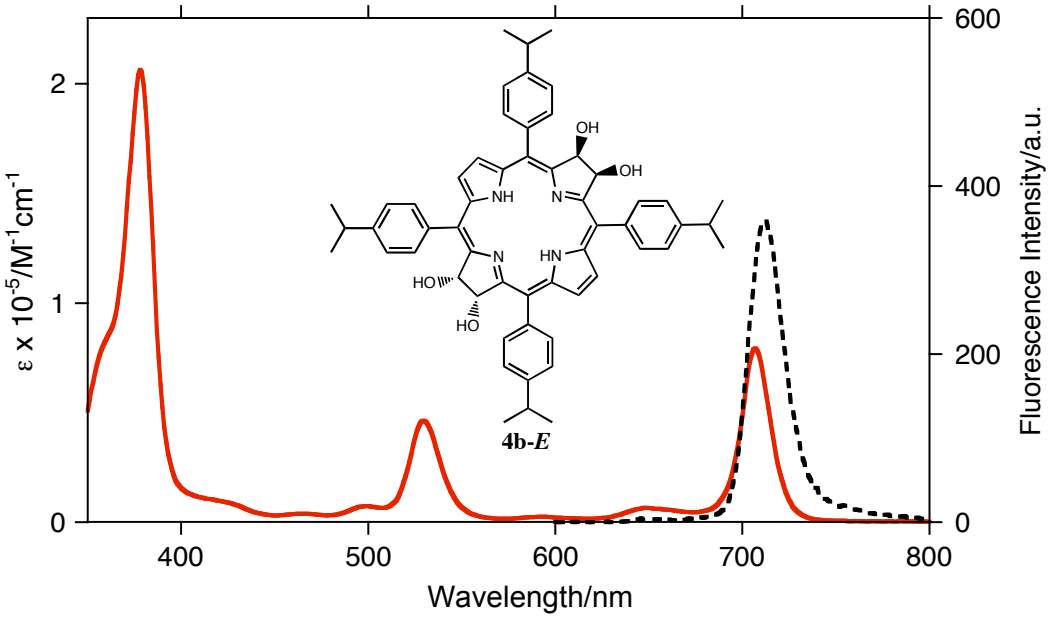

Figure ESI-11. UV-vis (solid red trace) and fluorescence (broken black trace) spectra of **4b—*E*** in CH_2Cl_2

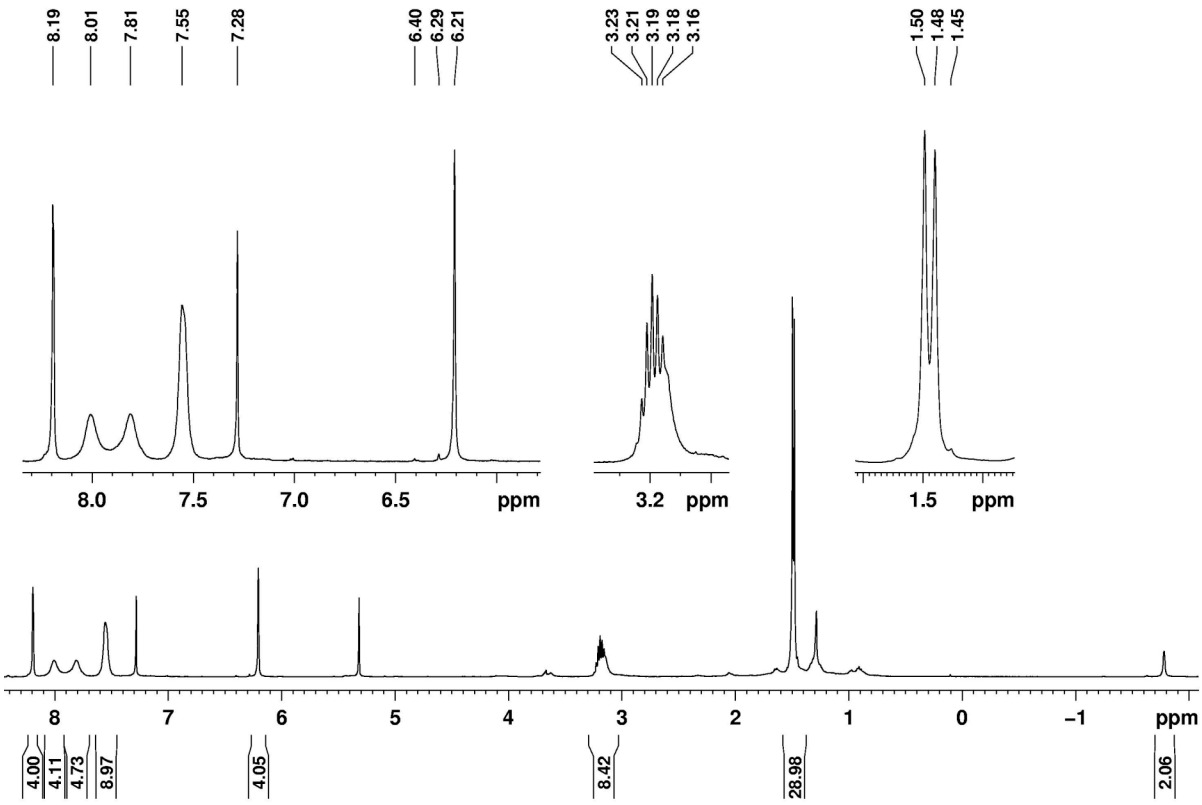

Figure ESI-12. ^{1}H NMR spectrum (400 MHz, $CDCl_3$) of **4b-*E***

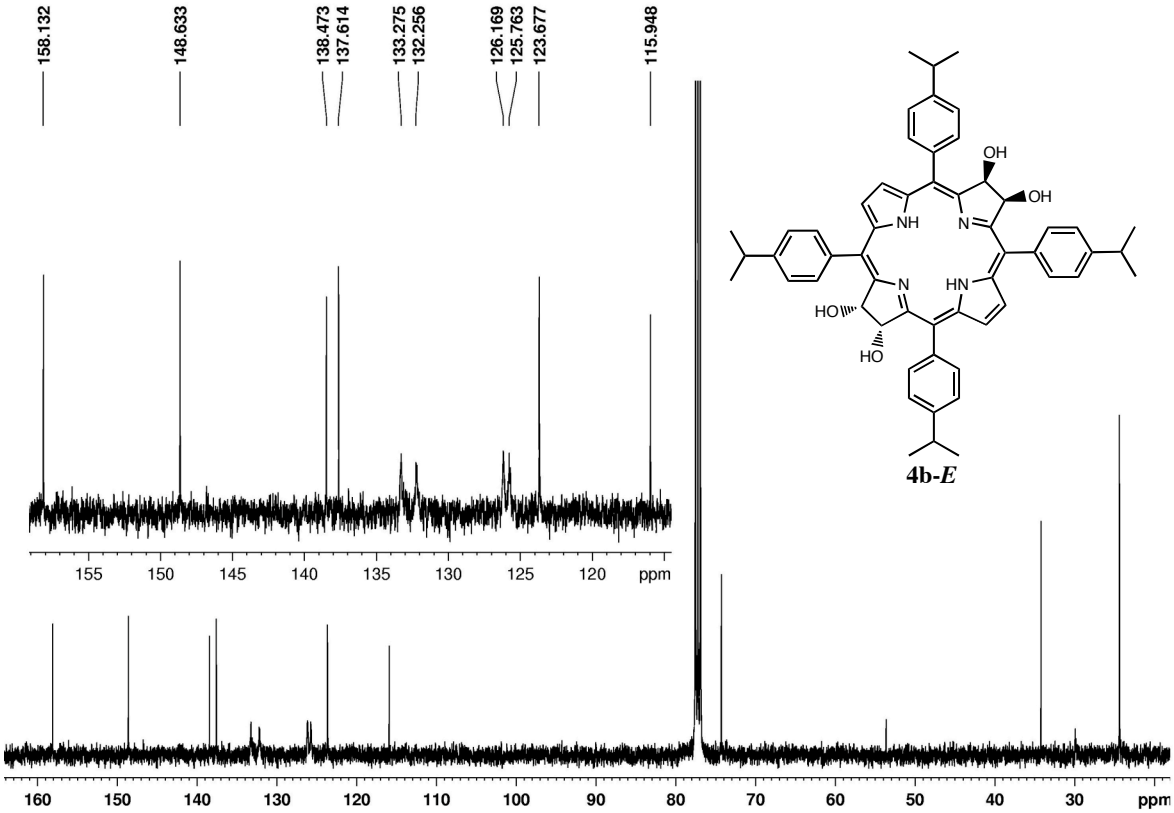

Figure ESI-13. ^{13}C NMR spectrum (100 MHz, $CDCl_3$) of **4b-*E***

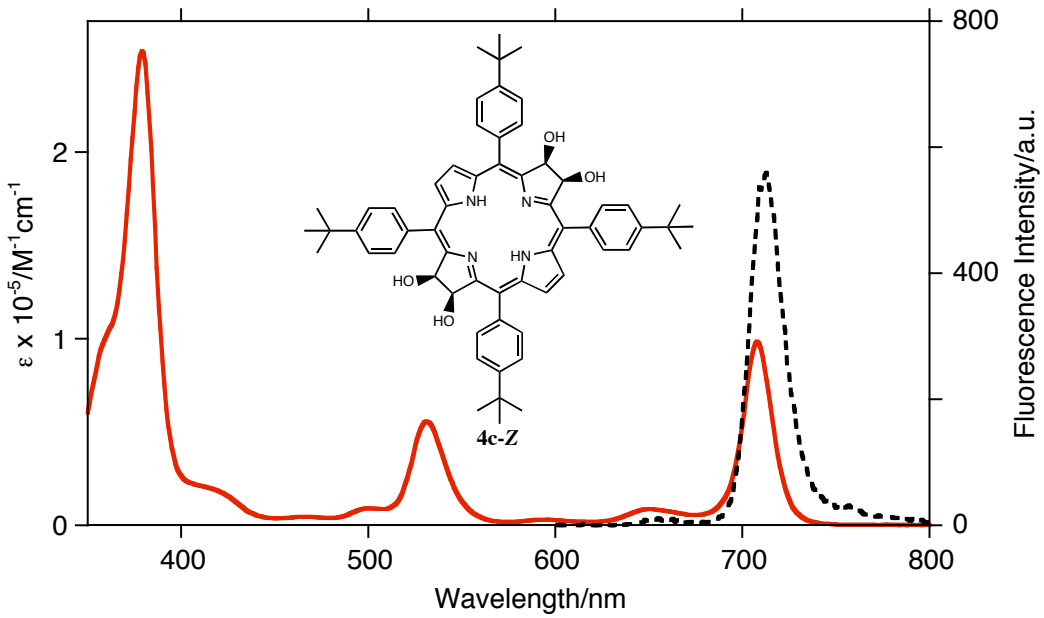

Figure ESI-14. UV-vis (solid red trace) and fluorescence (broken black trace) spectra of **4c-*Z*** in CH_2Cl_2

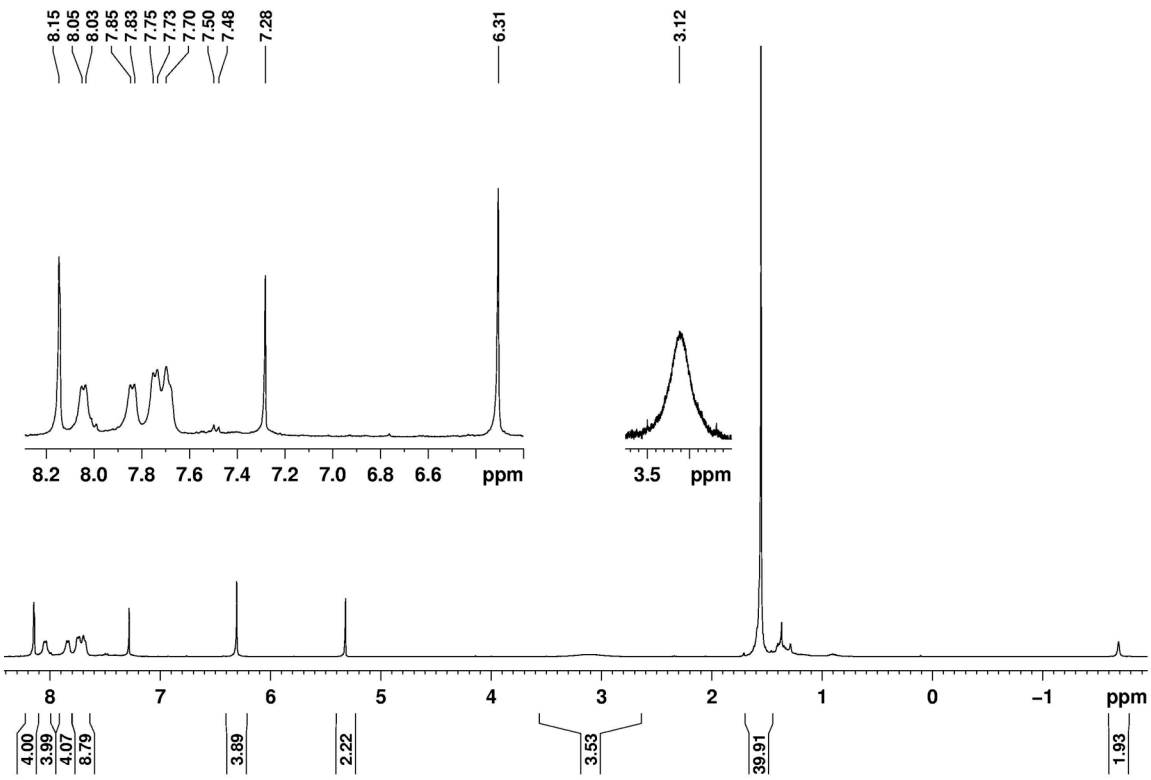

Figure ESI-15. ^{1}H NMR spectrum (400 MHz, $CDCl_3$) of **4c-*Z***

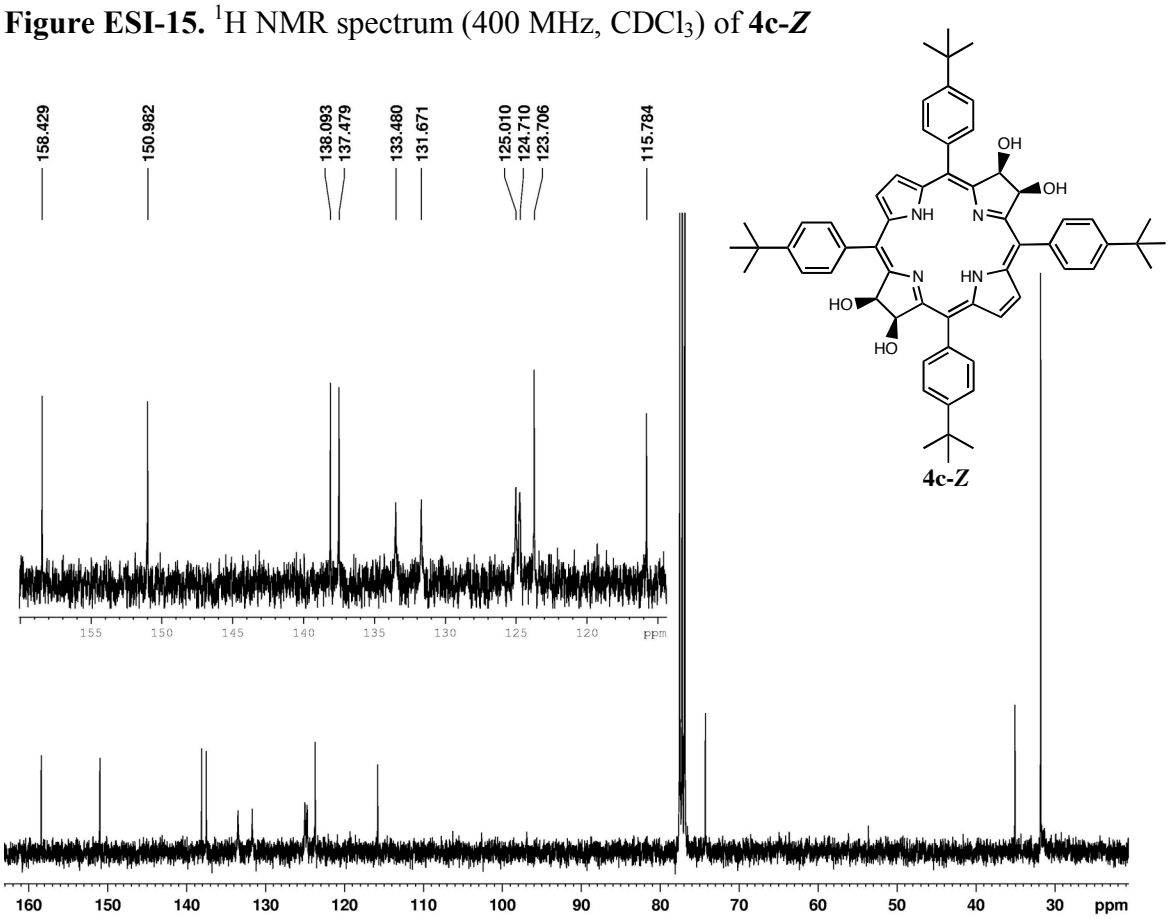

Figure ESI-16. ^{13}C NMR spectrum (100 MHz, $CDCl_3$) of **4c-*Z***

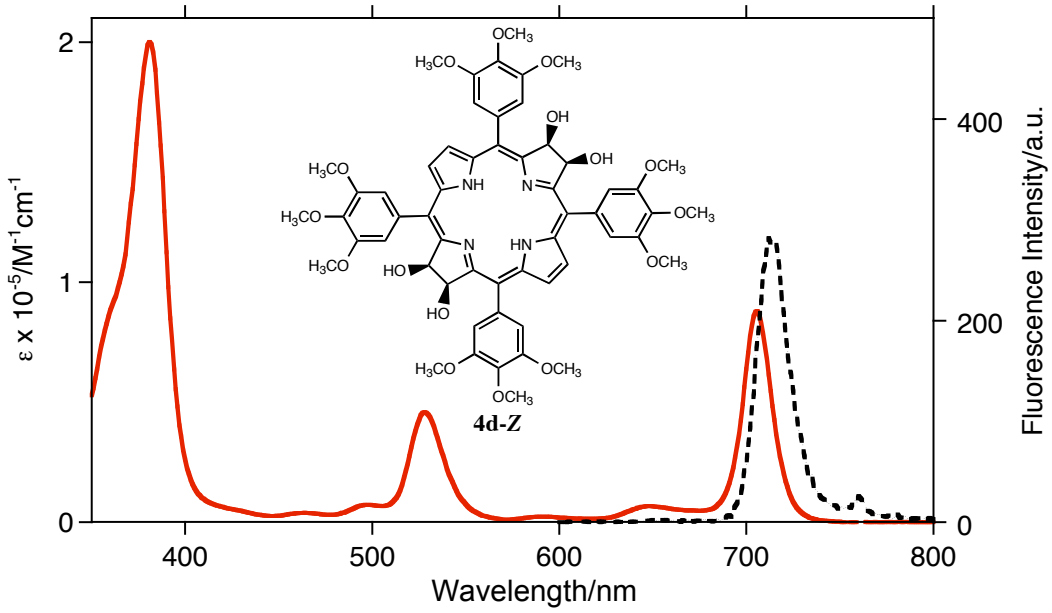

Figure ESI-17. UV-vis (solid red trace) and fluorescence (broken black trace) spectra of **4d-*Z*** in CH_2Cl_2

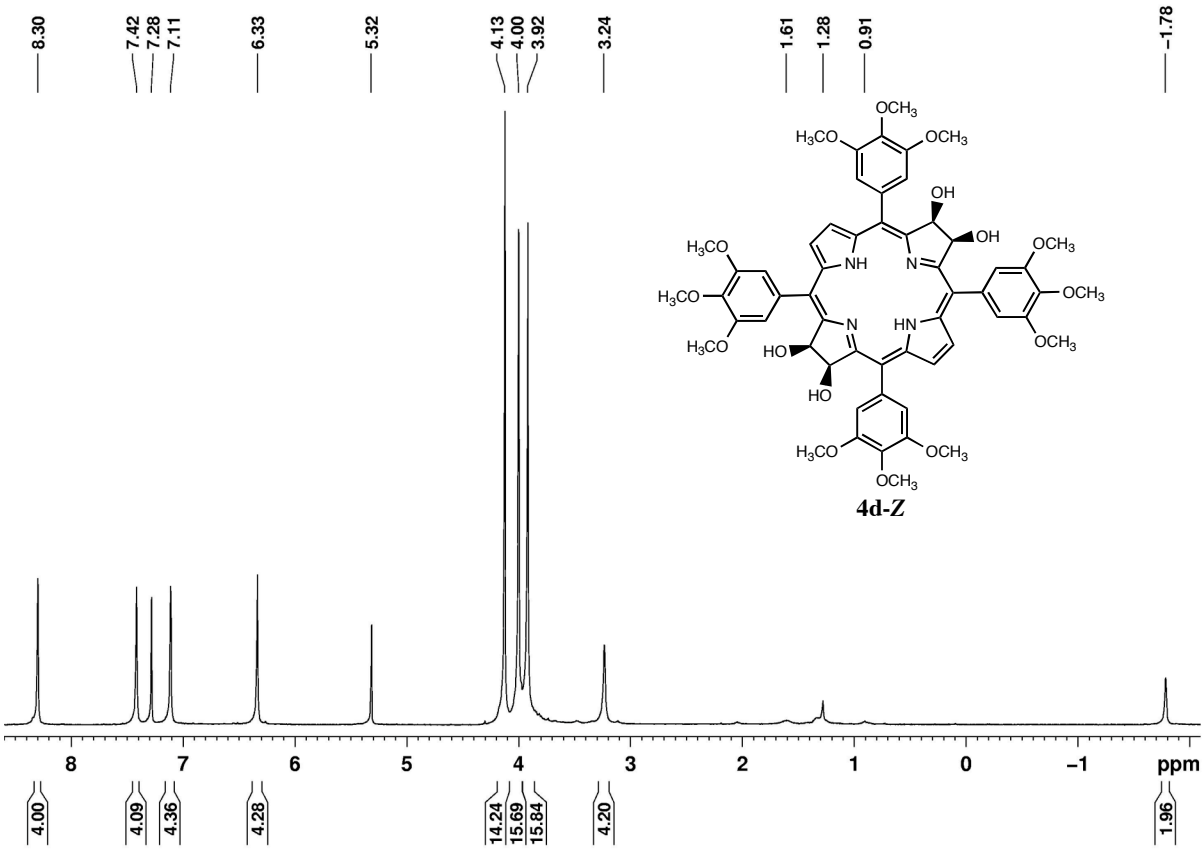

Figure ESI-18. ^{1}H NMR spectrum (400 MHz, $CDCl_3$) of **4d-*Z***

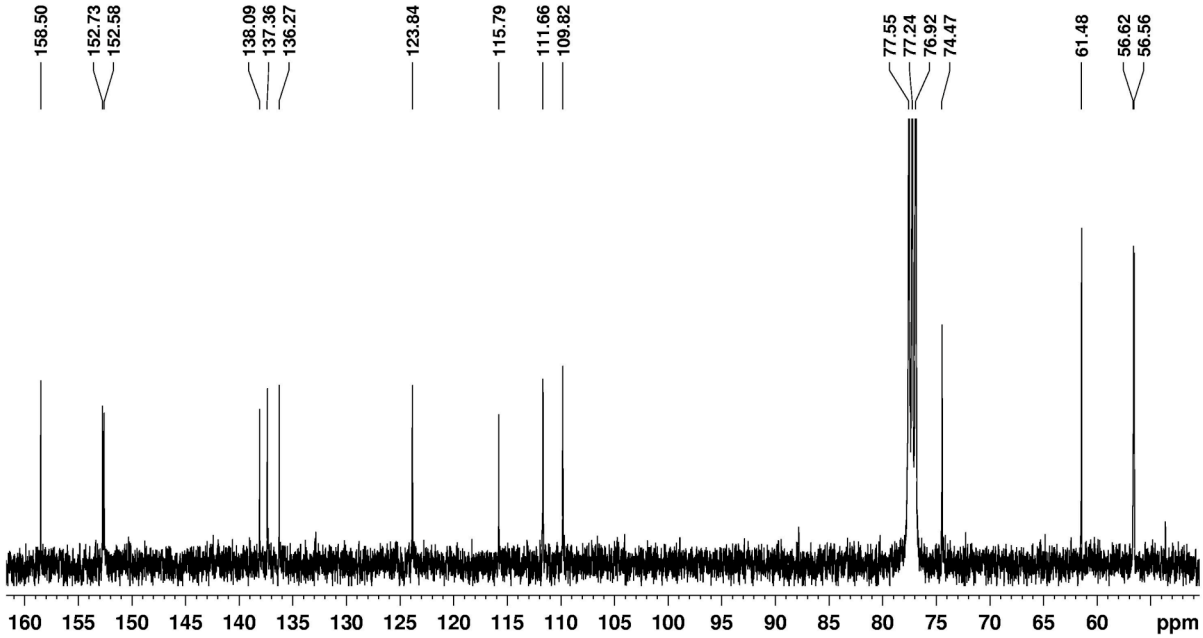

Figure ESI-19. ^{13}C NMR spectrum (100 MHz, $CDCl_3$) of **4d-*Z***

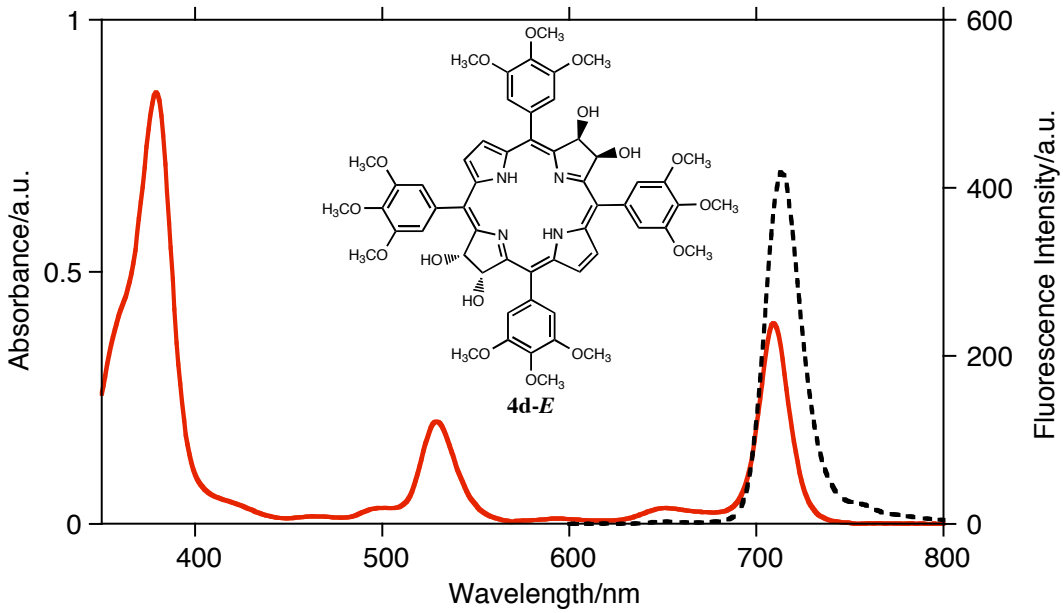

Figure ESI-20. UV-vis (solid red trace) and fluorescence (broken black trace) spectra of **4d-*E*** in CH_2Cl_2

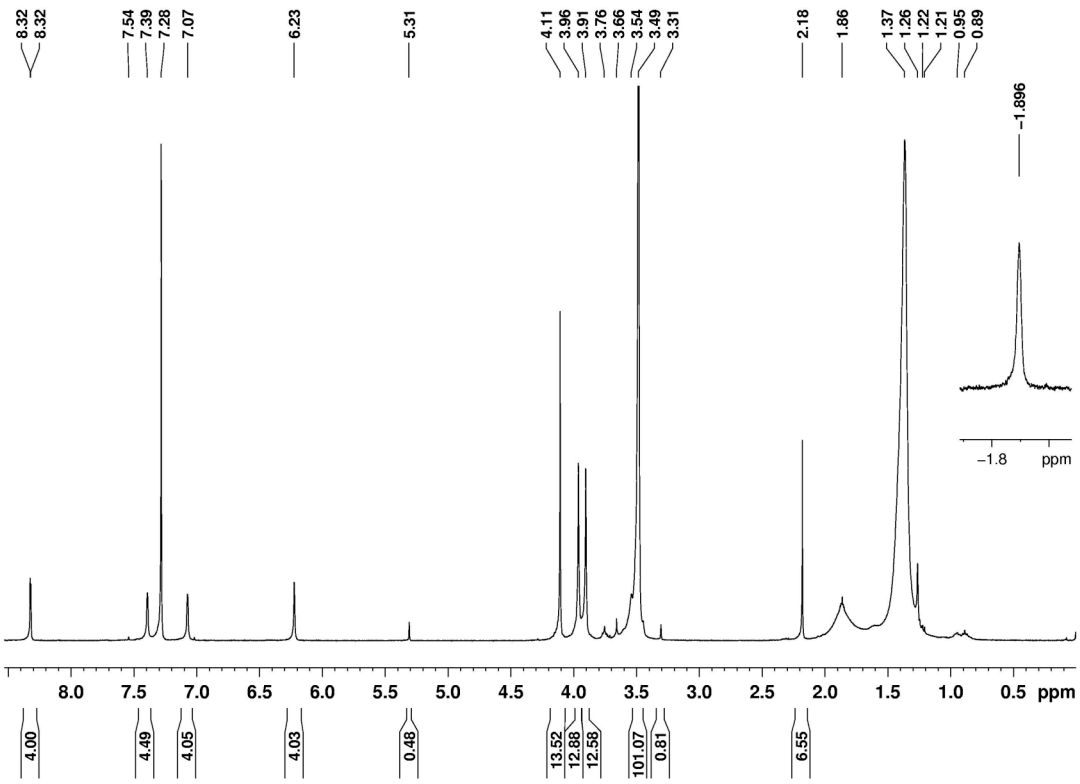

Figure ESI-21. ^{1}H NMR spectrum (400 MHz, $CDCl_3$) of **4d-*E***

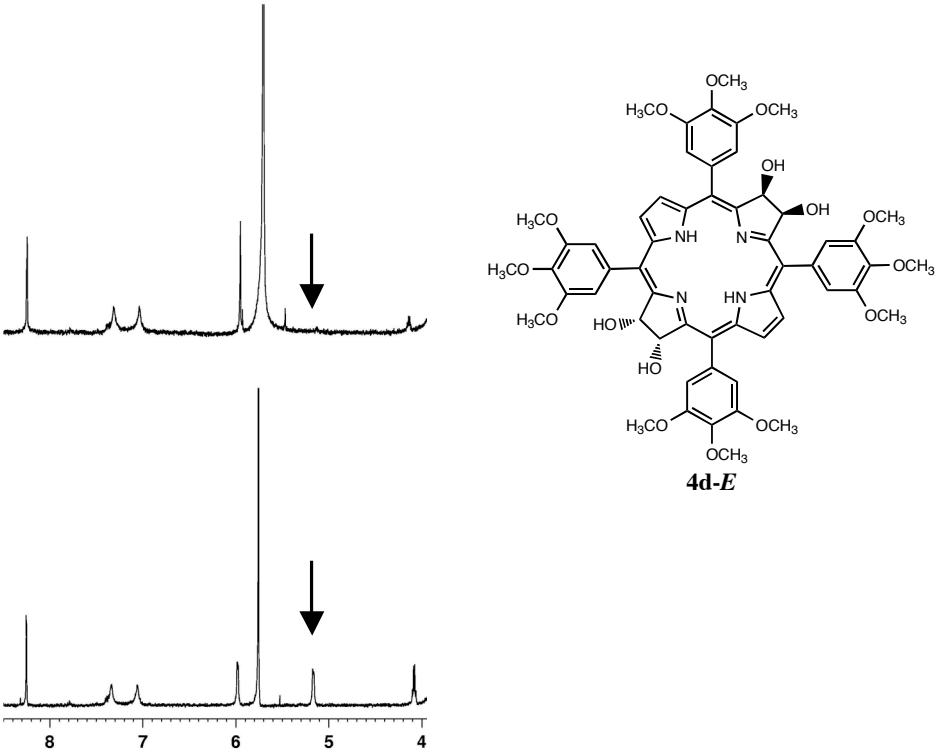

Figure ESI-22. Comparison of ^{1}H NMR spectra (400 MHz, DMSO-d_6) of **4d-*E***, before (bottom spectrum) and after a D_2O wash (top spectrum). Arrow indicates position of the –OH signal.

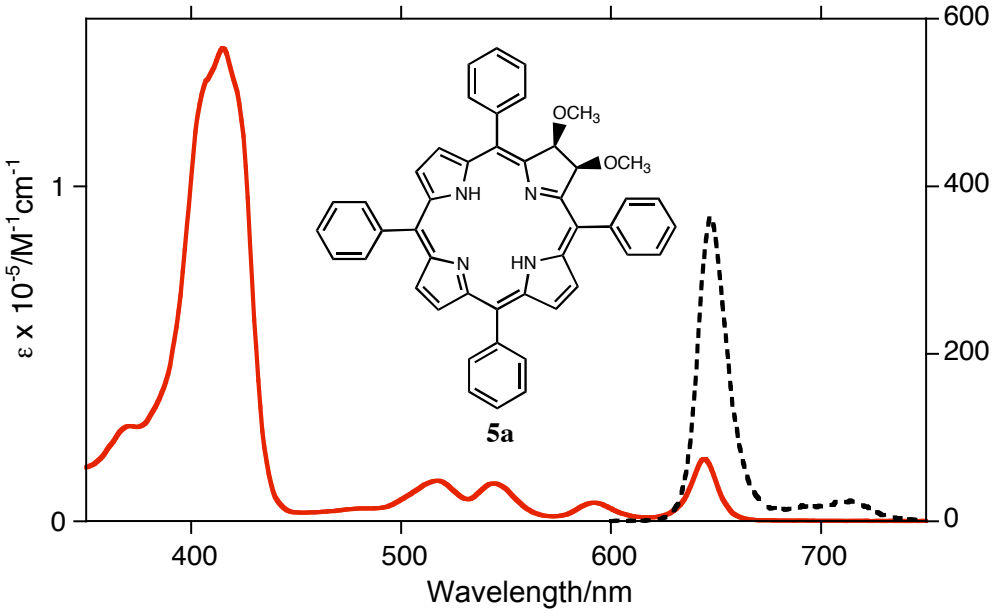

Figure ESI-23. UV-vis (solid red trace) and fluorescence (broken black trace) spectra of **5a** in CH_2Cl_2

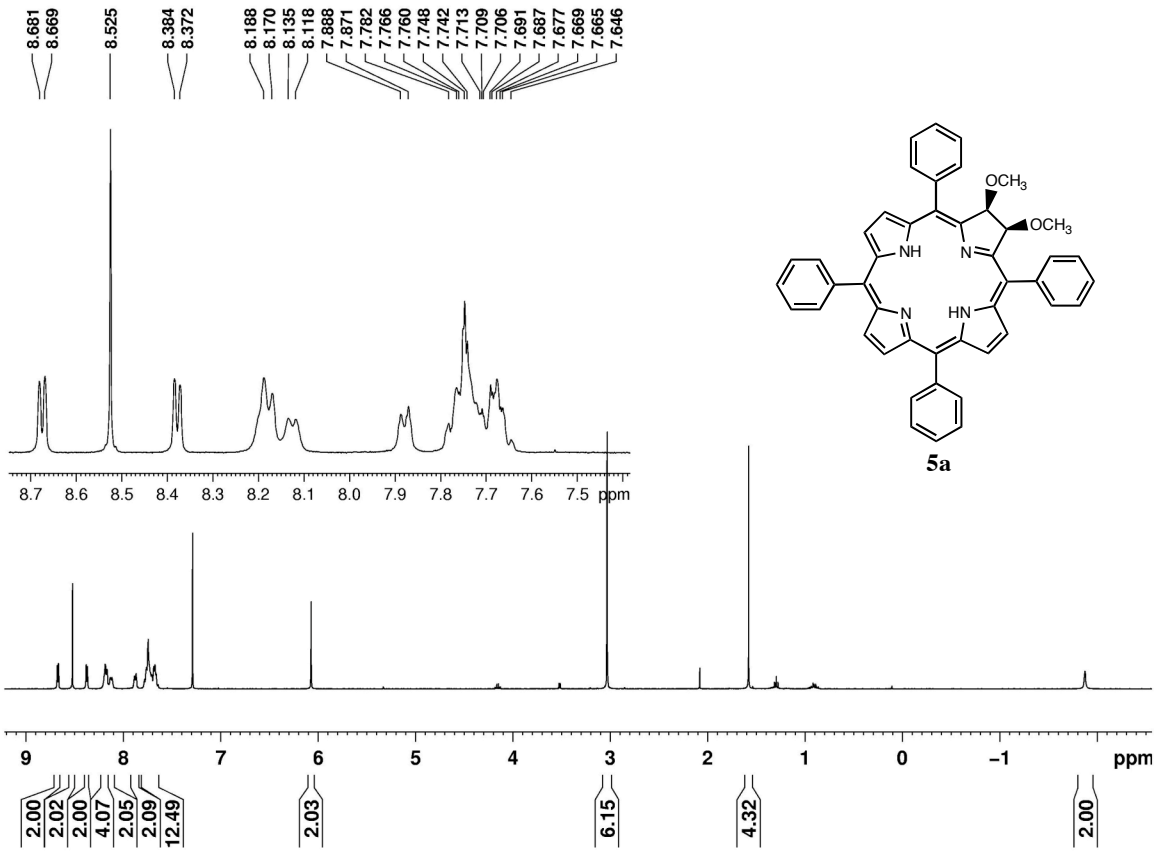

Figure ESI-24. ^{1}H NMR (400 MHz, $CDCl_3$) spectrum of **5a**

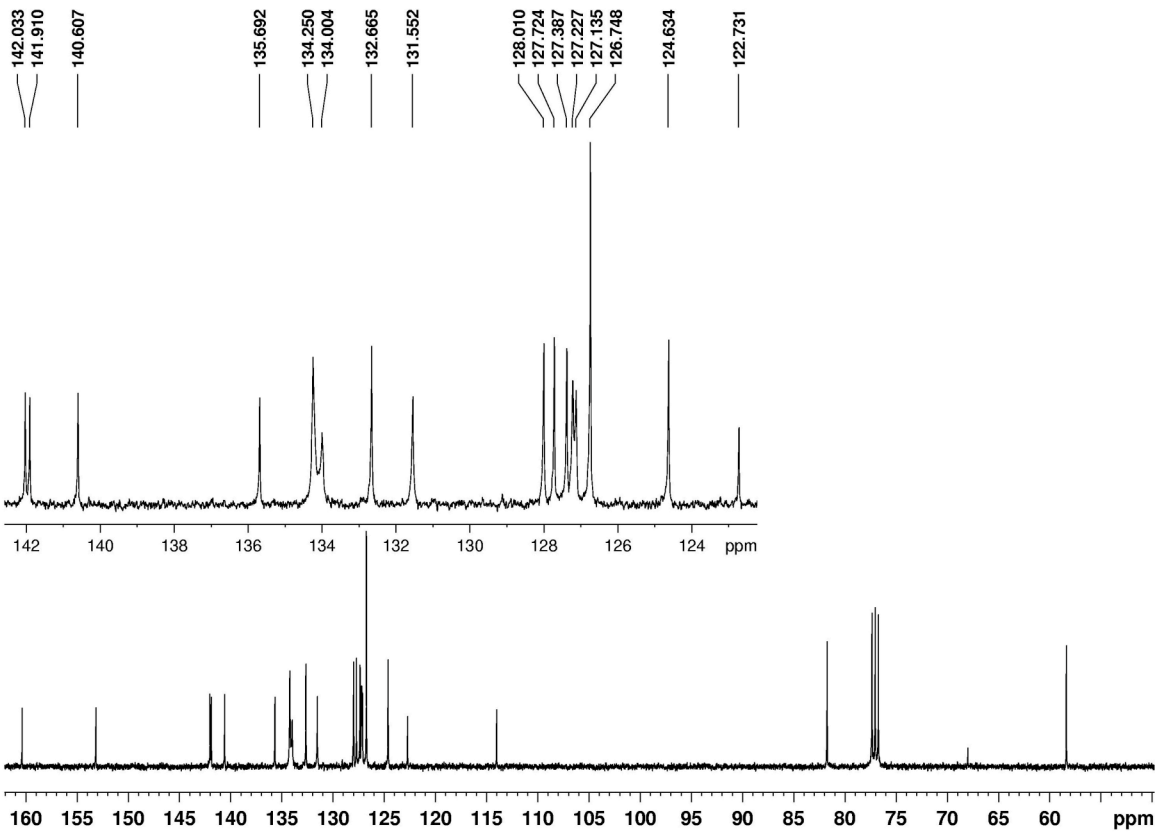

Figure ESI-25. ^{13}C NMR (100 MHz, $CDCl_3$) spectrum of **5a**

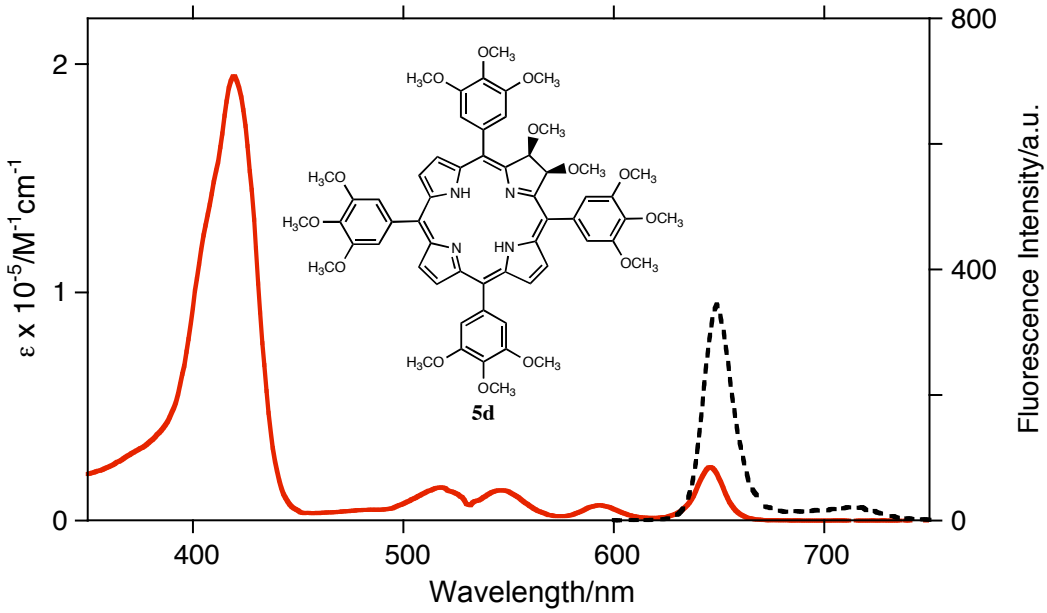

Figure ESI-26. UV-vis (solid red trace) and fluorescence (broken black trace) spectra of **5d** in CH_2Cl_2

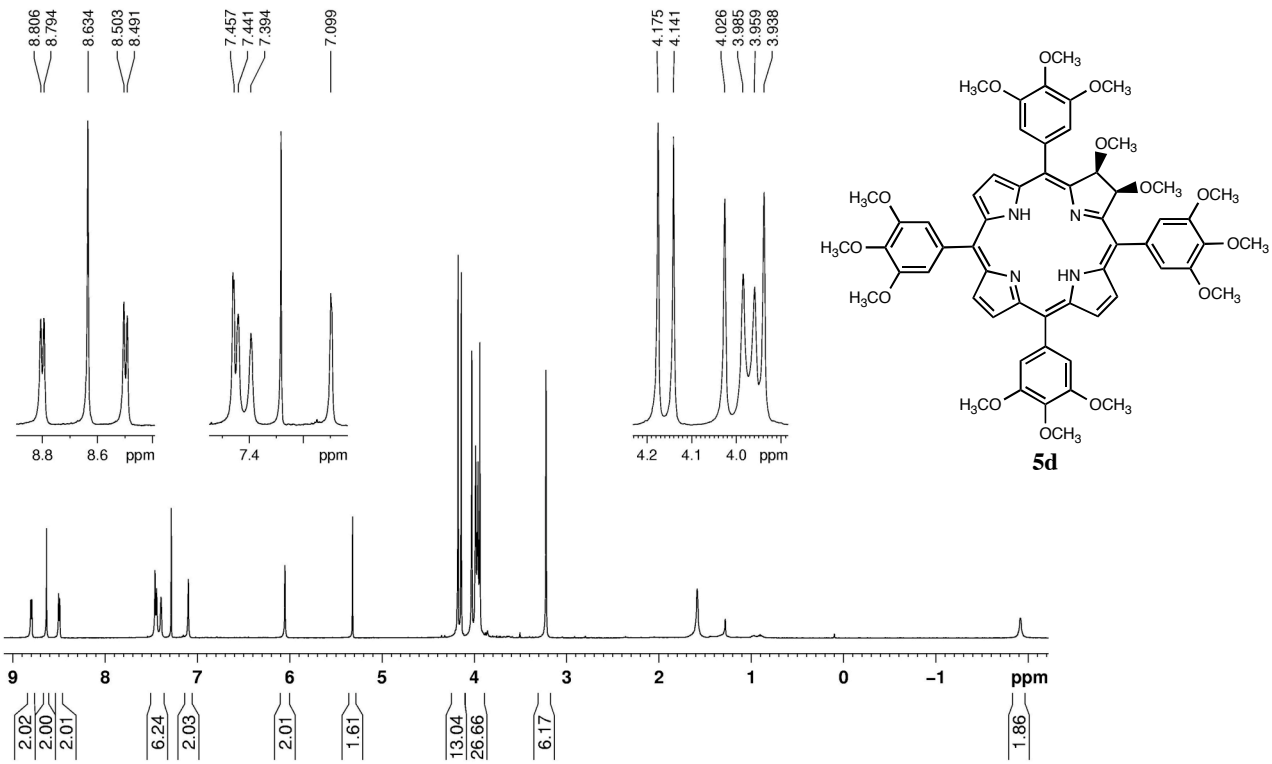

Figure ESI-27. ^{1}H NMR spectrum (400 MHz, $CDCl_3$) of **5d**

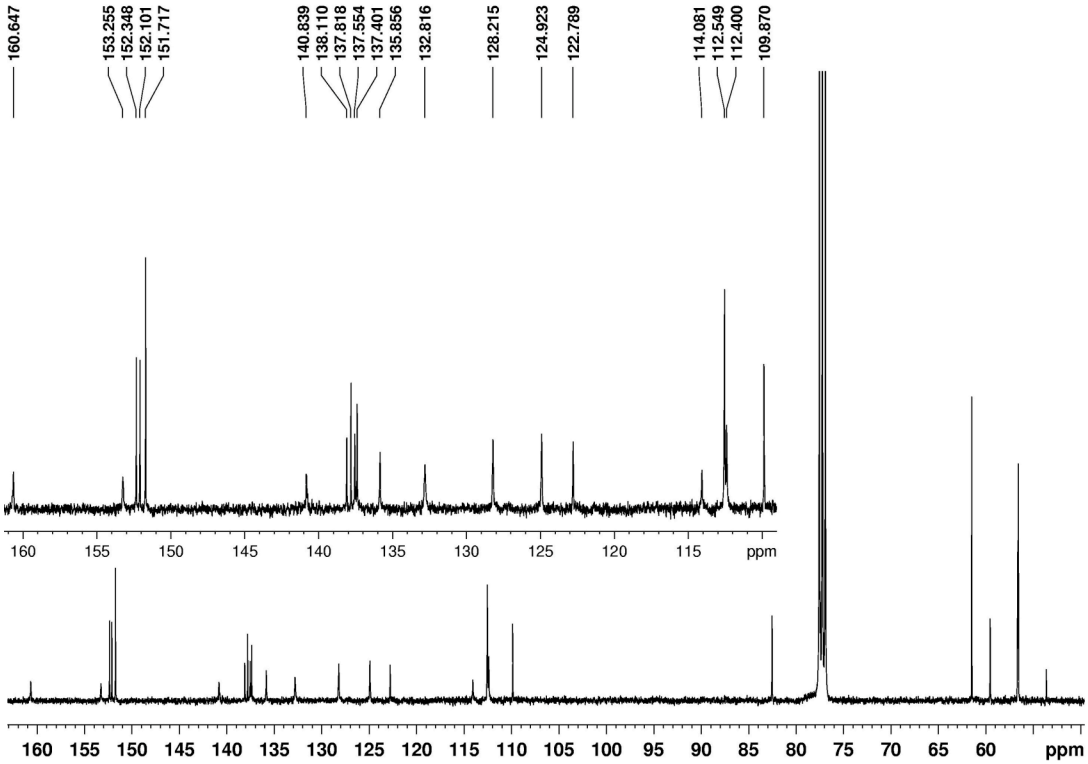

Figure ESI-28. ^{13}C NMR (100 MHz, $CDCl_3$) spectrum of **5d**

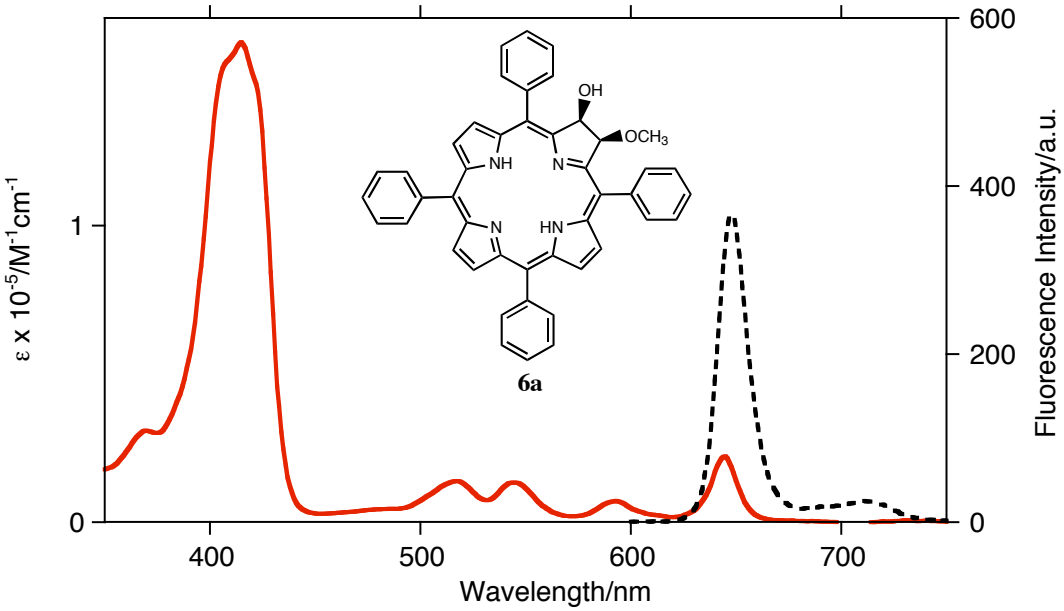

Figure ESI-29. UV-vis (solid red trace) and fluorescence (broken black trace) spectra of **6a** in CH_2Cl_2

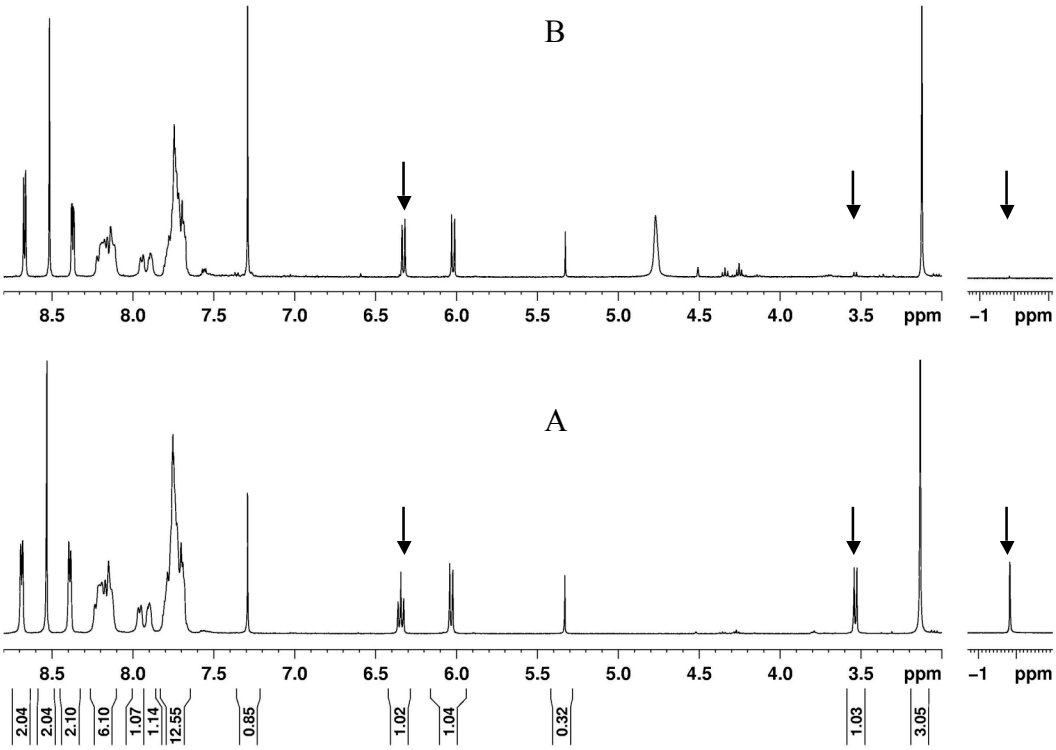

Figure ESI-30. ^{1}H NMR spectrum (400 MHz, $CDCl_3$) of **6a** before (A) and after (B) a D_2O wash

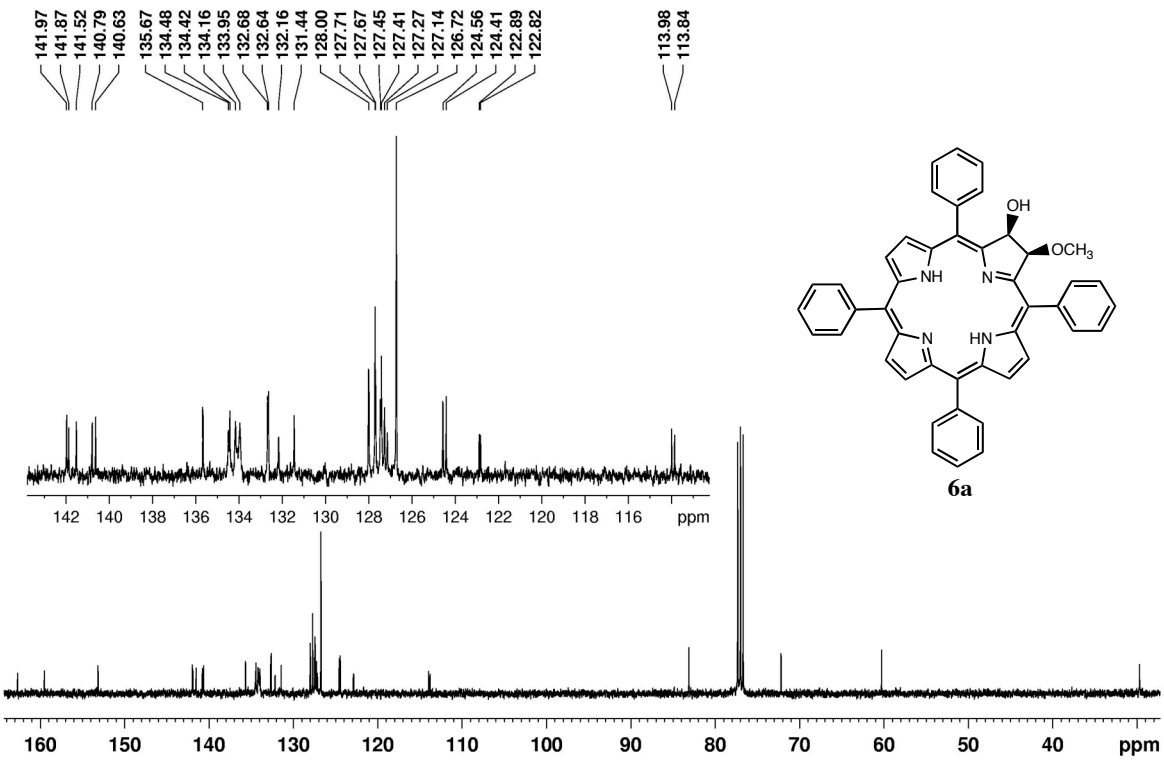

Figure ESI-31. ^{13}C NMR spectrum (100 MHz, $CDCl_3$) of **6a**

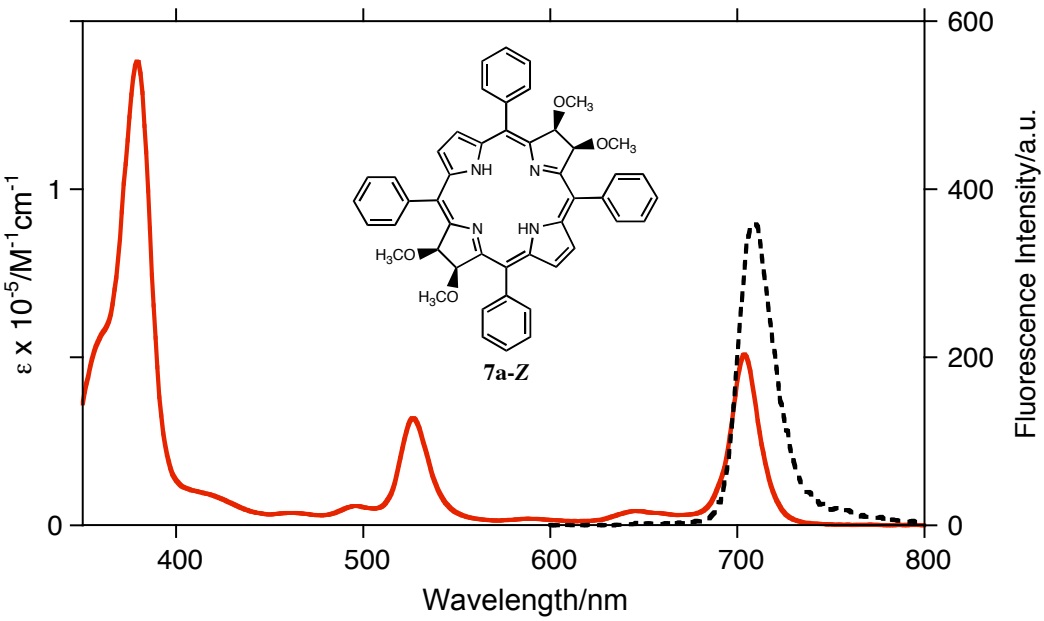

Figure ESI-32. UV-vis (solid red trace) and fluorescence (broken black trace) spectra of **7a-*Z*** in CH_2Cl_2

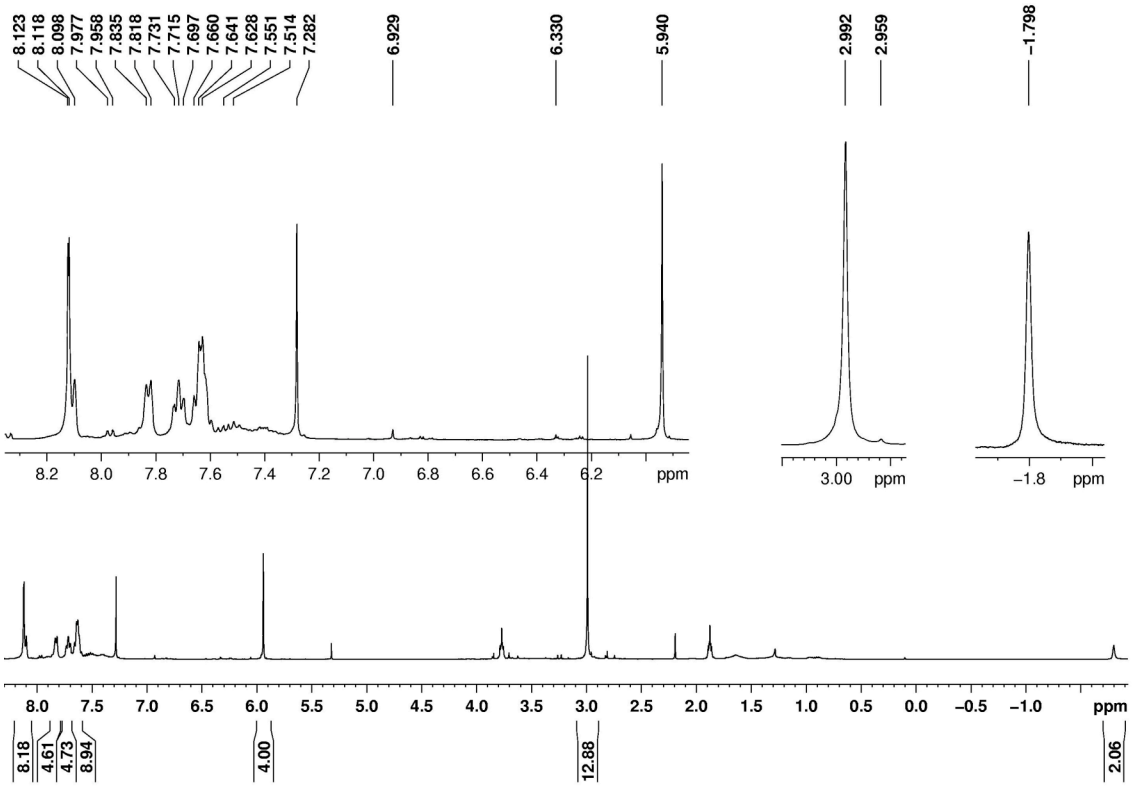

Figure ESI-33. ^{1}H NMR spectrum (400 MHz, $CDCl_3$) of **7a-*Z***

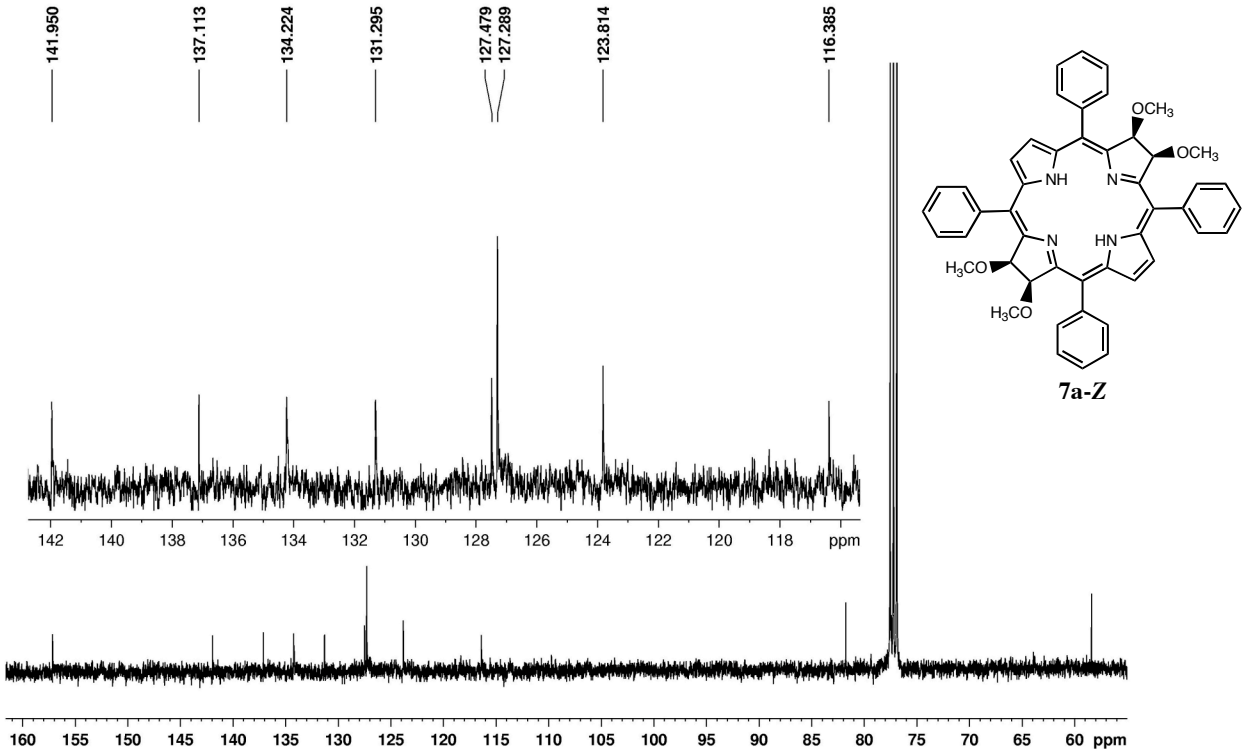

Figure ESI-34. ^{13}C NMR spectrum (100 MHz, $CDCl_3$) of **7a-*Z***

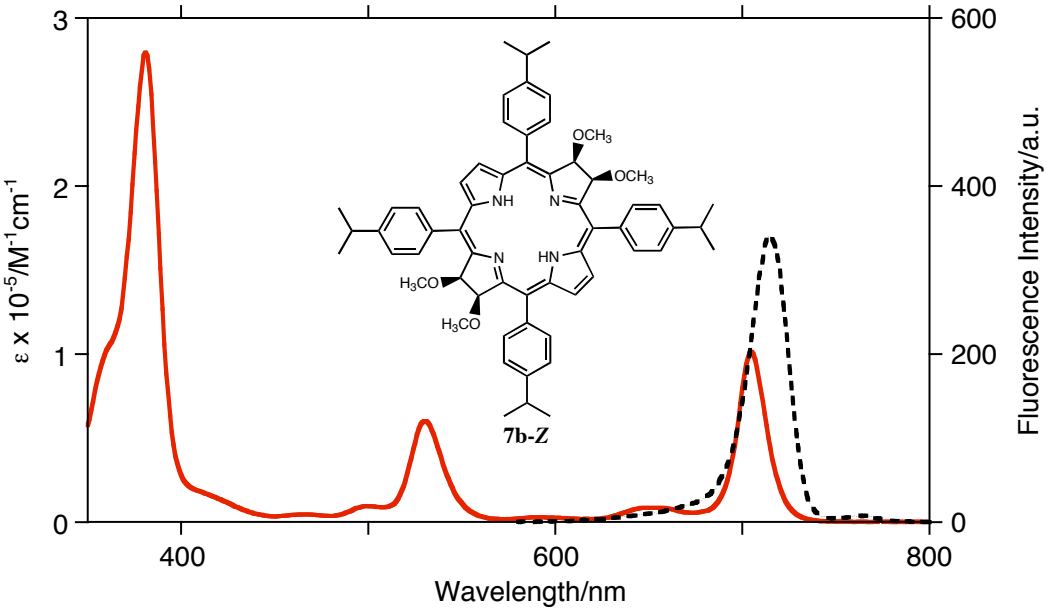

Figure ESI-35. UV-vis (solid red trace) and fluorescence (broken black trace) spectra of **7b-*Z*** in CH_2Cl_2

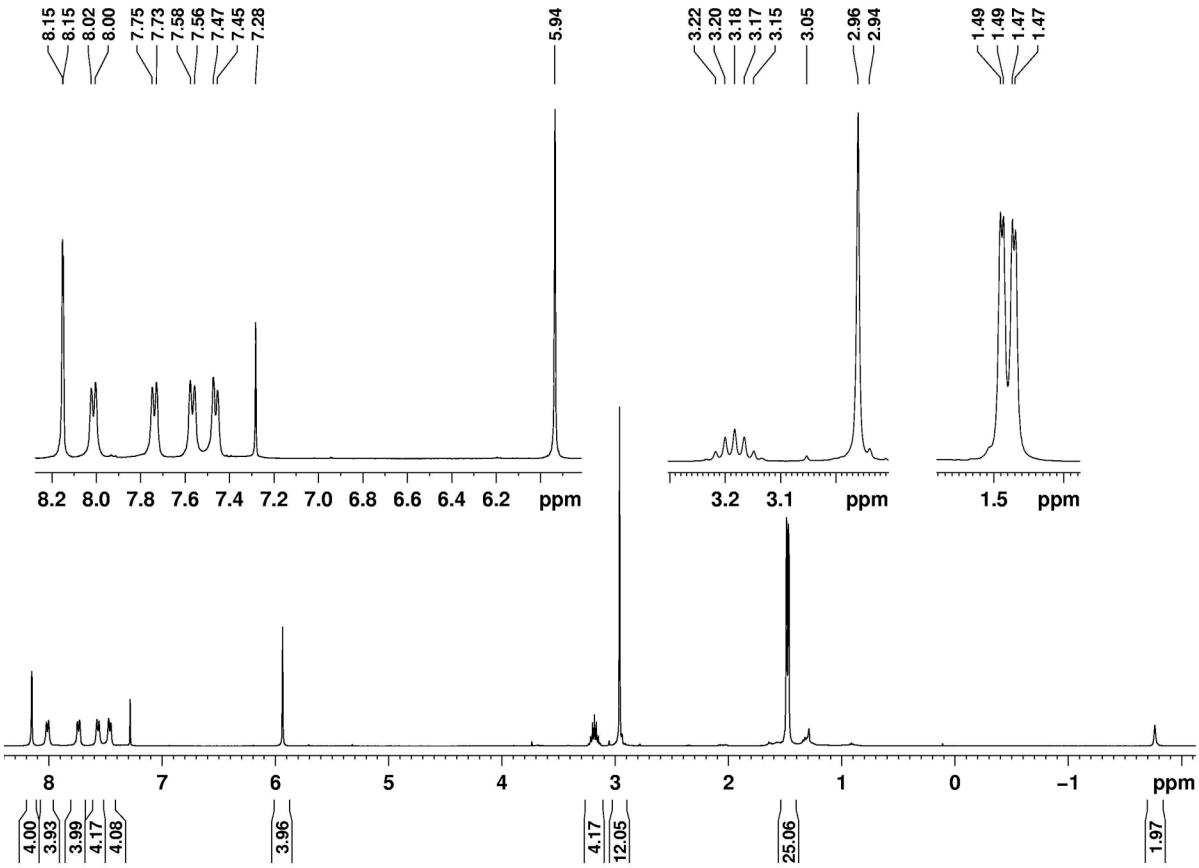

Figure ESI-36. ^{1}H NMR spectrum (400 MHz, $CDCl_3$) of **7b-*Z***

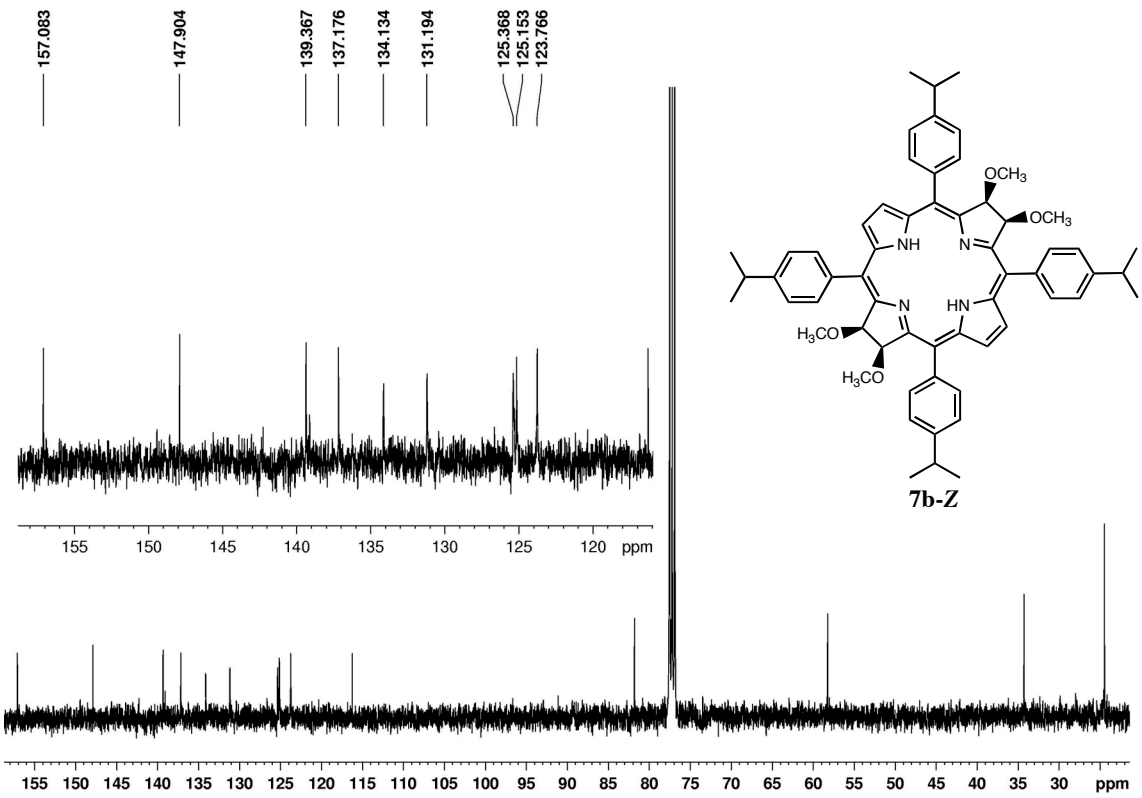

Figure ESI-37. ^{13}C NMR spectrum (100 MHz, $CDCl_3$) of **7b-*Z***

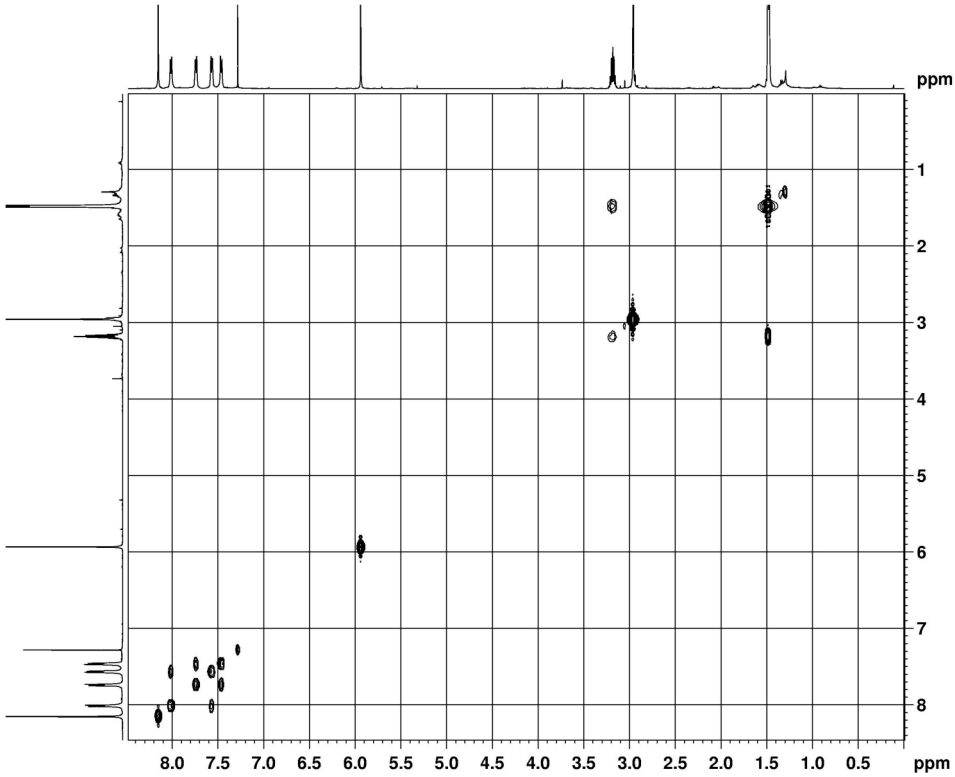

Figure ESI-38. H,H-COSY spectrum (500 MHz, $CDCl_3$) of **7b-*Z***

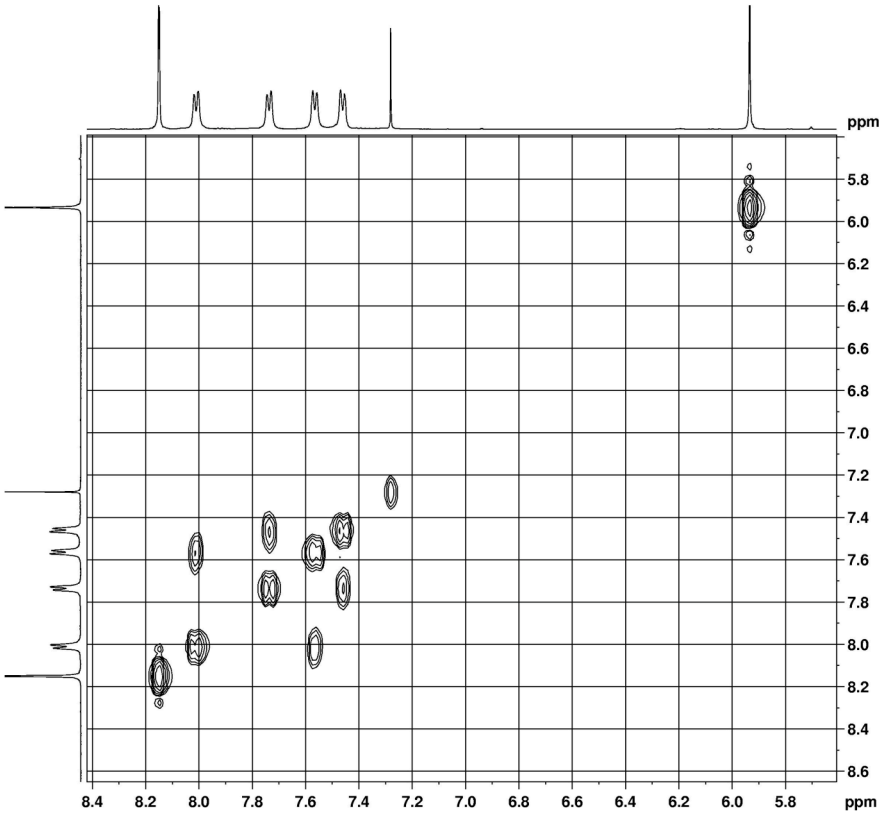

Figure ESI-39. Expansion of the aromatic region of the H,H-COSY spectrum (500 MHz, $CDCl_3$) spectrum of **7b-*Z***

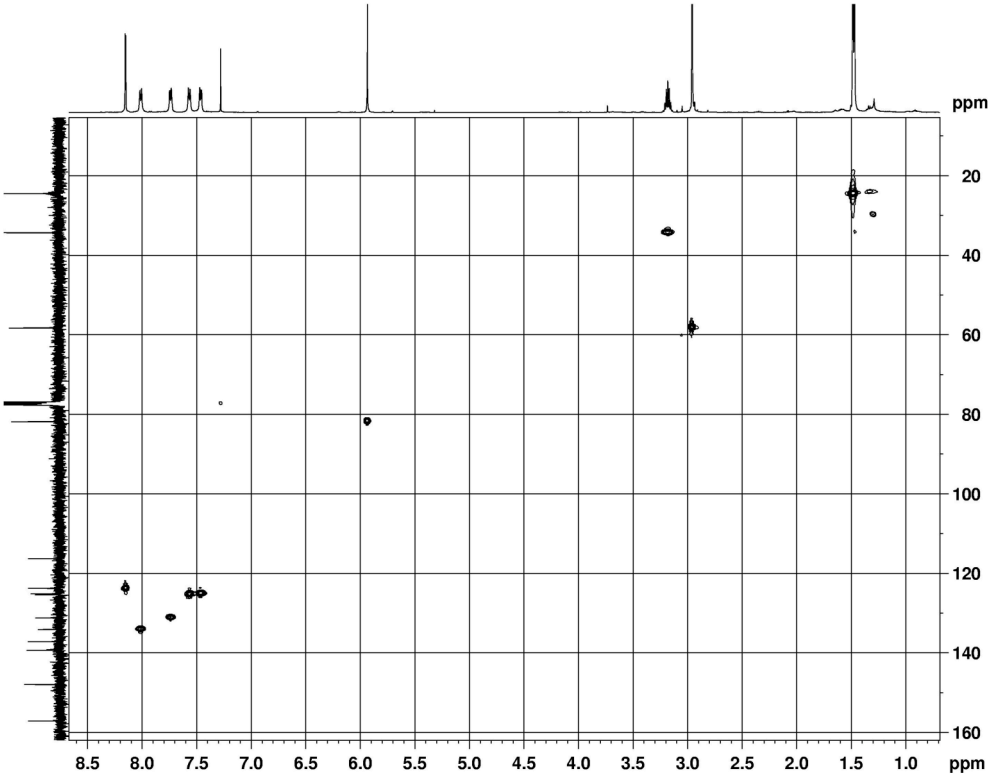

Figure ESI-40. HSQC spectrum (500 MHz, $CDCl_3$) of **7b-*Z***

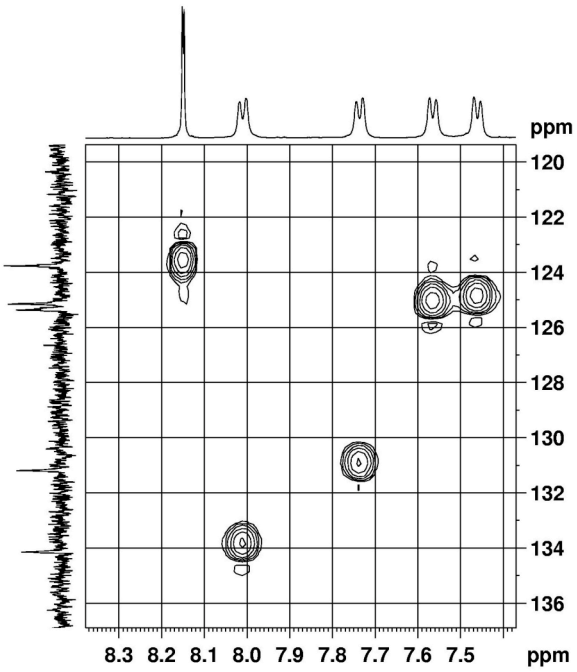

Figure ESI-41. Expansion of the aromatic region of the HSQC spectrum (500 MHz, $CDCl_3$) spectrum of **7b-*Z***

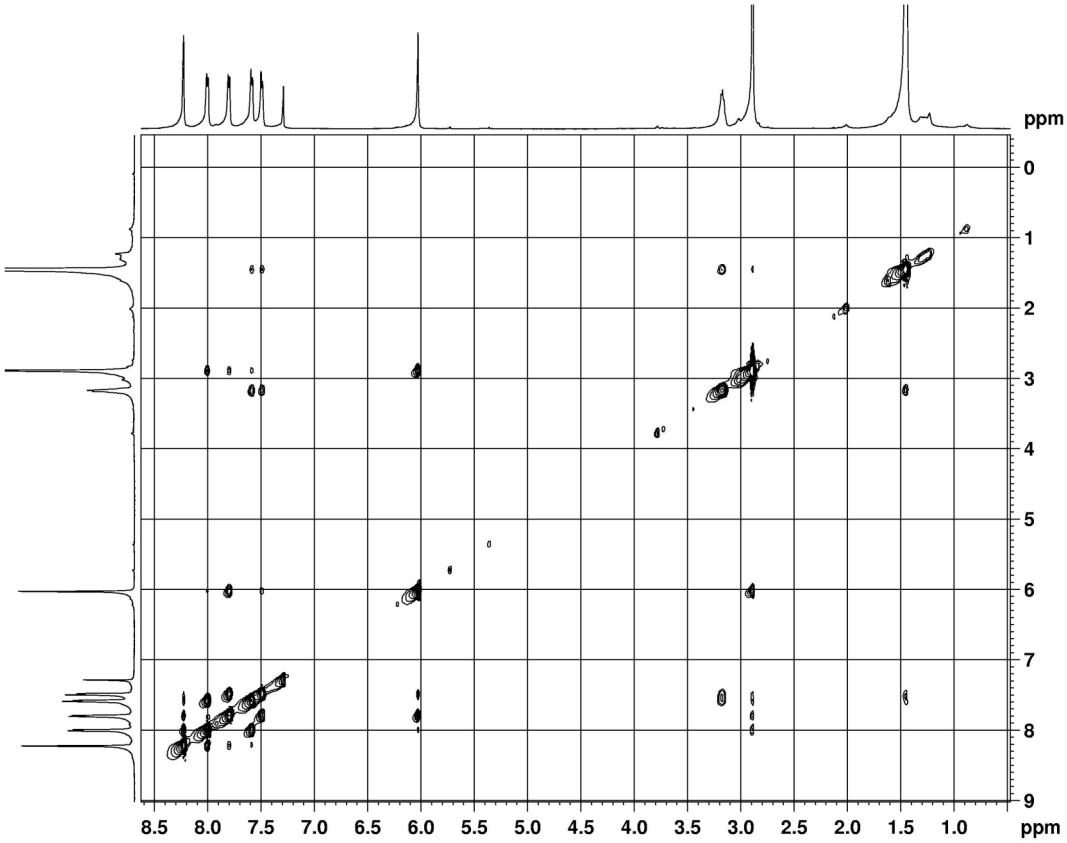

Figure ESI-42. NOESY spectrum (500 MHz, $CDCl_3$, -40°C) of **7b-*Z***

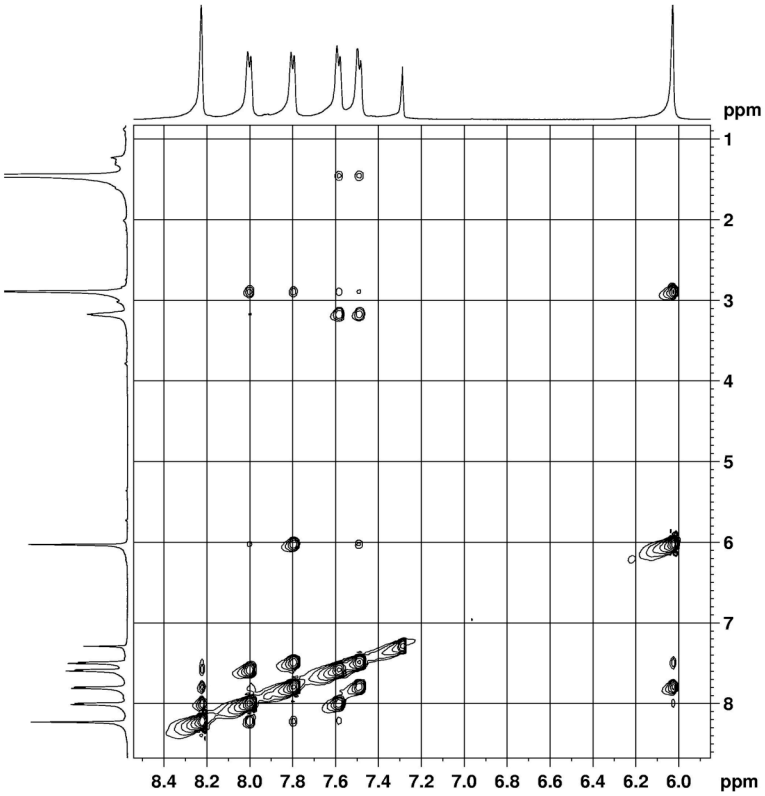

Figure ESI-43. Expansion of the aromatic region of the NOESY spectrum (500 MHz, $CDCl_3$, -40°C) of **7b-*Z***

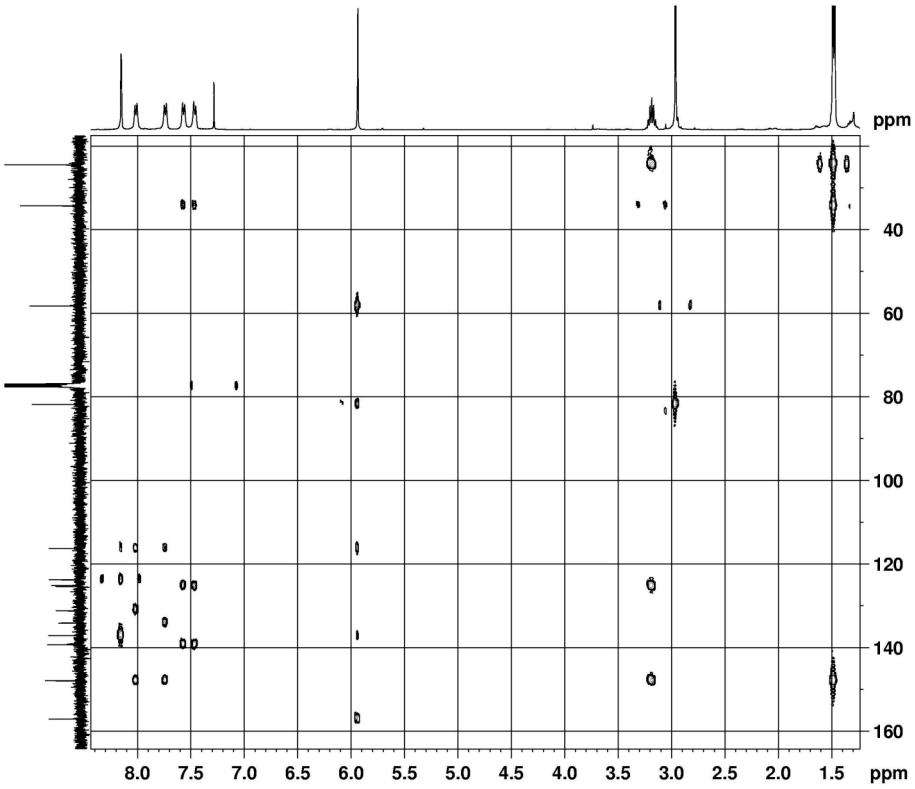

Figure ESI-44. HMBC Spectrum (500 MHz, $CDCl_3$) of **7b-*Z***

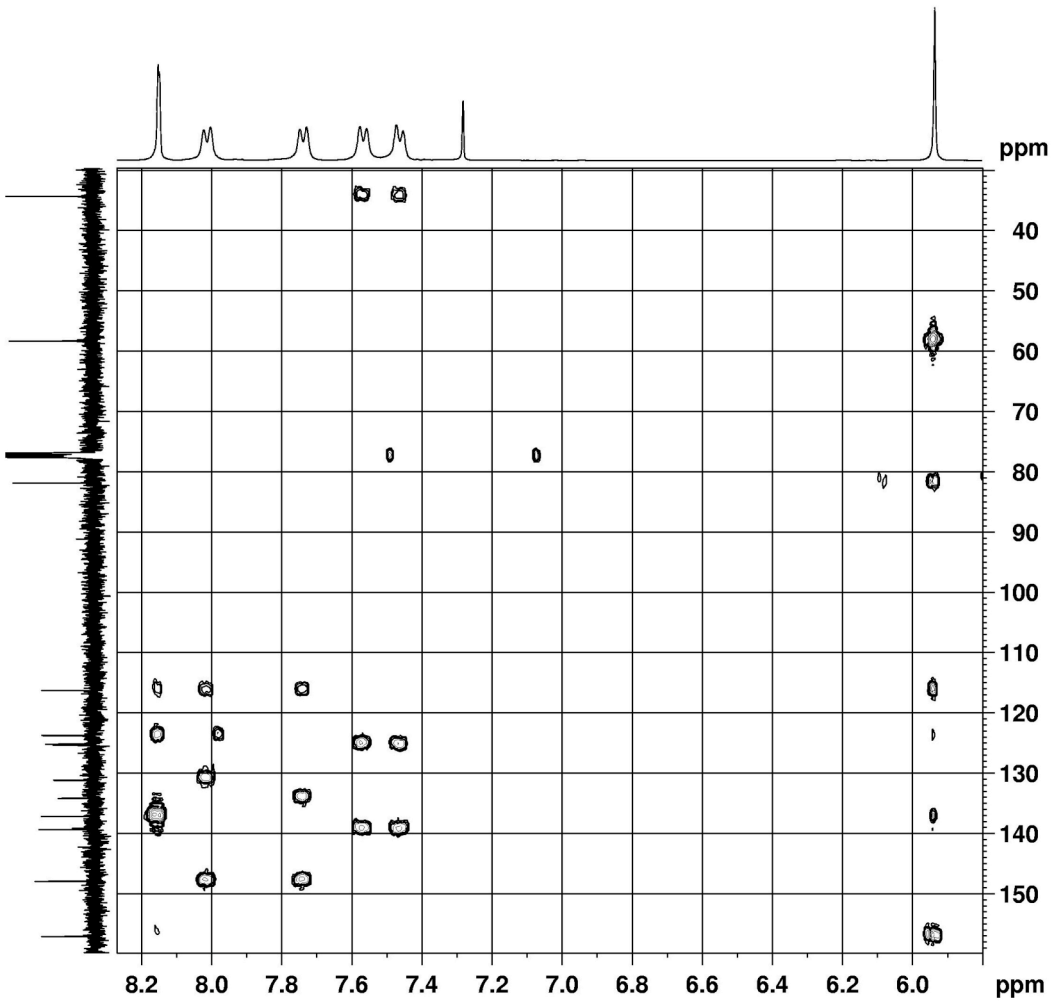

Figure ESI-45. Partial of the HMBC spectrum (500 MHz, $CDCl_3$) of **7b-*Z***

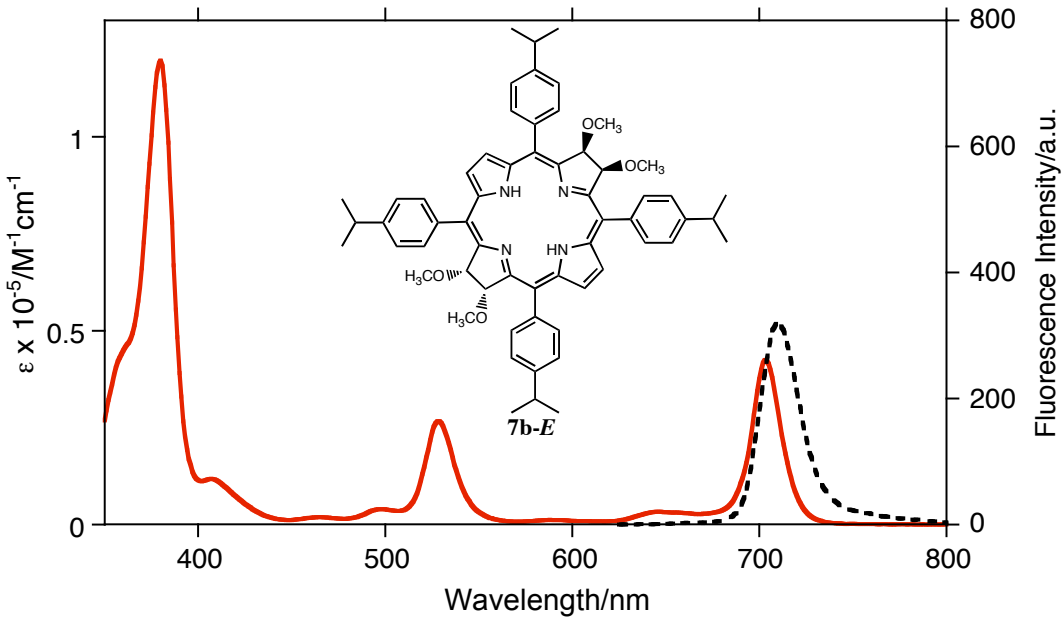

Figure ESI-46. UV-vis (solid red trace) and fluorescence (broken black trace) spectra of **7b-*E*** in CH_2Cl_2

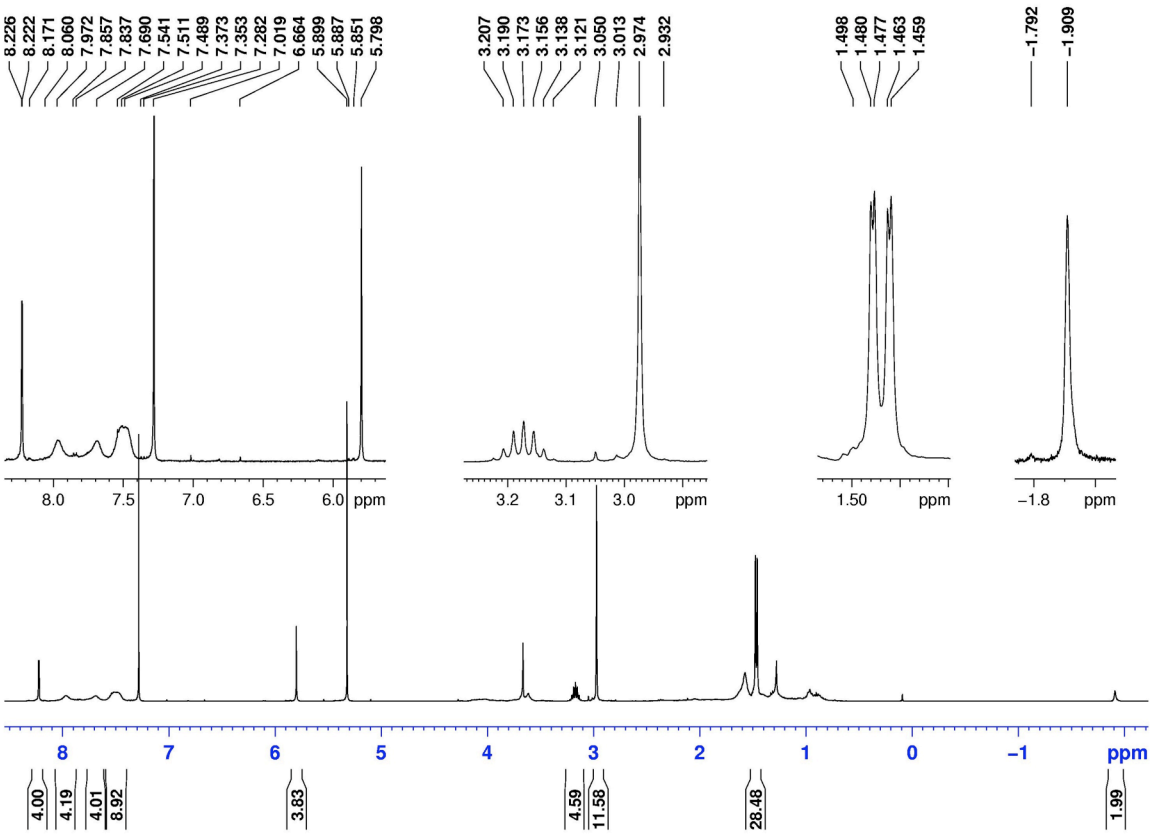

Figure ESI-47. ^{1}H NMR spectrum (400 MHz, $CDCl_3$) of **7b-*E***

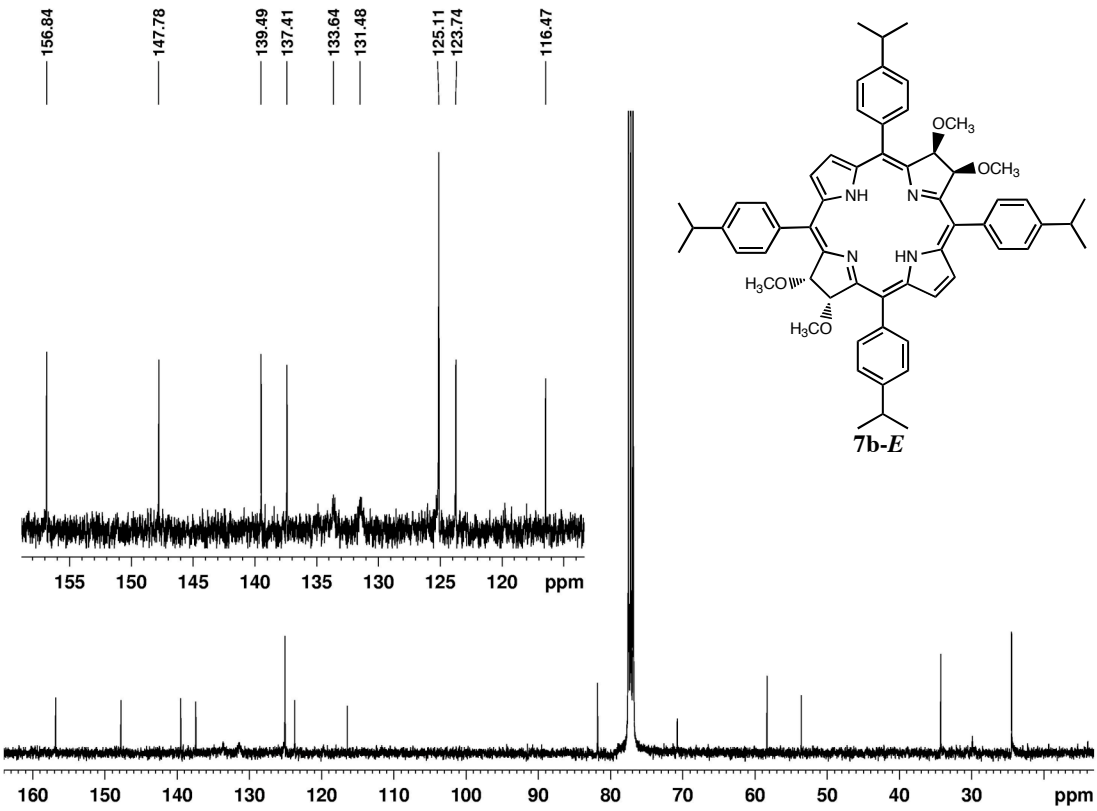

Figure ESI-48. ^{13}C NMR (100 MHz, $CDCl_3$) spectrum of **7b-*E***

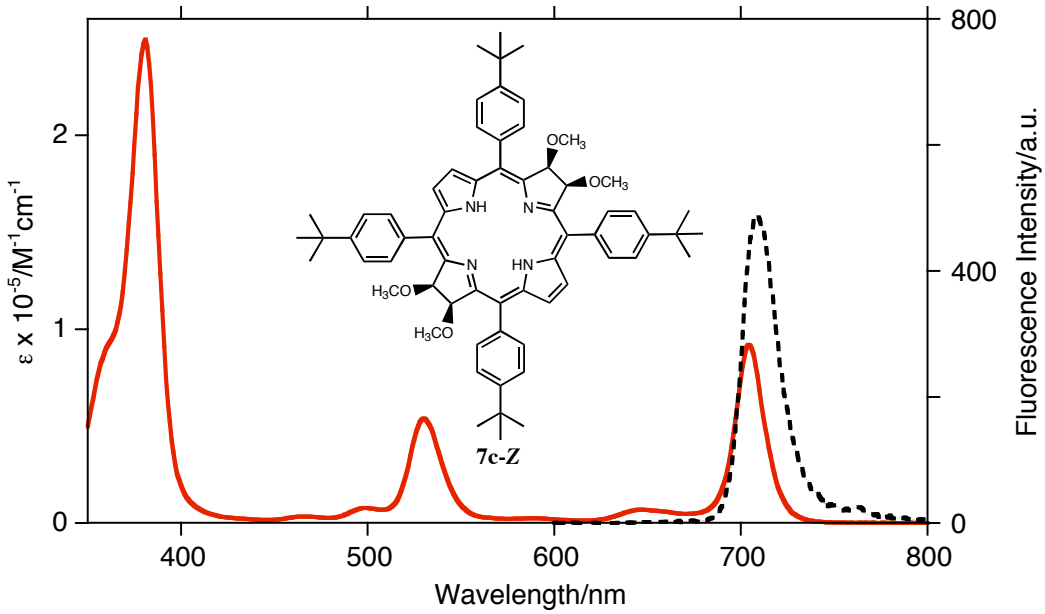

Figure ESI-49. UV-vis (solid red trace) and fluorescence (broken black trace) spectra of **7c-*Z*** in CH_2Cl_2

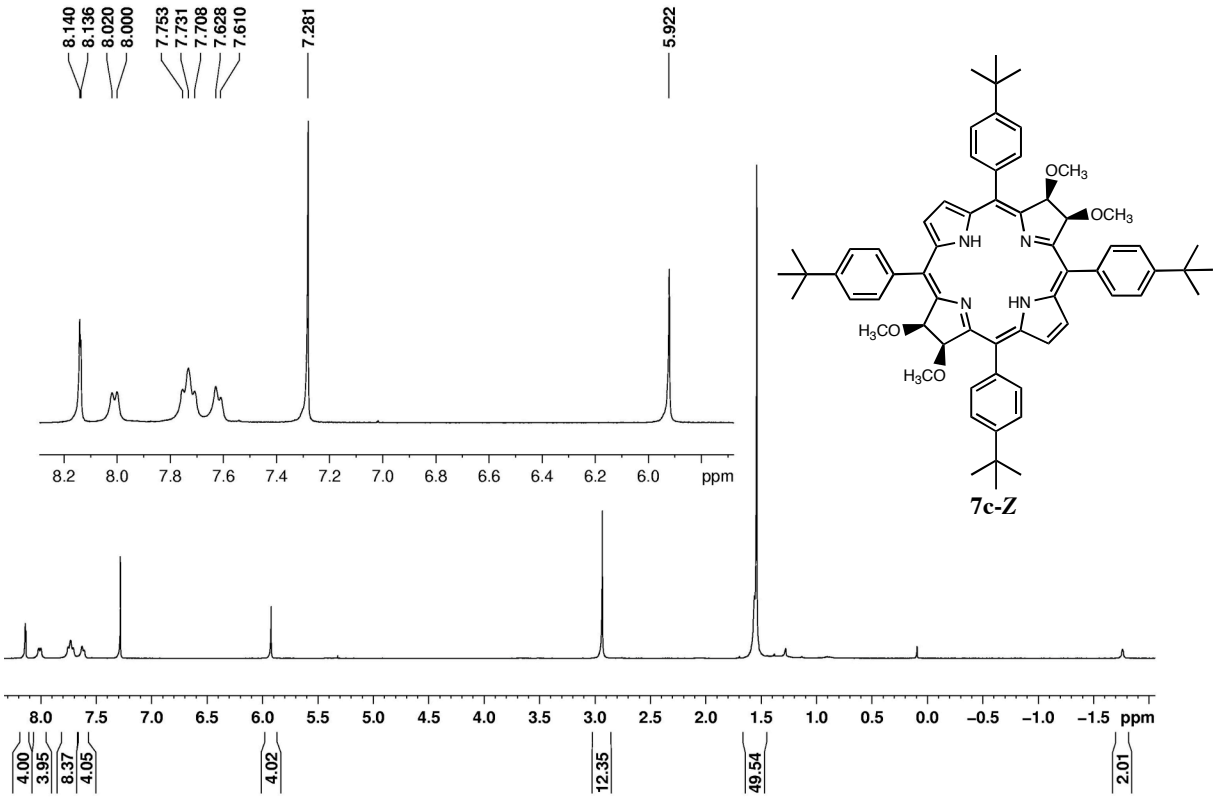

Figure ESI-50. ^{1}H NMR spectrum (400 MHz, $CDCl_3$) of **7c-*Z***

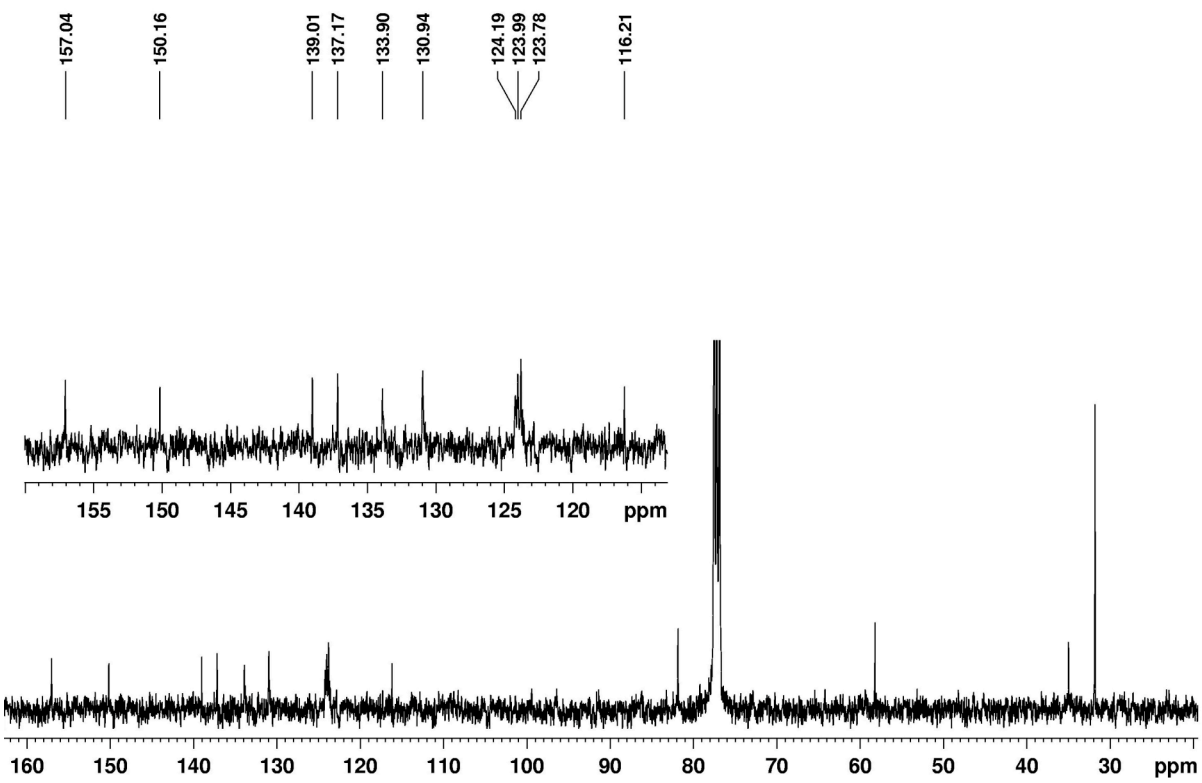

Figure ESI-51. ^{13}C NMR spectrum (100 MHz, $CDCl_3$) of **7c-*Z***

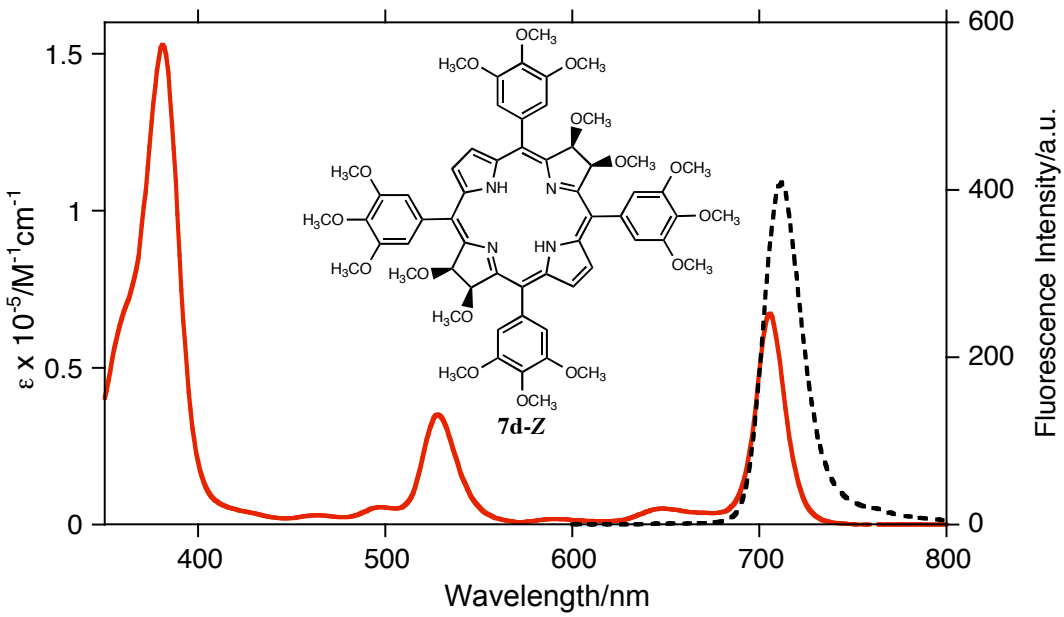

Figure ESI-52. UV-vis (solid red trace) and fluorescence (broken black trace) spectra of **7d-*Z*** in CH_2Cl_2

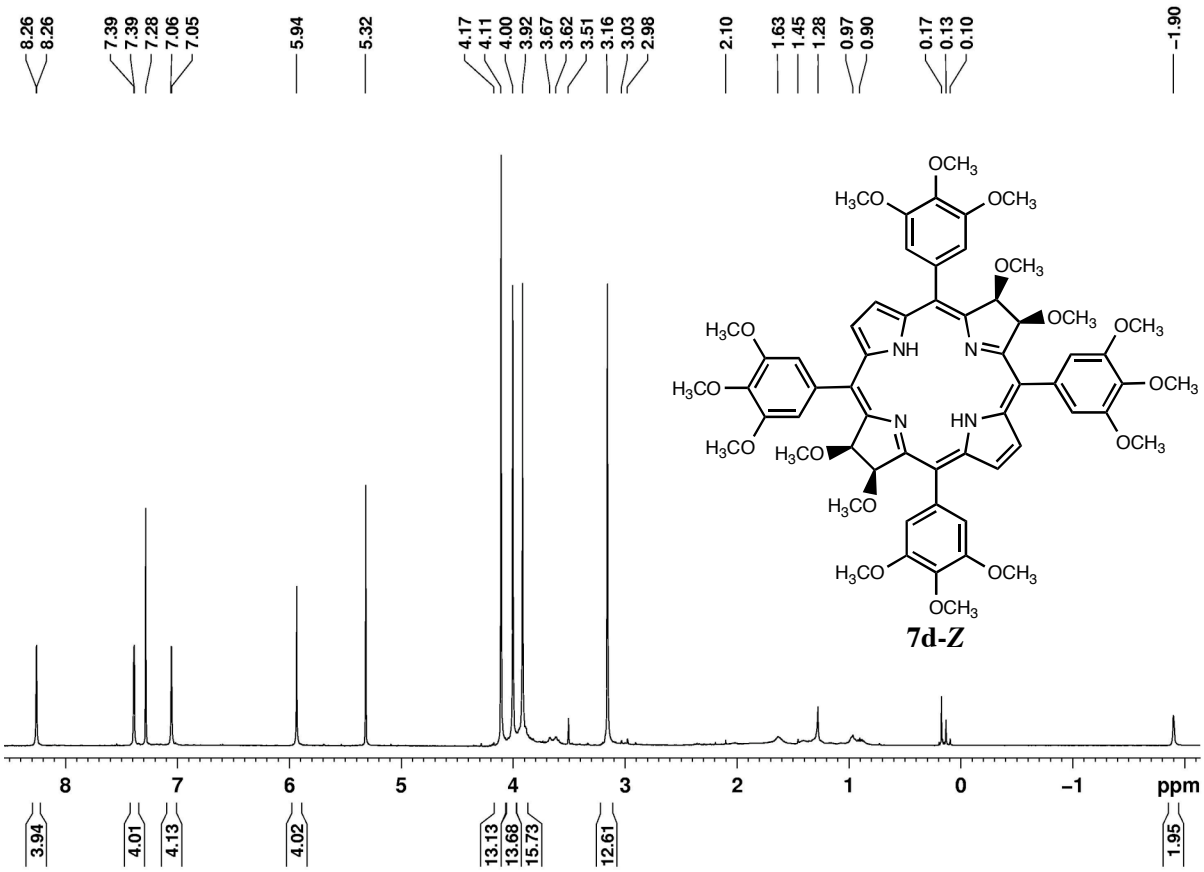

Figure ESI-53. ^{1}H NMR spectrum (400 MHz, $CDCl_3$) of **7d-*Z***

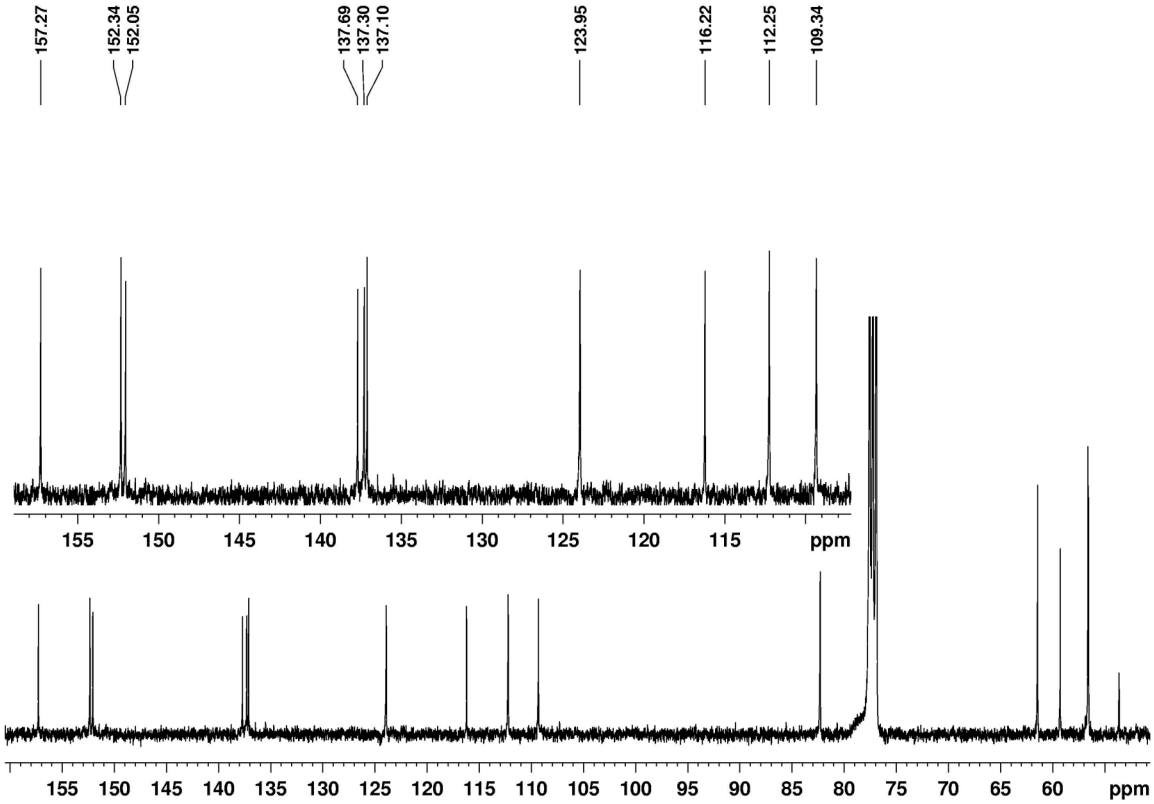

Figure ESI-54. ^{13}C NMR spectrum (100 MHz, $CDCl_3$) of **7d-*Z***

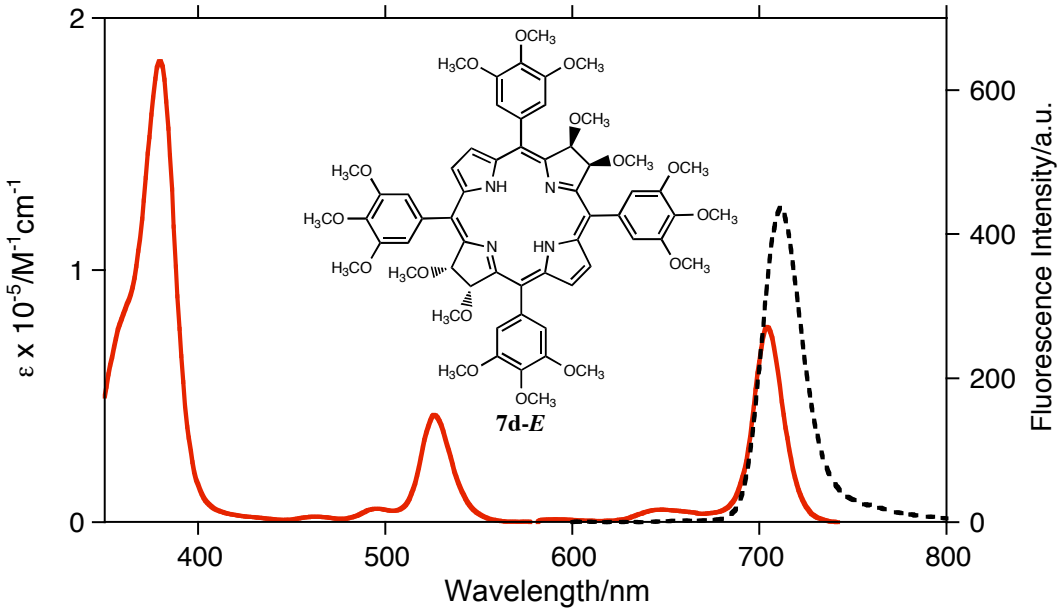

Figure ESI-55. UV-vis (solid red trace) and fluorescence (broken black trace) spectra of **7d-*E*** in CH_2Cl_2

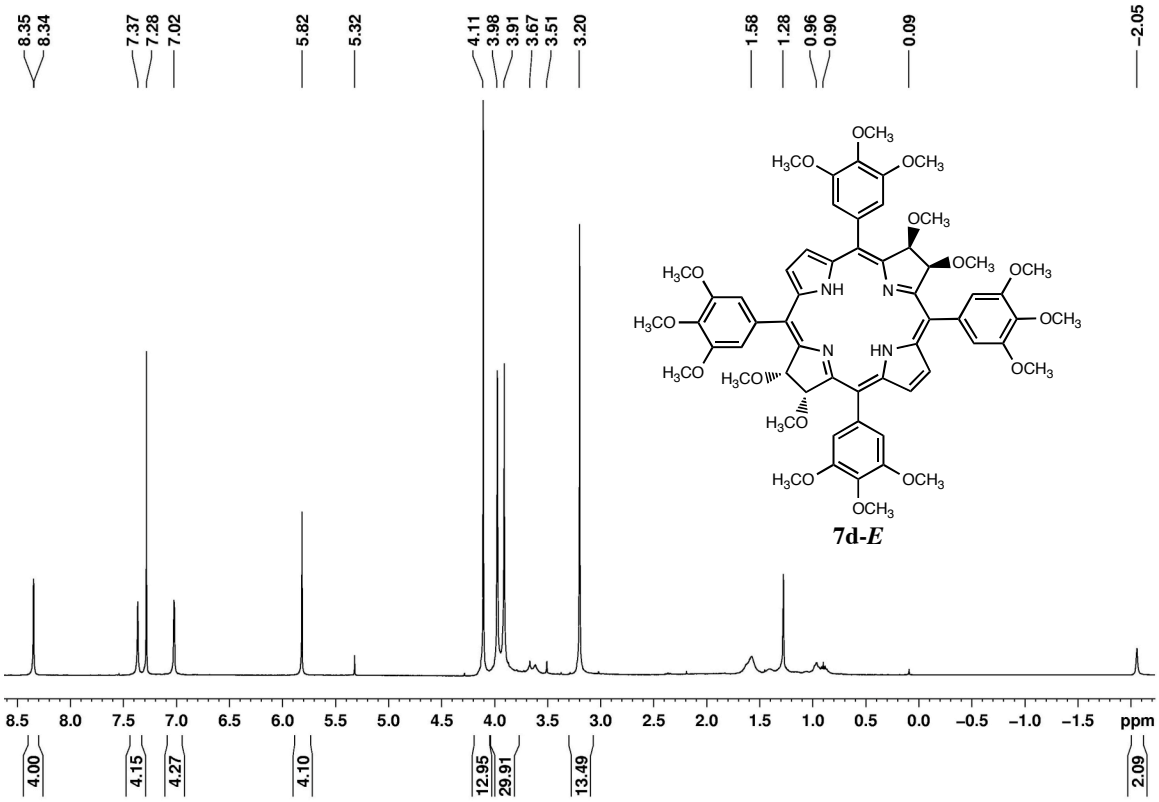

Figure ESI-56. ^{1}H NMR spectrum (400 MHz, $CDCl_3$) of **7d-*E***

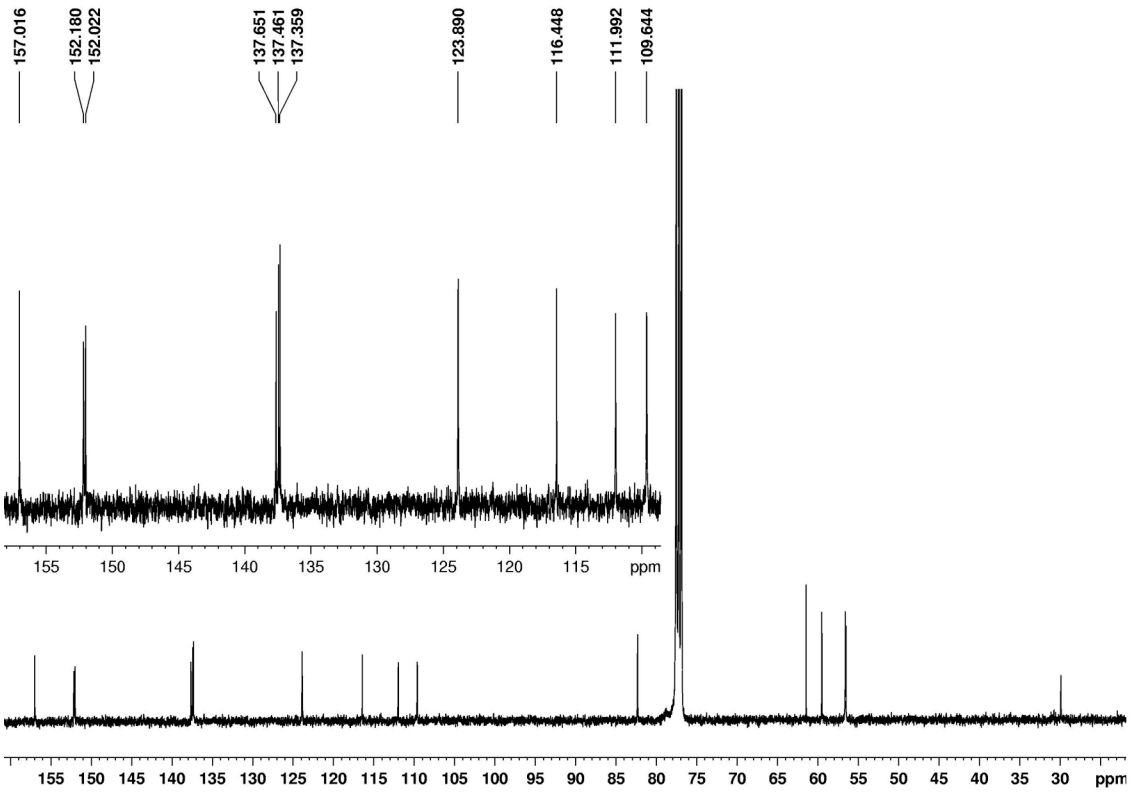

Figure ESI-57. ^{13}C NMR spectrum (100 MHz, $CDCl_3$) of **7d-*E***

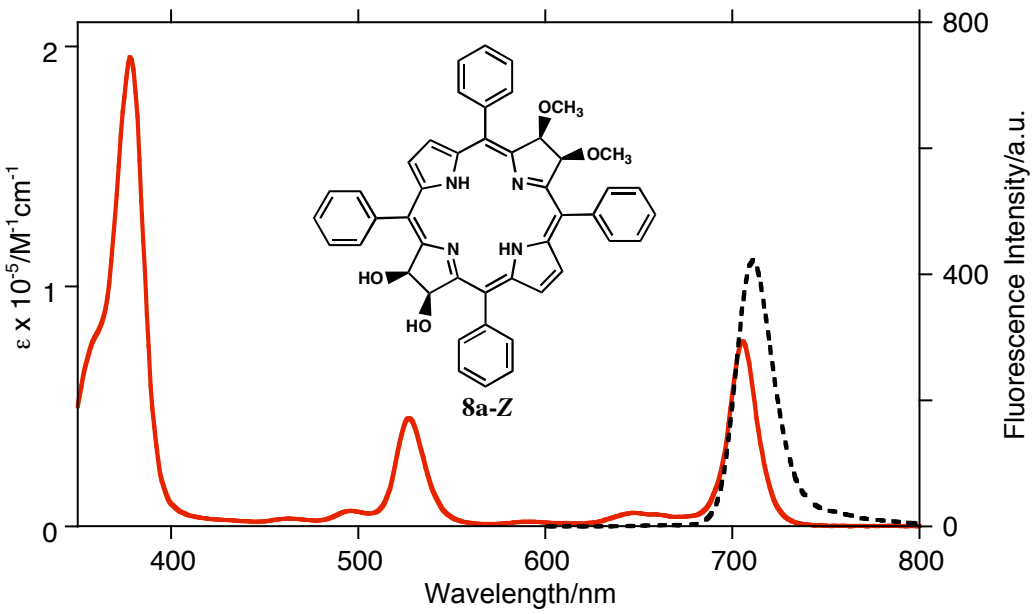

Figure ESI-58. UV-vis (solid red trace) and fluorescence (broken black trace) spectra of **8a-*Z*** in CH_2Cl_2

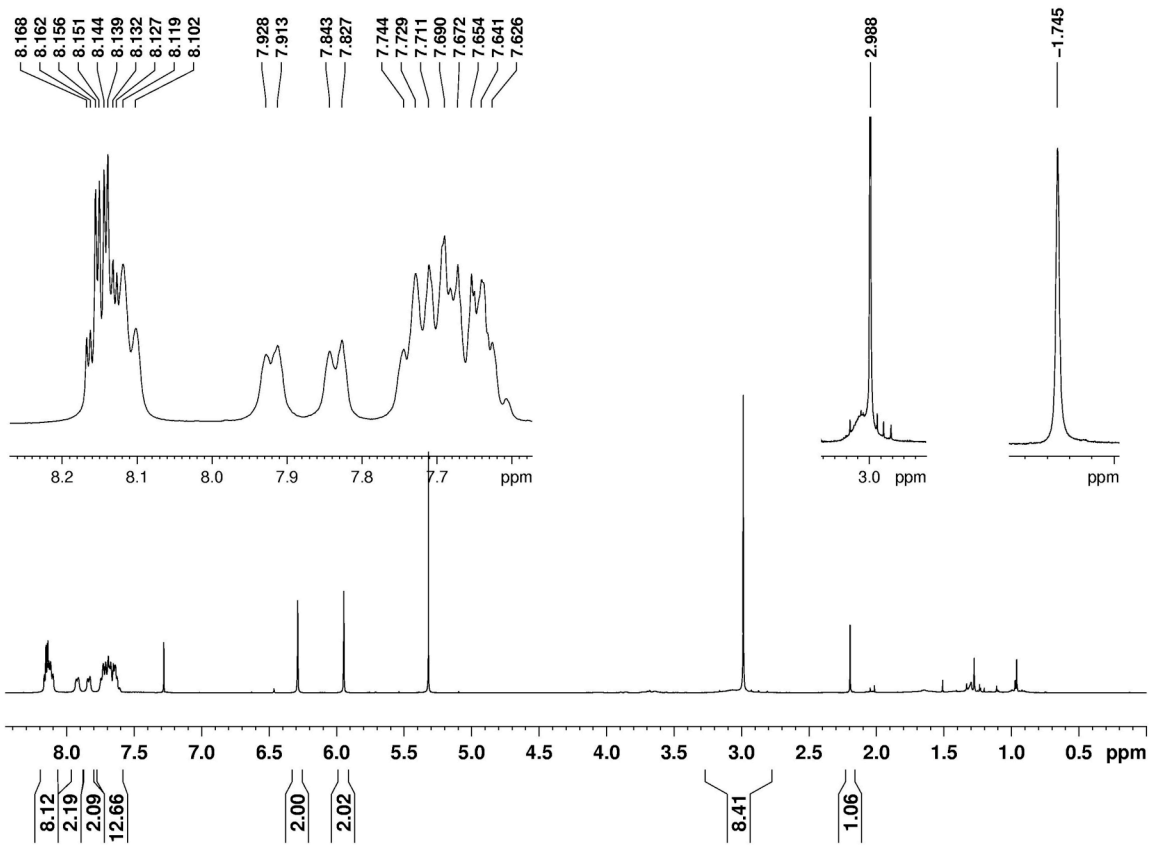

Figure ESI-59. ^{1}H NMR spectrum (400 MHz, $CDCl_3$) of **8a-*Z***

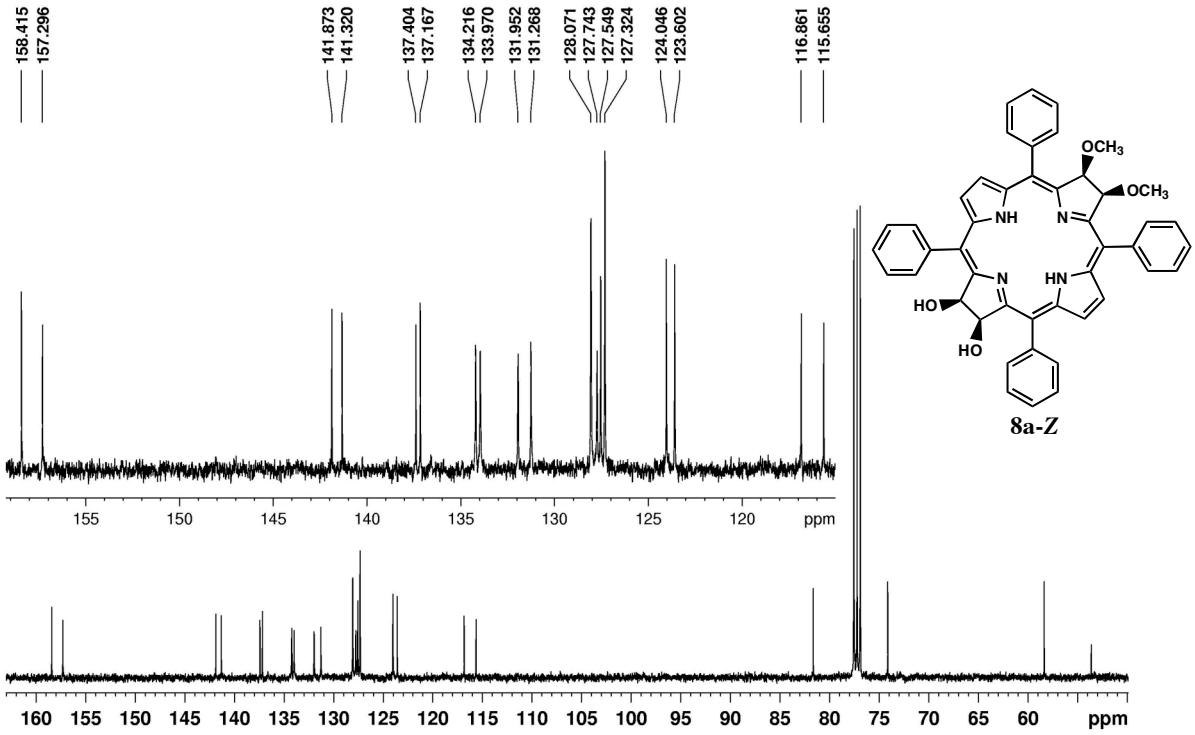

Figure ESI-60. ^{13}C NMR spectrum (100 MHz, $CDCl_3$) of **8a-*Z***

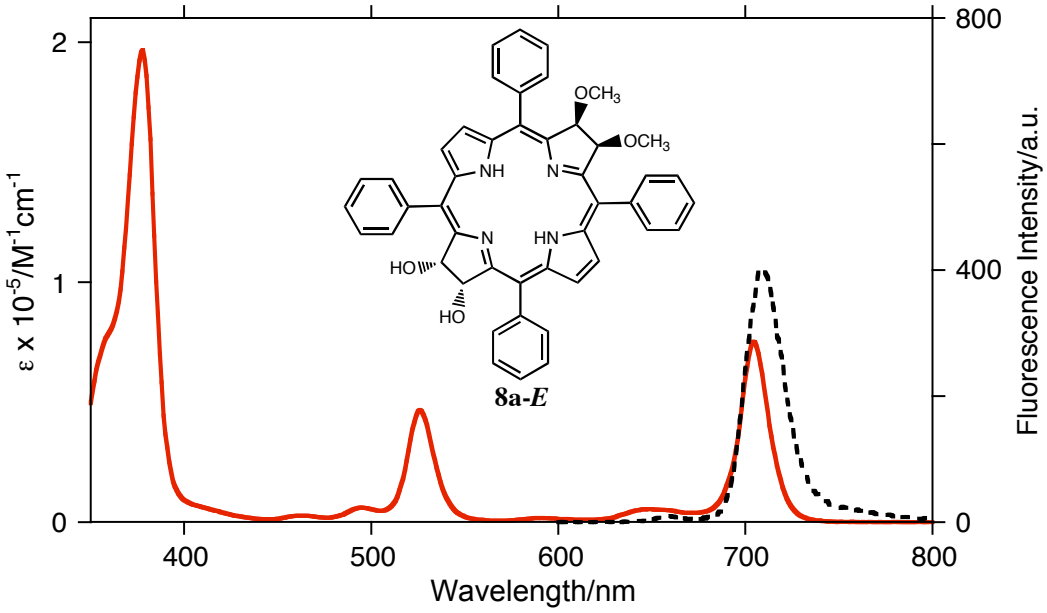

Figure ESI-61. UV-vis (solid red trace) and fluorescence (broken black trace) spectra of **8a-*E*** in CH_2Cl_2

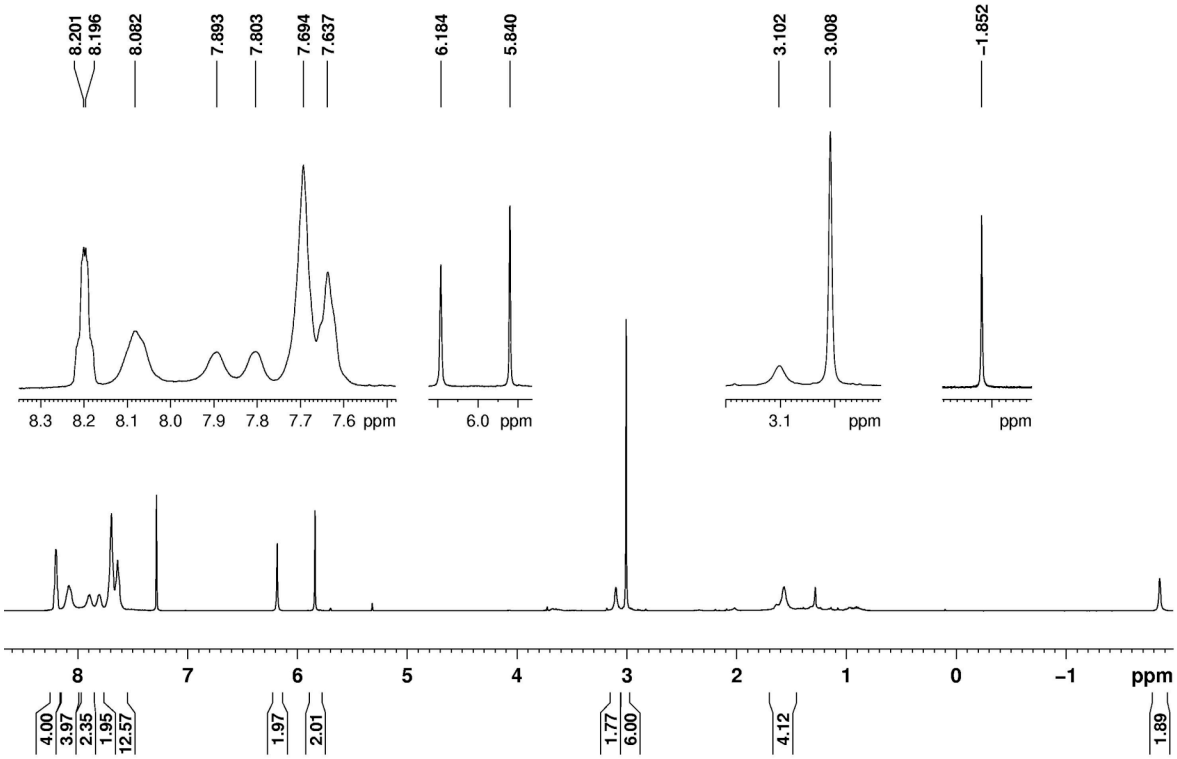

Figure ESI-62. ^{1}H NMR spectrum (400 MHz, $CDCl_3$) of **8a-*E***

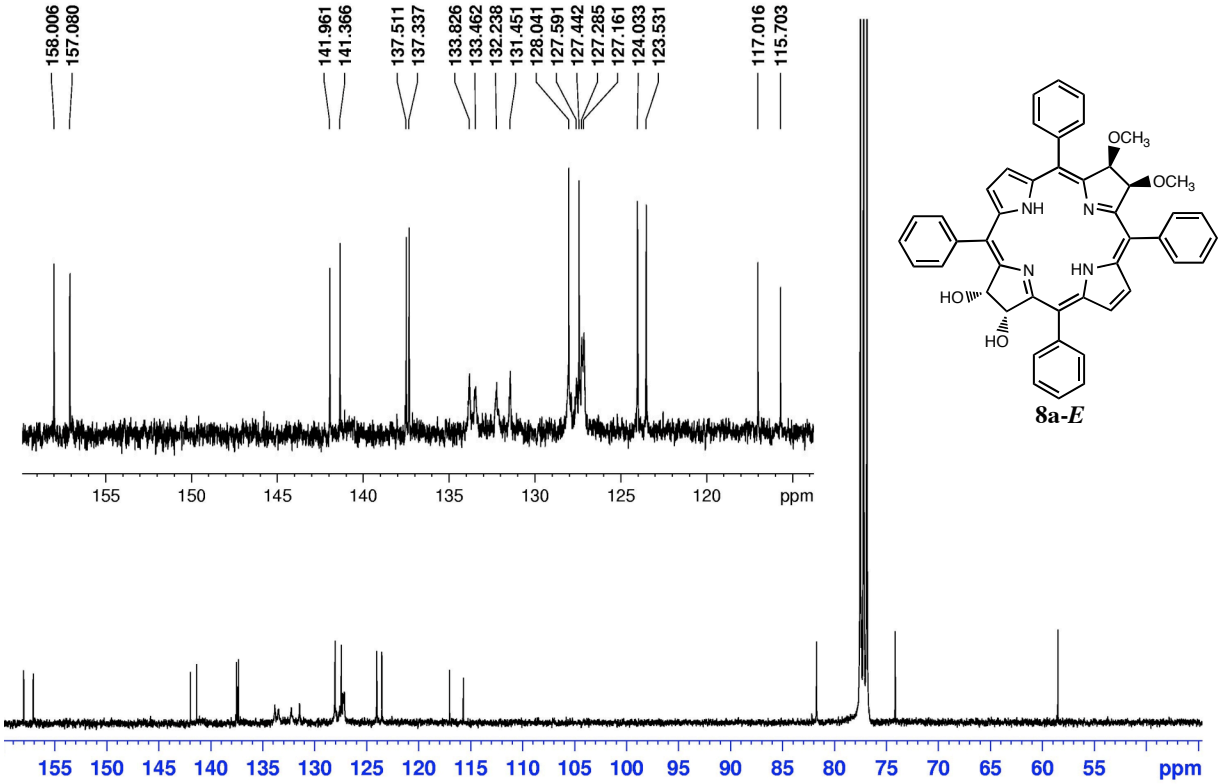

Figure ESI-63. ^{13}C NMR spectrum (100 MHz, $CDCl_3$) of **8a-*E***

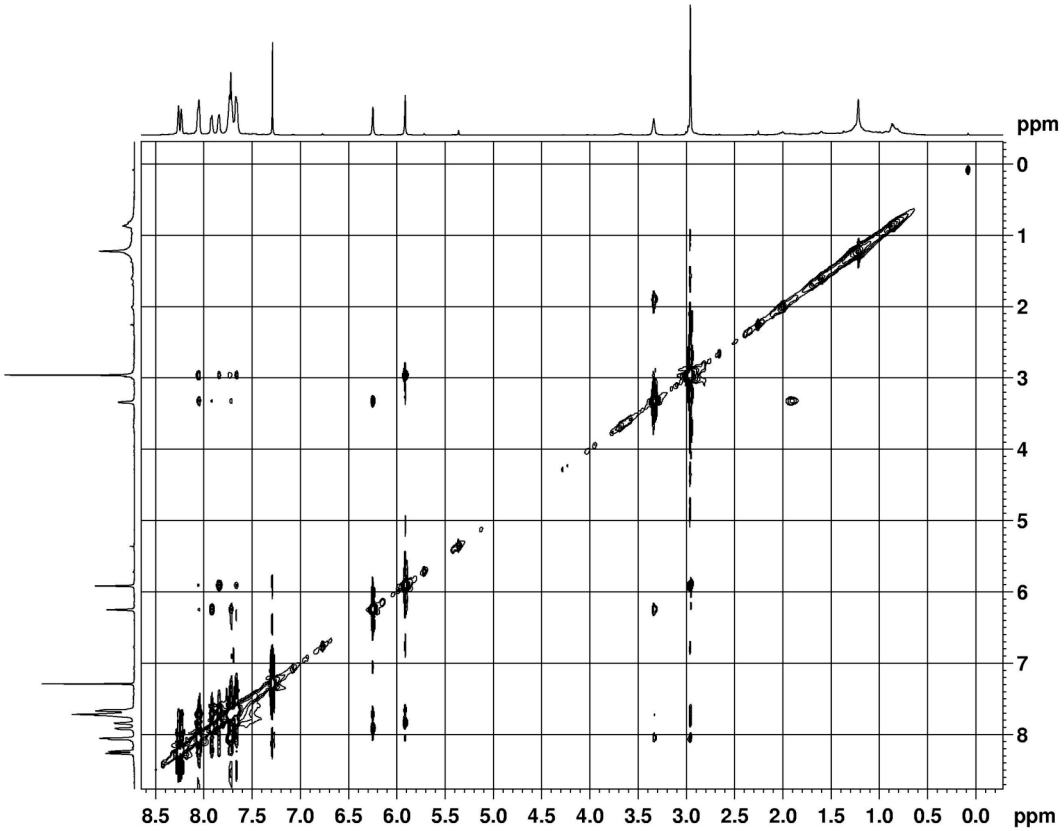

Figure ESI-64. NOESY (500 MHz, $CDCl_3$, -40°C) spectrum of **8a-*E***

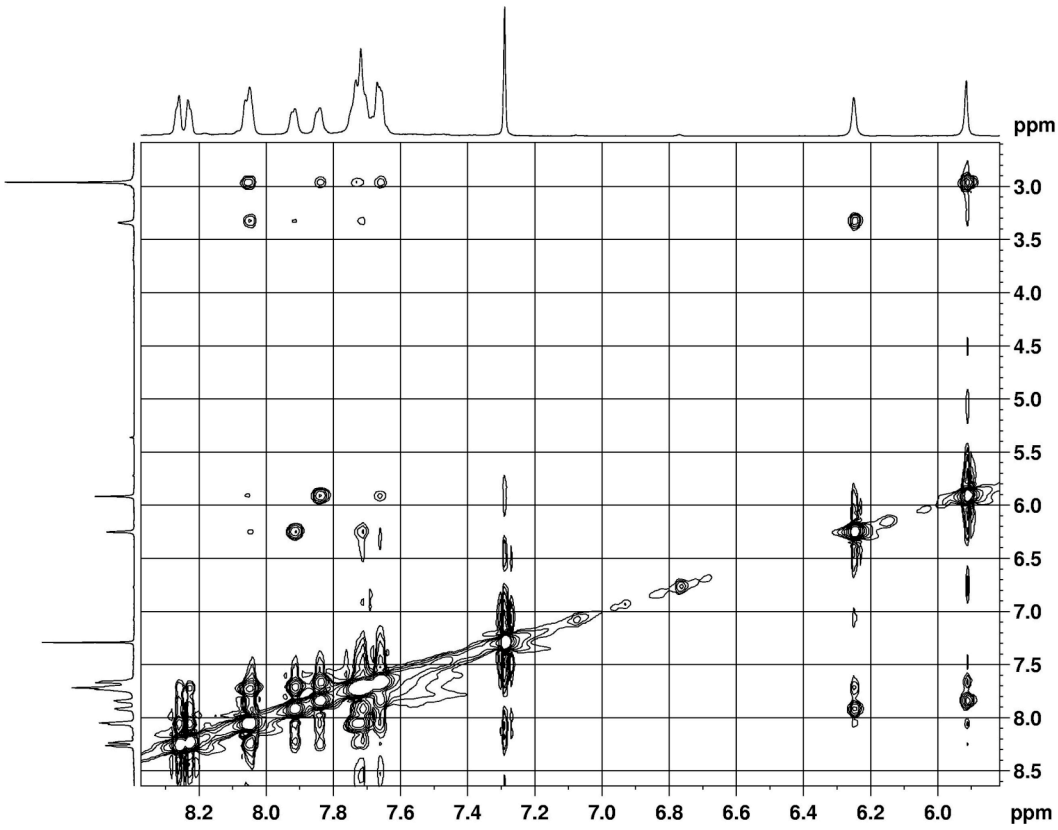

Figure ESI-65. Expansion of the NOESY spectrum (500 MHz, $CDCl_3$, -40°C) of **8a-*E***

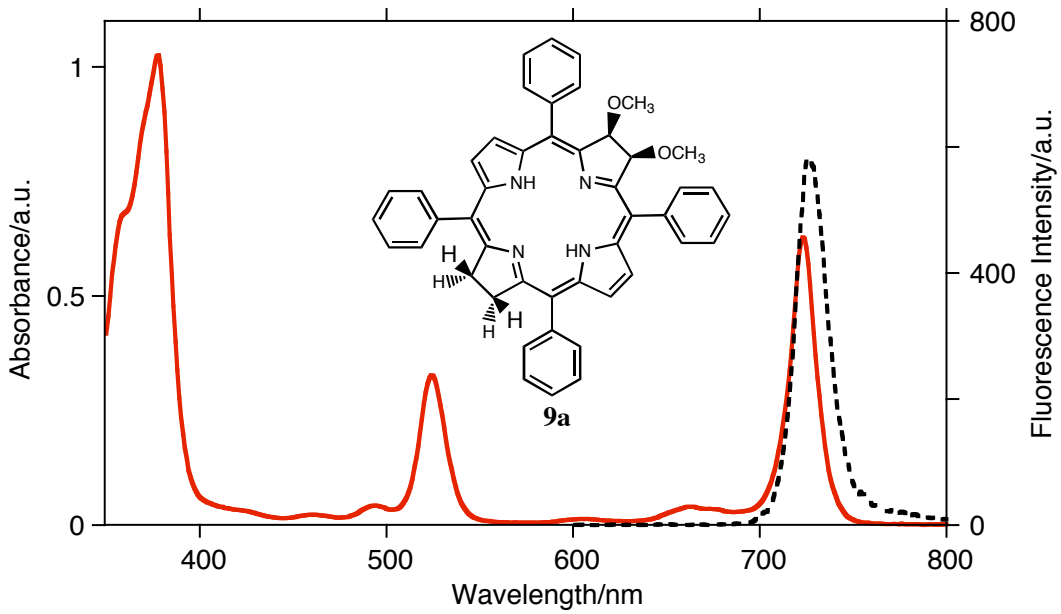

Figure ESI-66. UV-vis (solid red trace) and fluorescence (broken black trace) spectra of **9a** in CH_2Cl_2

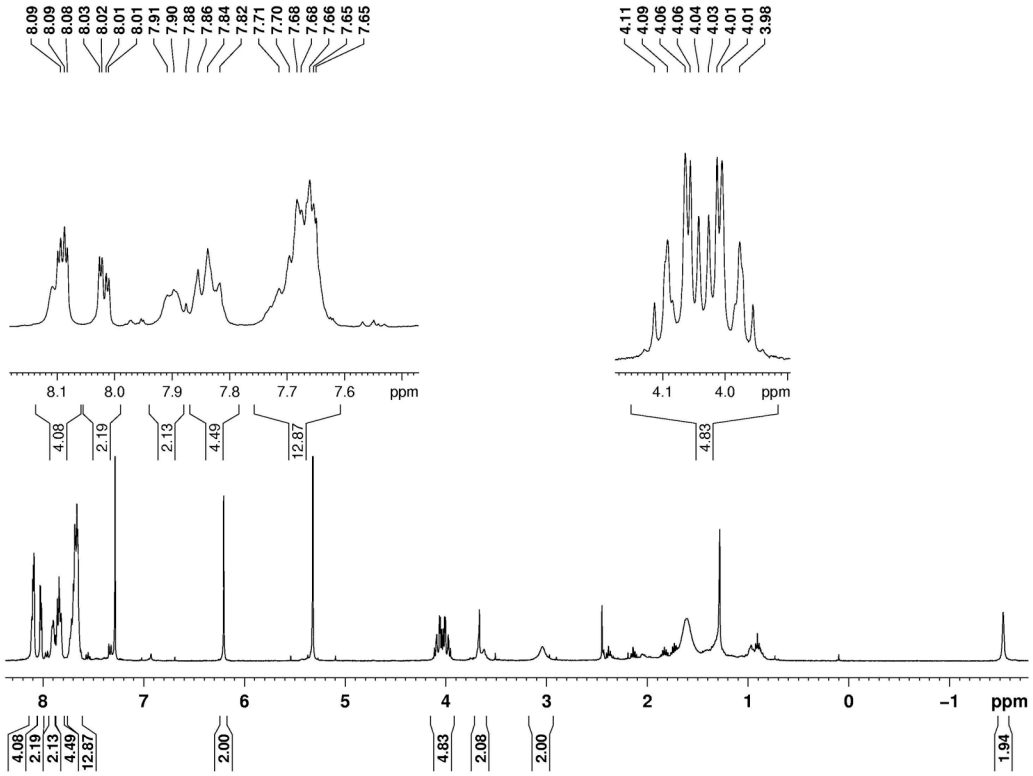

Figure ESI-67. ^{1}H NMR Spectrum (400 MHz, $CDCl_3$) of **9a**

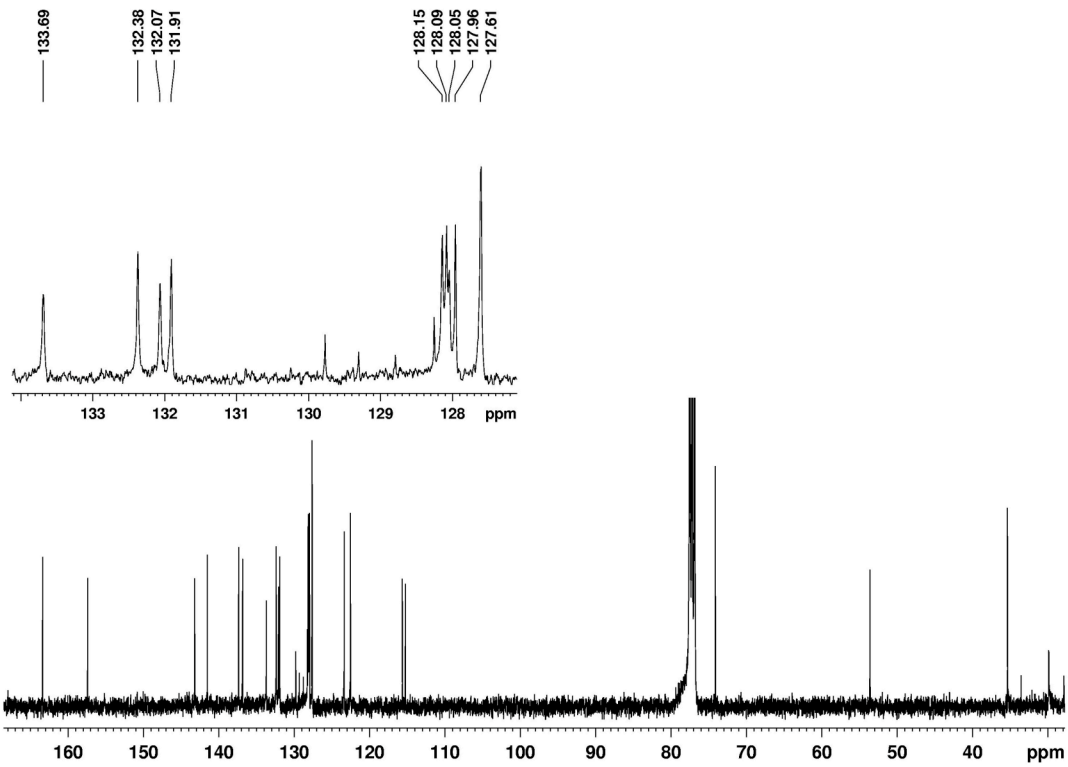

Figure ESI-68. ^{13}C NMR spectrum (100 MHz, $CDCl_3$) of **9a**

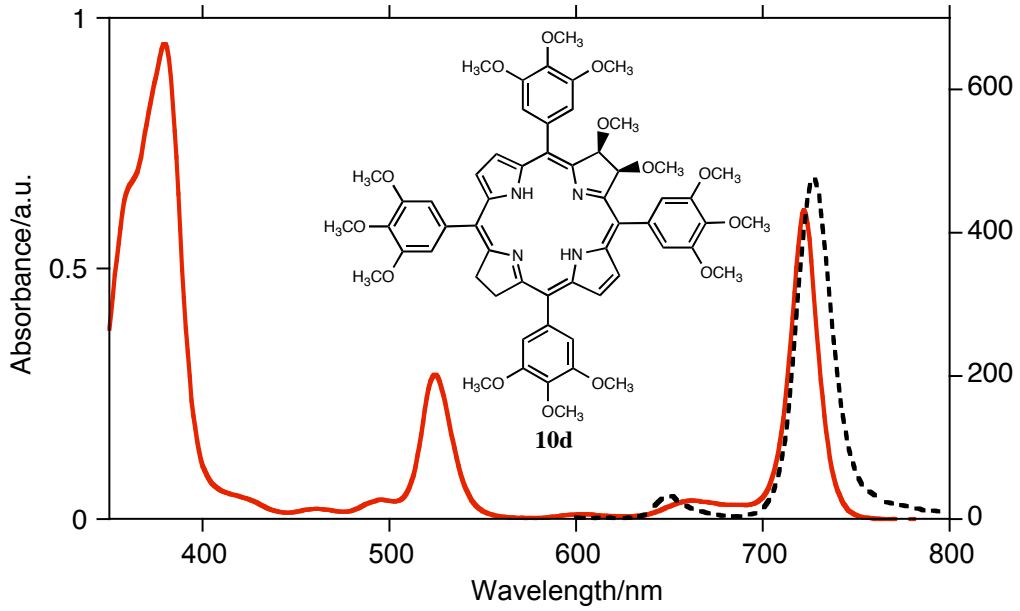

Figure ESI-69. UV-vis (solid red trace) and fluorescence (broken black trace) spectrum of **10d** in CH_2Cl_2

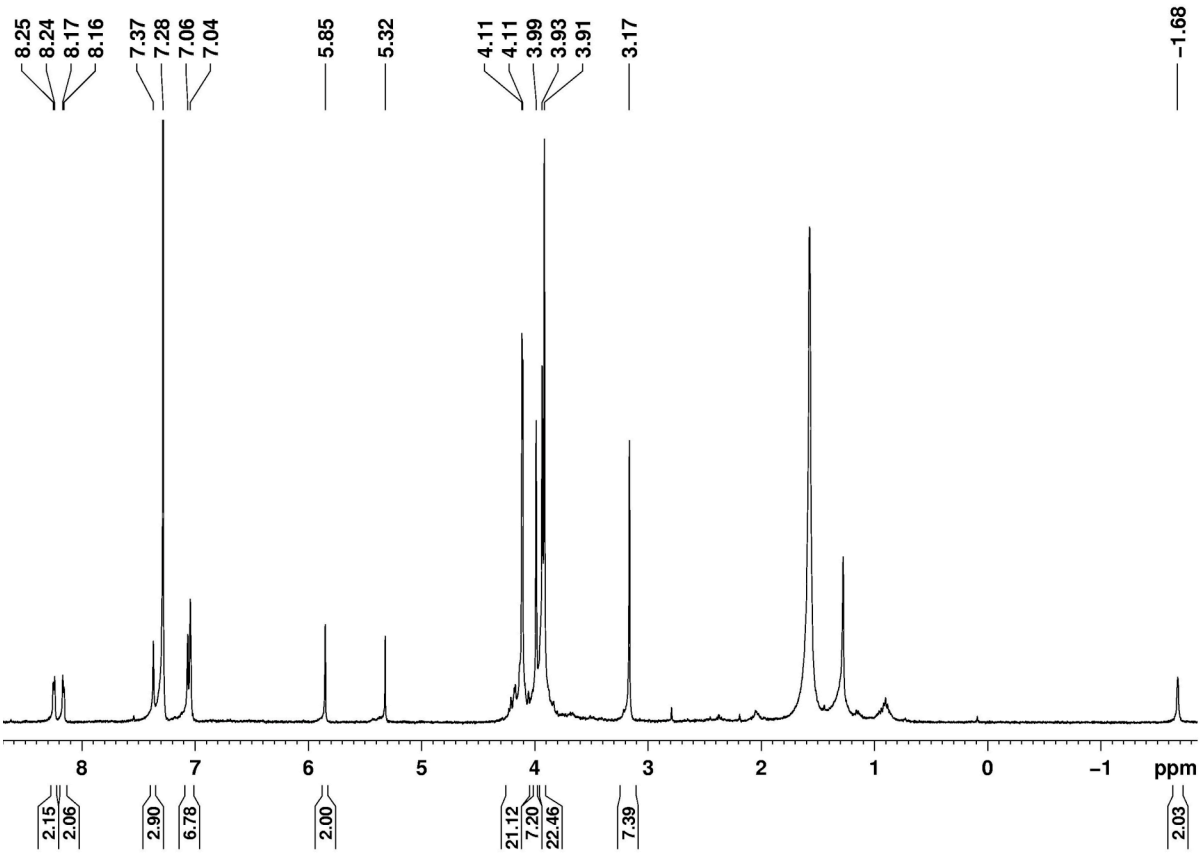

Figure ESI-70. ^{1}H NMR Spectrum (400 MHz, $CDCl_3$) of **10d**

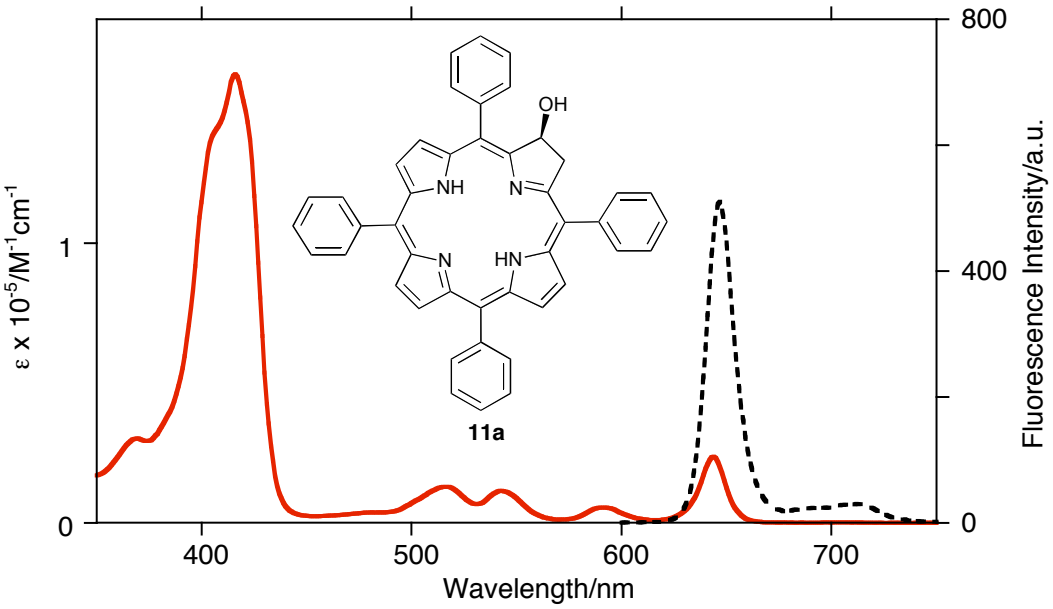

Figure ESI-71. UV-vis (solid red trace) and fluorescence (broken black trace) spectra of **11a** in CH_2Cl_2

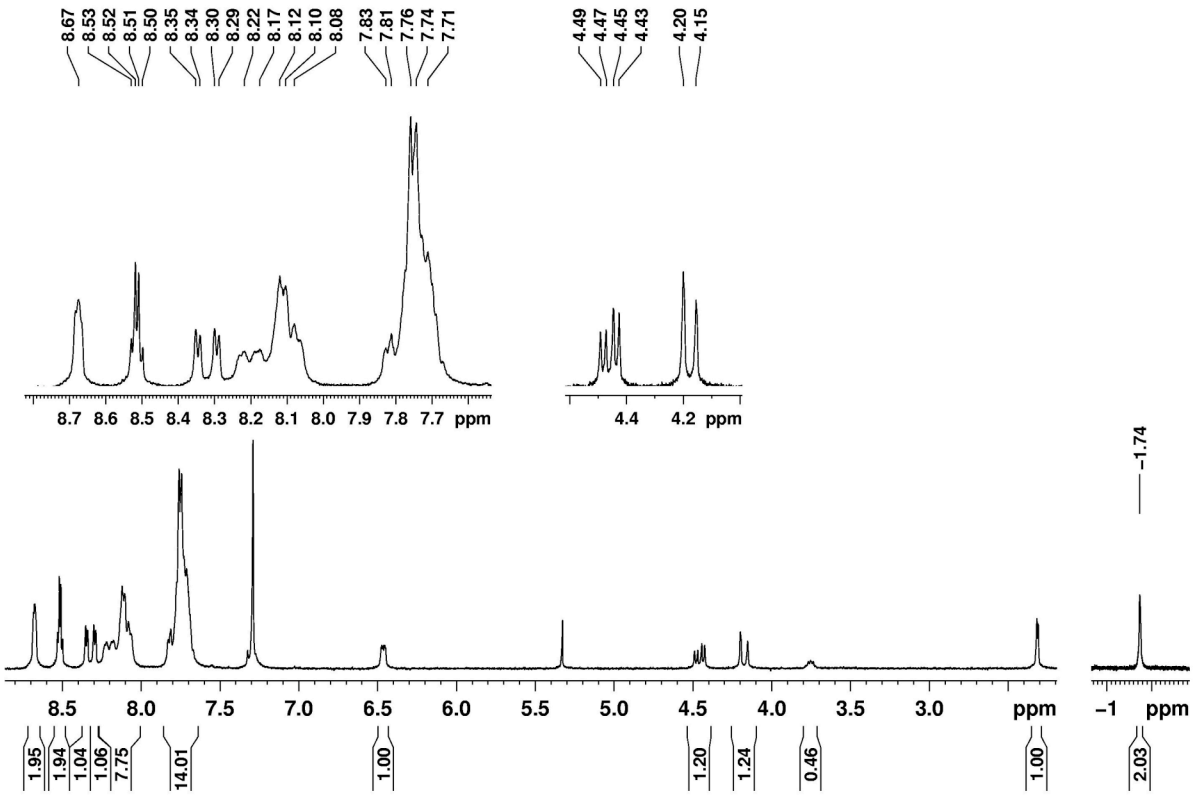

Figure ESI-72. ^{1}H NMR Spectrum (400 MHz, $CDCl_3$) of **11a**

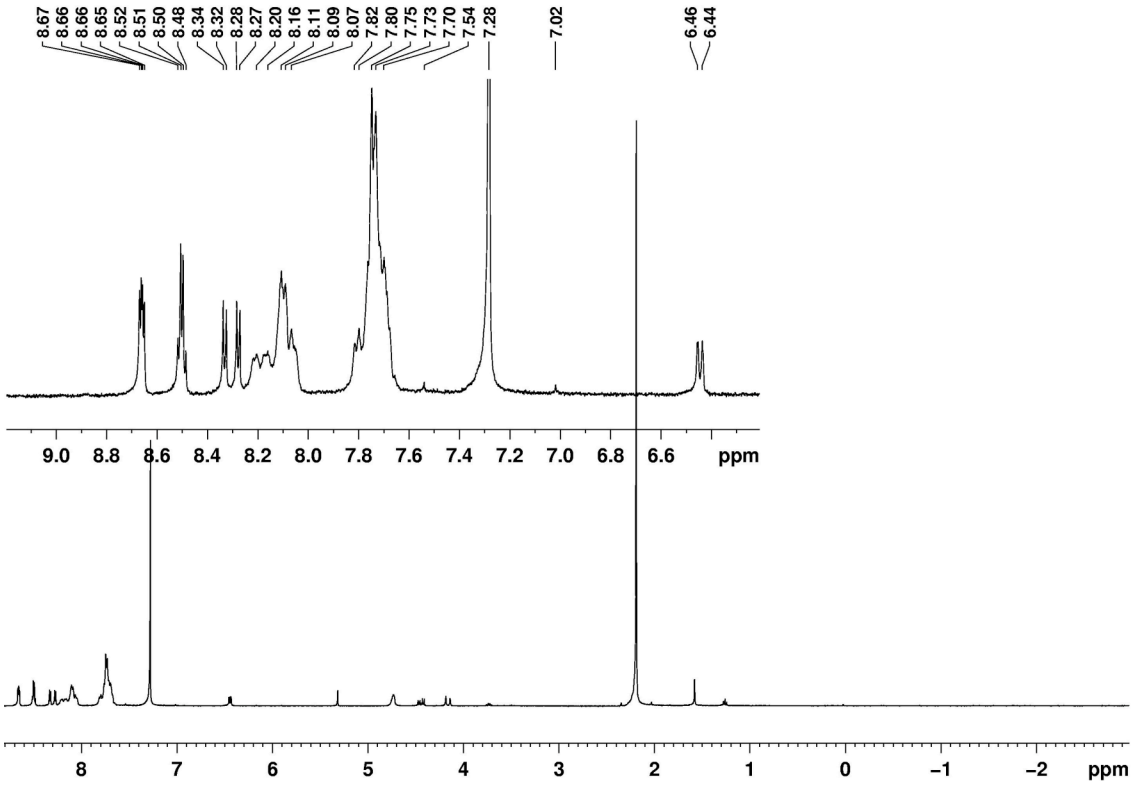

Figure ESI-73. ^{1}H NMR Spectrum (400 MHz, $CDCl_3$) of **11a** after a D_2O wash

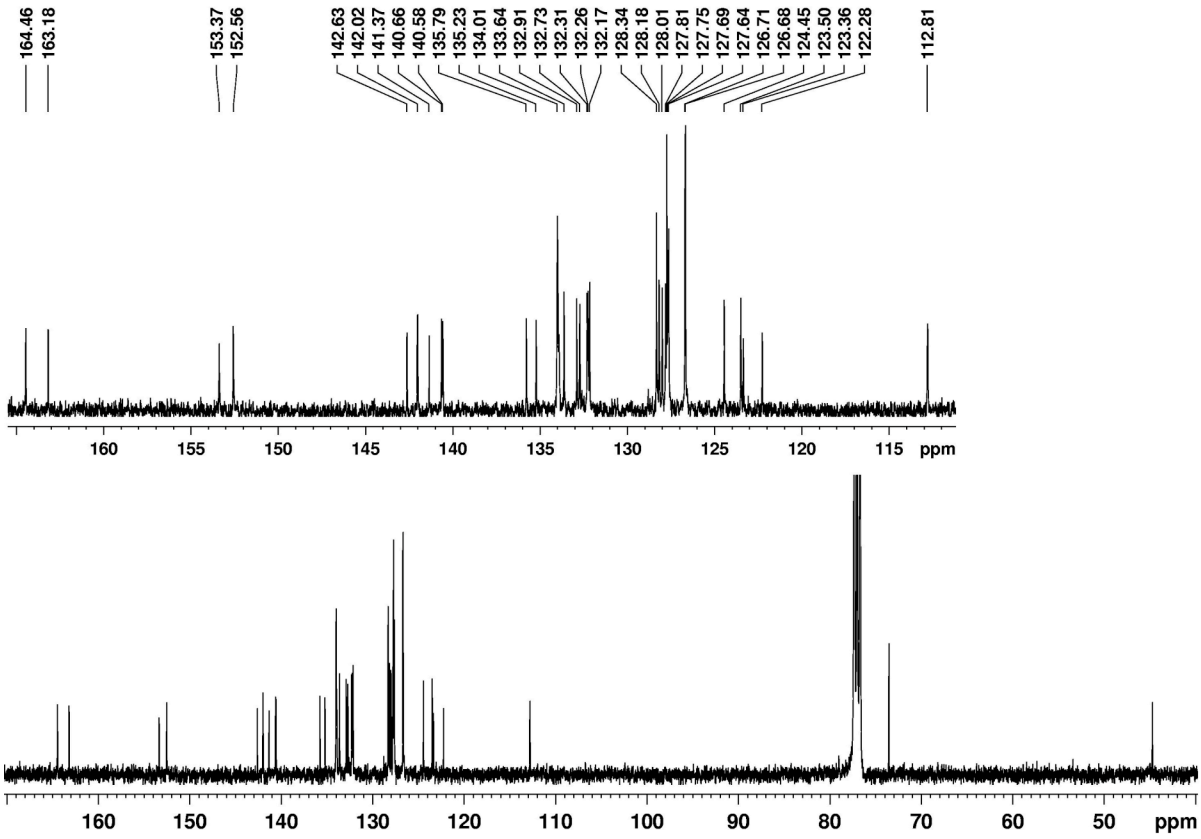

Figure ESI-74. ^{13}C NMR Spectrum (100 MHz, $CDCl_3$) of **11a**

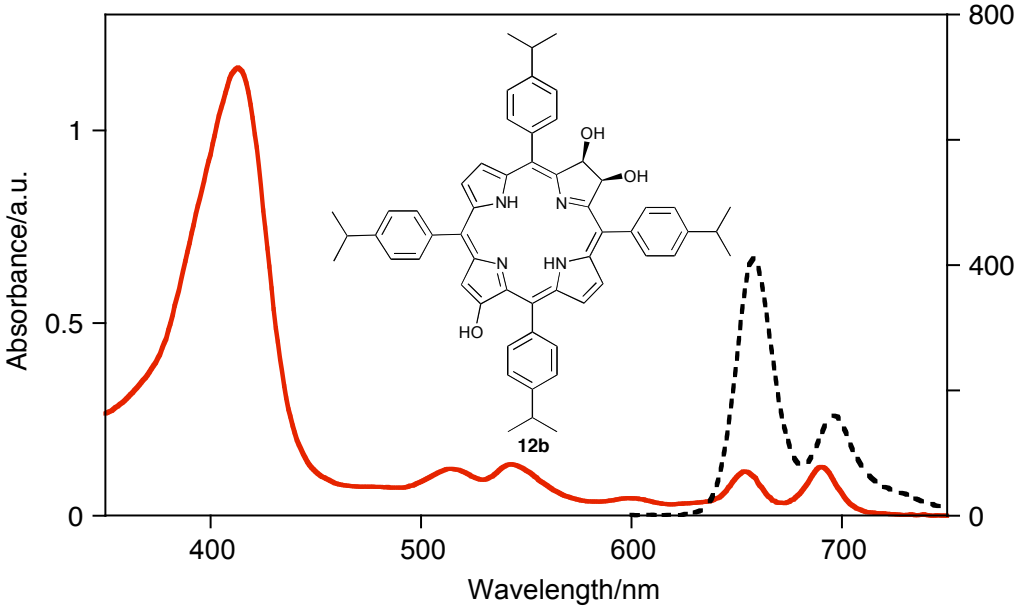

Figure ESI-75. UV-vis (solid red trace) and fluorescence (broken black trace) spectra of **12b** in CH_2Cl_2

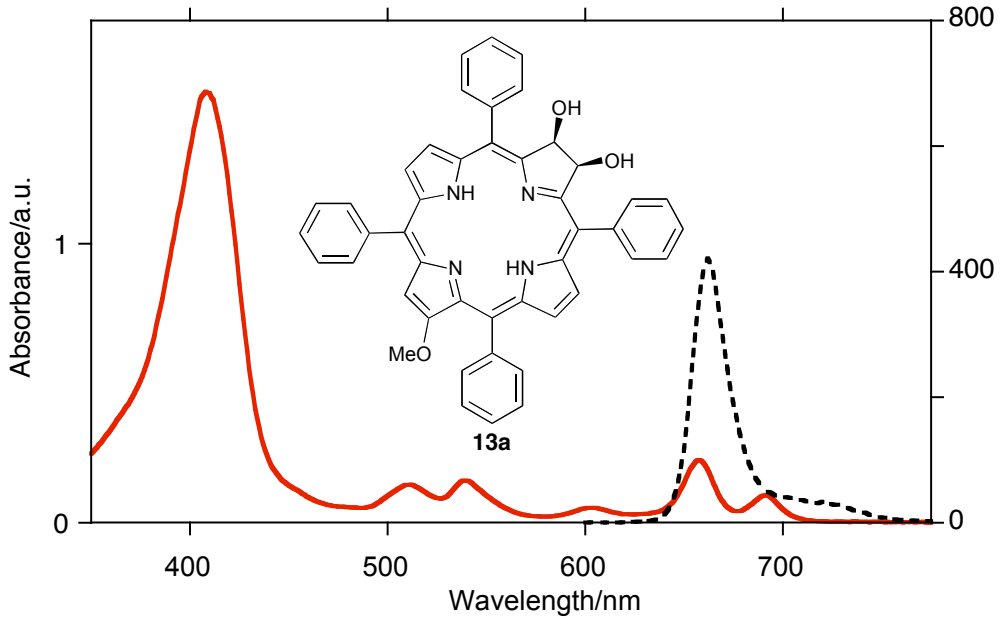

Figure ESI-76. UV-vis (solid red trace) and fluorescence (broken black trace) spectra of **13a** in CH_2Cl_2

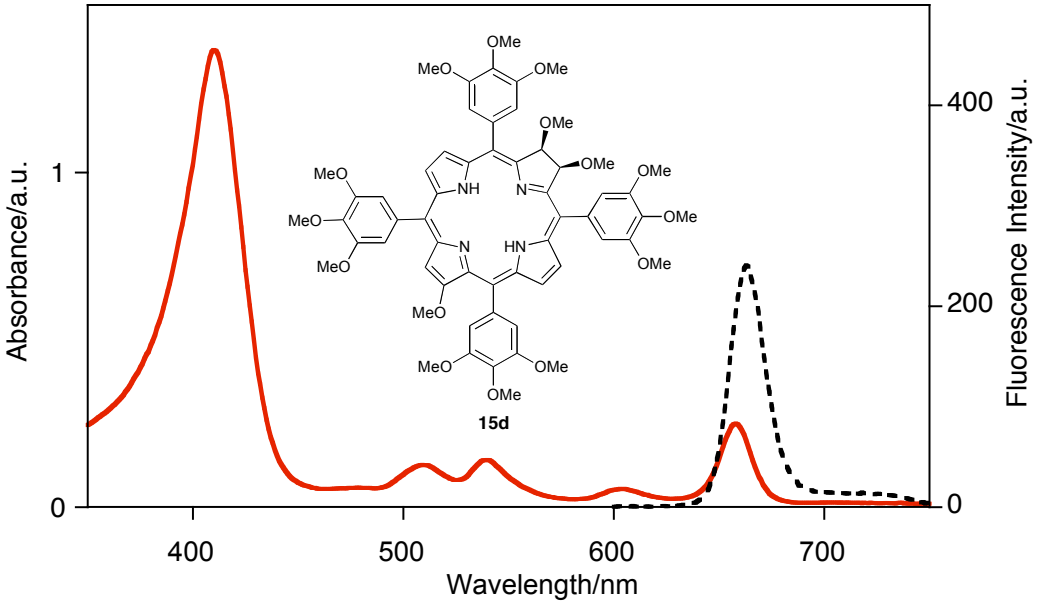

Figure ESI-77. UV-vis (solid red trace) and fluorescence (broken black trace) spectra of **15d** in CH_2Cl_2

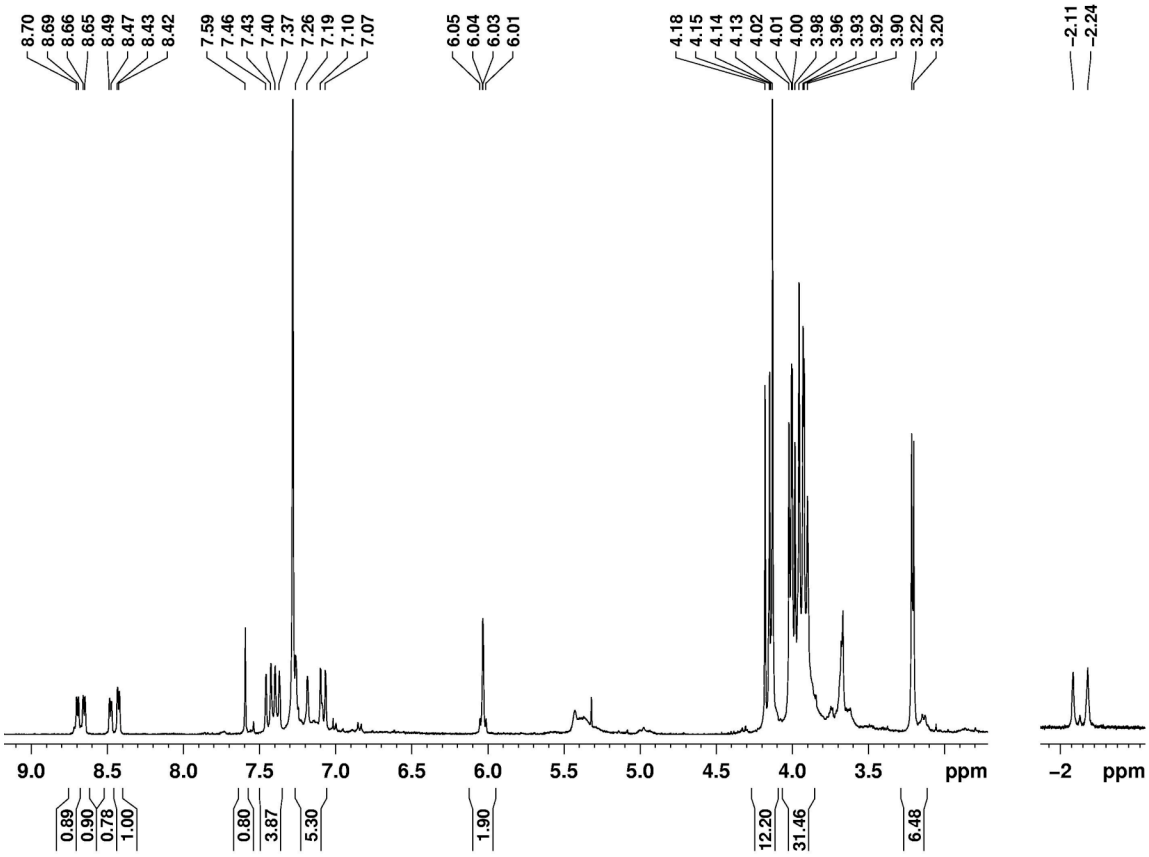

Figure ESI-78. ^{1}H NMR Spectrum (400 MHz, $CDCl_3$) of **15d**

Comparison of the UV-Vis spectra of *E* and *Z* isomers of selected tetraol and tetramethoxy bacteriochlorin derivatives:

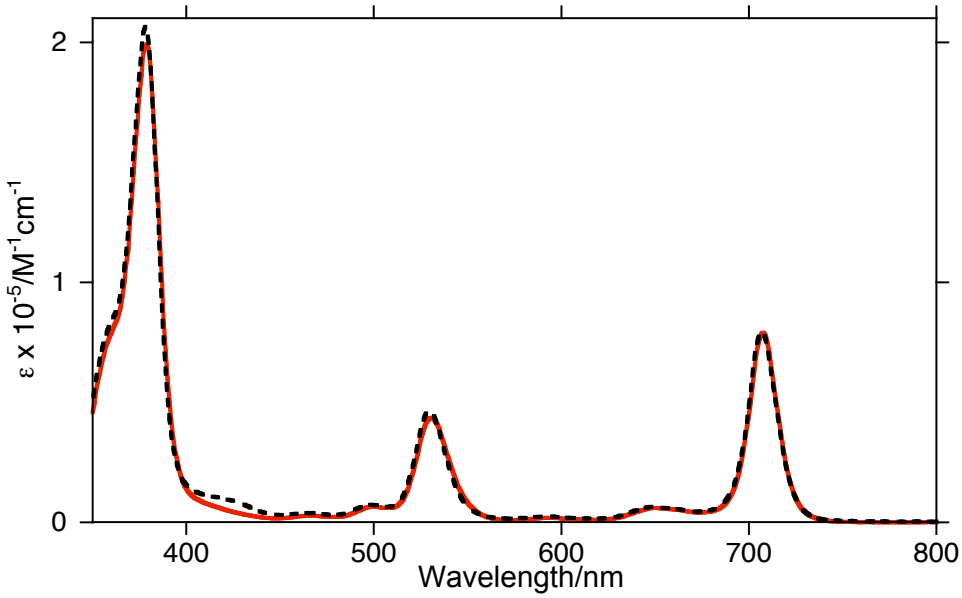

Figure ESI-79. UV-vis spectra of **4b-*Z*** (solid red trace) vs **4b-*E*** (broken black trace) in CH_2Cl_2

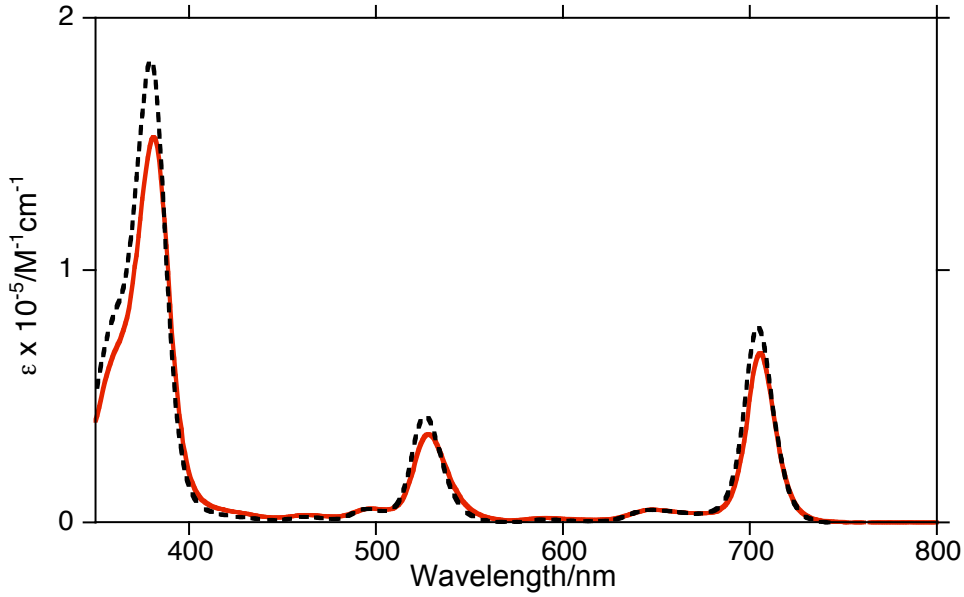

Figure ESI-80. UV-vis spectra of **7d-*Z*** (solid red trace) vs **7d-*E*** (broken black trace) in CH_2Cl_2

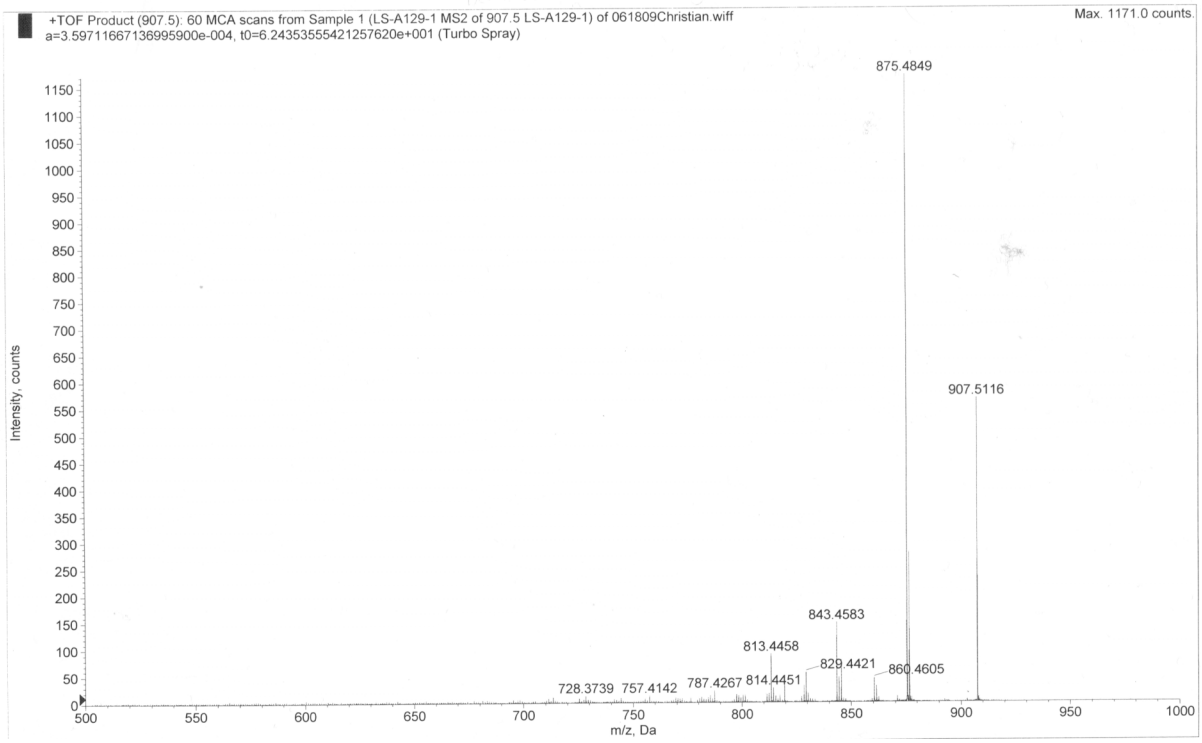

Figure ESI-81. Collision-induced tandem mass spectrum (ESI+, 100%CH_3CN) of **7b-*Z***

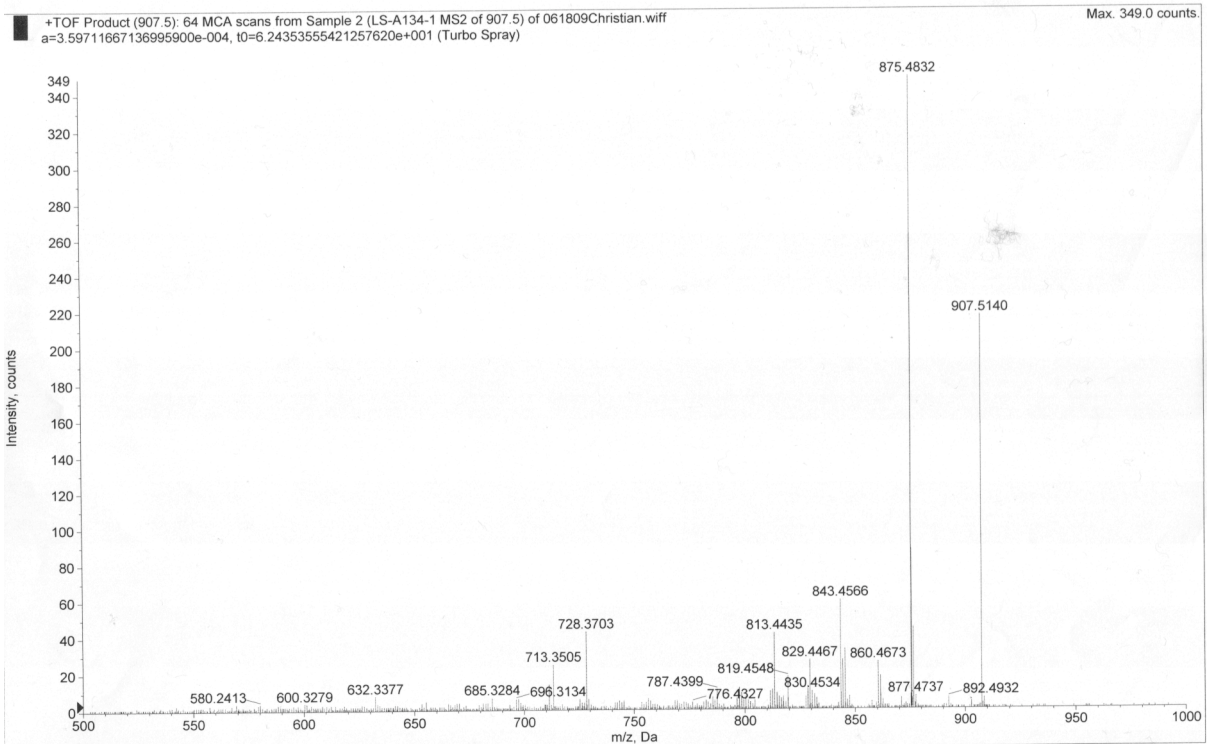

Figure ESI-82. Collision-induced tandem mass spectrum (ESI+, 100%CH_3CN) of **7b-*E***

X-ray Crystal Structure Determination – General

Diffraction data were collected on a Bruker AXS SMART6000 CCD at 150(2) K (compound **5a**) or a Bruker AXS SMART APEX CCD diffractometer at 100(2) K (all others) using monochromatic Mo Kα radiation with omega scan technique. The unit cells were determined, the data were collected, integrated corrected for absorption using SMART v5.628, SAINT v6.28A and SADABS v2.03 (compound **5a**) or the Apex2 suite of programs (all others). The structures were solved by direct methods and refined by full matrix least squares against F2 against all reflections using SHELXTL. All hydrogen atoms were placed in calculated positions and were isotropically refined with a displacement parameter of 1.5 (methyl, hydroxyl) or 1.2 times (all others) that of the adjacent carbon, oxygen or nitrogen atom.

X-ray Crystal Structure Determination – Compound 4b-*E* · 4 MeOH

See also Table 3 (crystal Data) and the cif file of this structure.
The crystal used was found to be consisting of two independent crystallites. The orientation matrices for the two components were identified using the program Cell Now, and the two components were integrated using Saint.
The data were corrected for absorption using twinabs, and the structure was solved and refined using direct methods with only the non-overlapping reflections of component below a d-spacing threshold of 0.75.
The Rint value given is for all reflections before the cutoff at d = 0.75 and is based on agreement between observed single and composite intensities and those calculated from refined unique intensities and twin fractions (TWINABS (Sheldrick, 2007)).

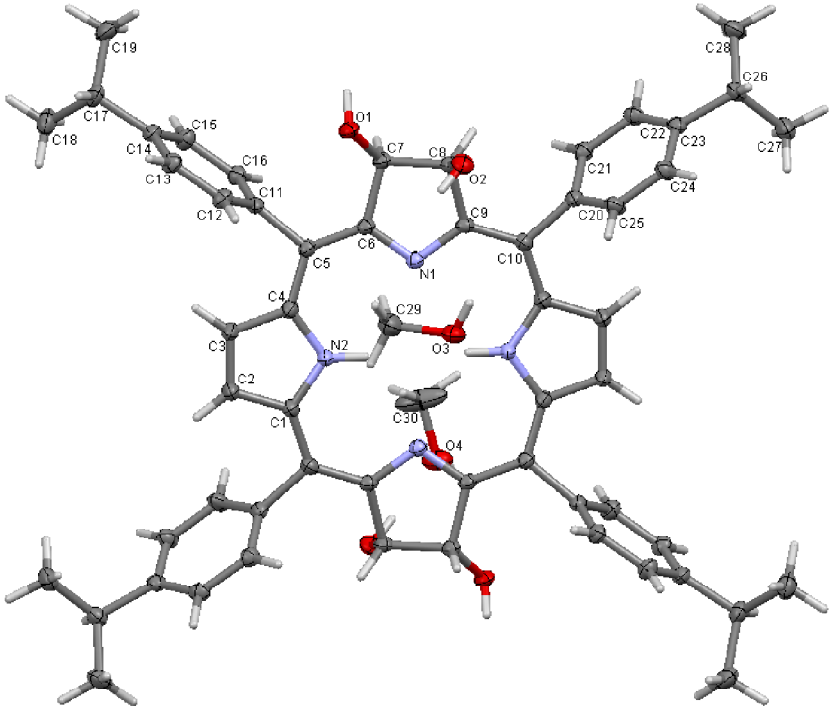

Figure ESI-83. ORTEP Representation of **4b-*E***, top view, and numbering used. Ellipsoids at 50% probability level. The molecule is located on a crystallographic inversion center.

X-ray Crystal Structure Determinations – 4d-*Z* · 4.62 $CHCl_3$
See also Table 3 (crystal Data) and the cif file of this structure

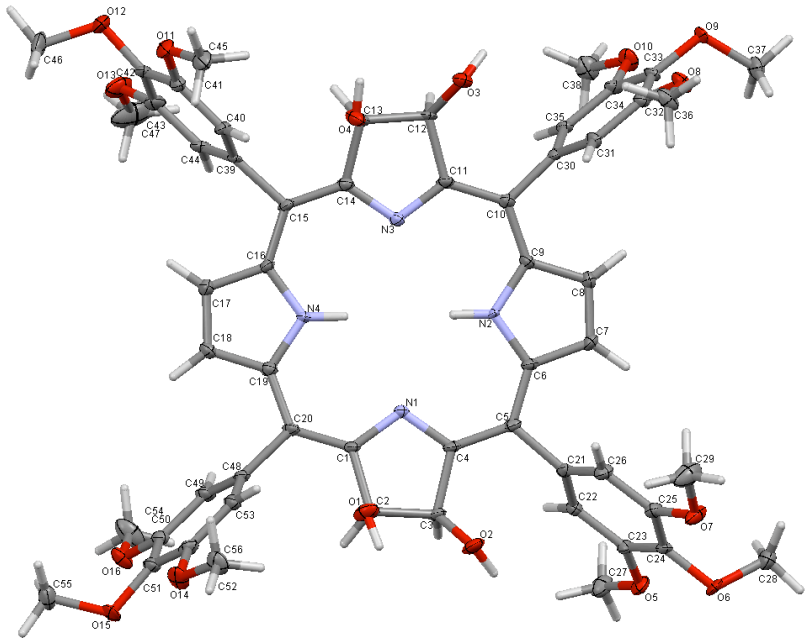

Figure ESI-84. ORTEP Representation of **4d-*Z***, top view, and numbering used. Ellipsoids at 50% probability level.

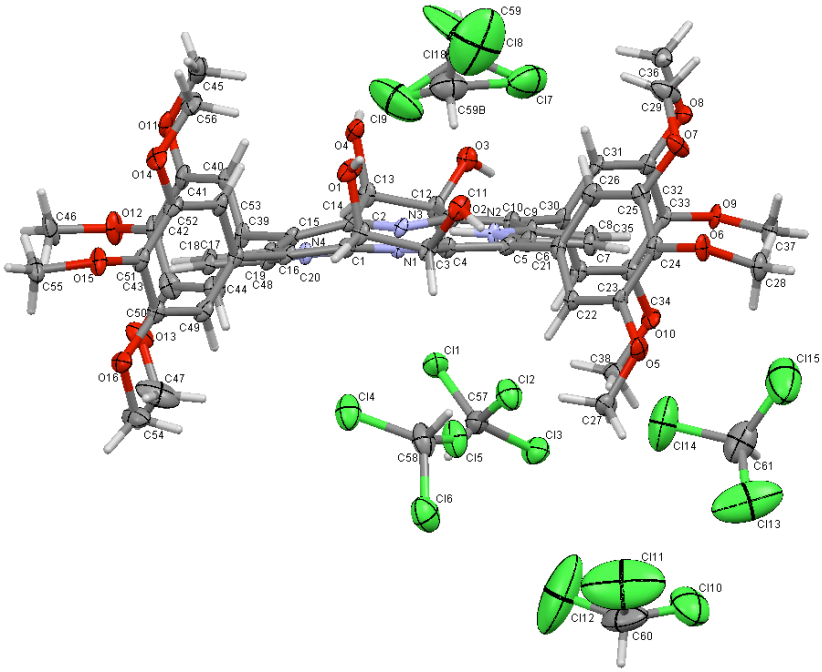

Figure ESI-85. ORTEP Representation of **4d-*Z***, side view, with $CHCl_3$ solvates. Ellipsoids at 50% probability level.

One chloroform molecule is inversion disordered over two sites with an occupancy ratio of 0.59(1) to 0.41(1). The carbon atoms in both moieties were constrained to have identical ADPs. Two other chloroform molecules refined to be only partially occupied with occupancies of 0.820(6) and 0.801(6), respectively.

X-ray Crystal Structure Determinations – 5a
See also Table 3 (crystal Data) and the cif file of this structure

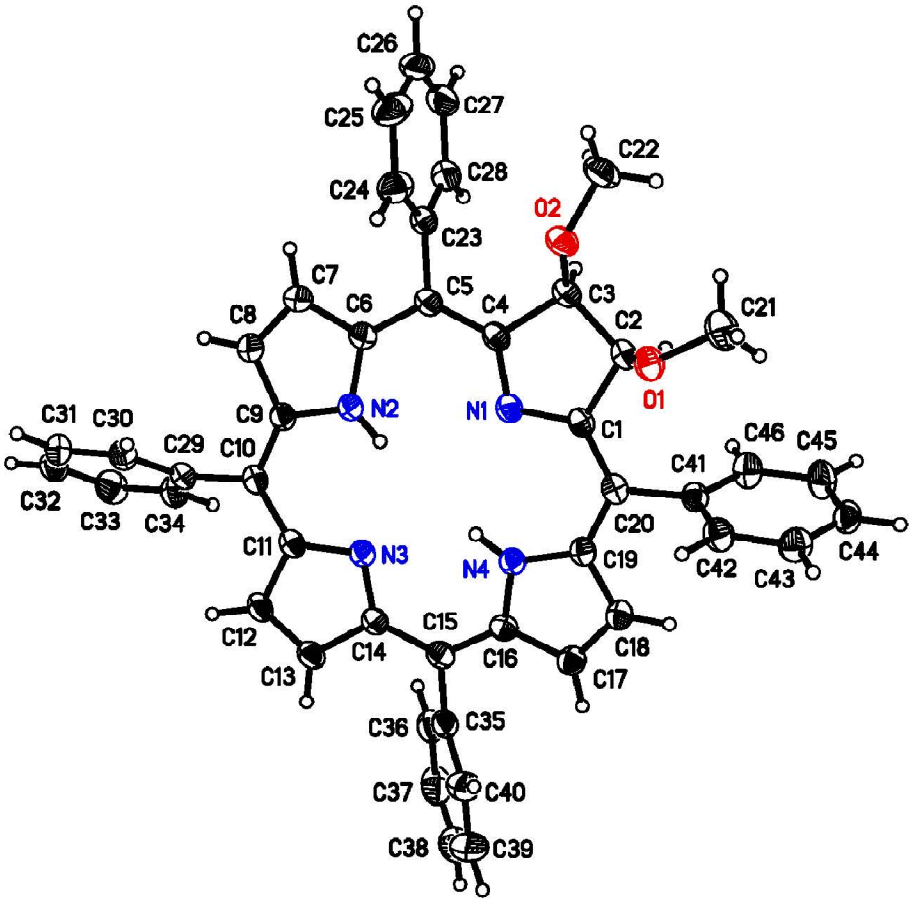

Figure ESI-86. ORTEP Representation of **5a,** and numbering used. Ellipsoids chosen at 50% probability.

X-ray Crystal Structure Determinations – 7d-*E* · 4 CH_2Cl_2
See also Table 3 (crystal Data) and the cif file of this structure

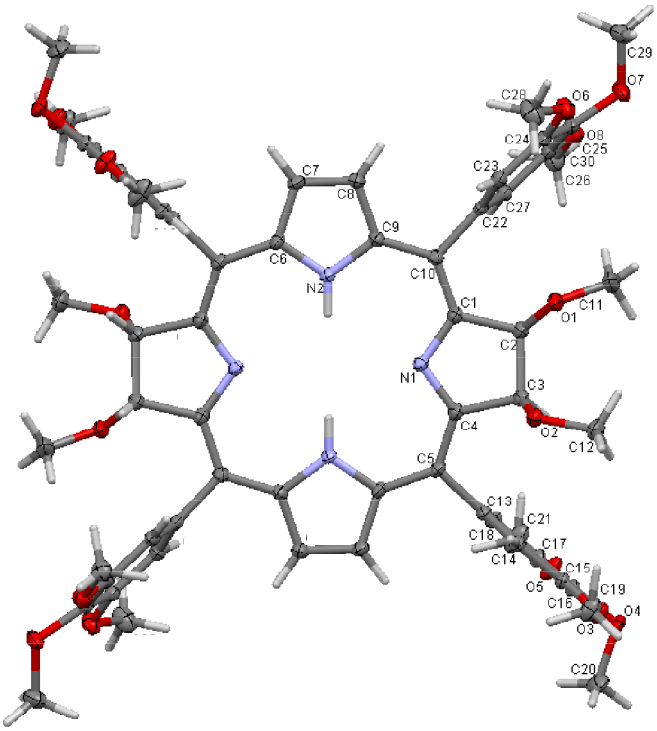

Figure ESI-87. ORTEP Representation of **7d-*E***, top view, and numbering system used. Molecule located on a crystallographic inversion center. Ellipsoids at 50% probability level.

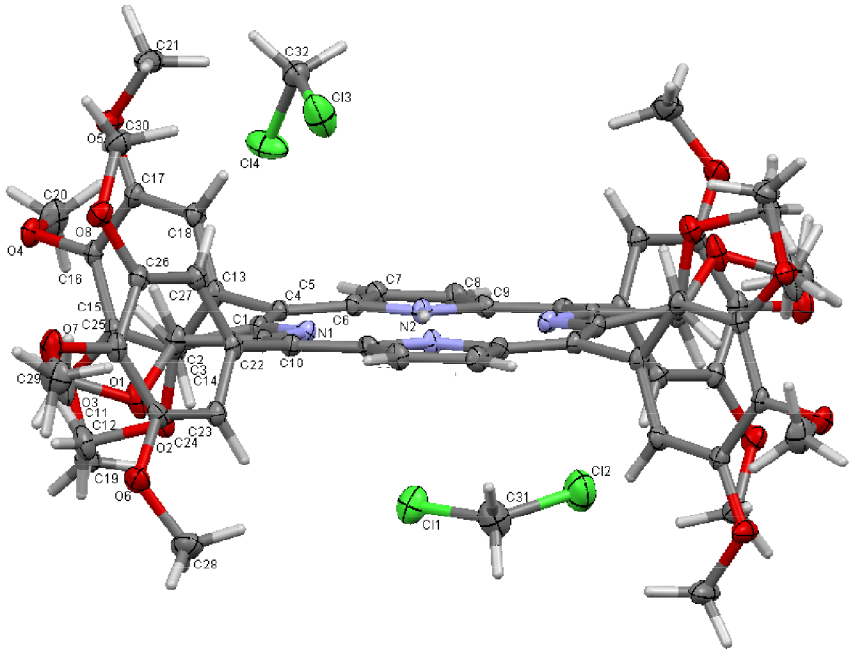

Figure ESI-88. ORTEP Representation of **7d-*E***, top view, with $CHCl_3$ solvates. The molecule is located on a crystallographic inversion center. Ellipsoids at 50% probability level.

X-ray Crystal Structure Determinations – 11a
See also Table 3 (crystal Data) and the cif file of this structure

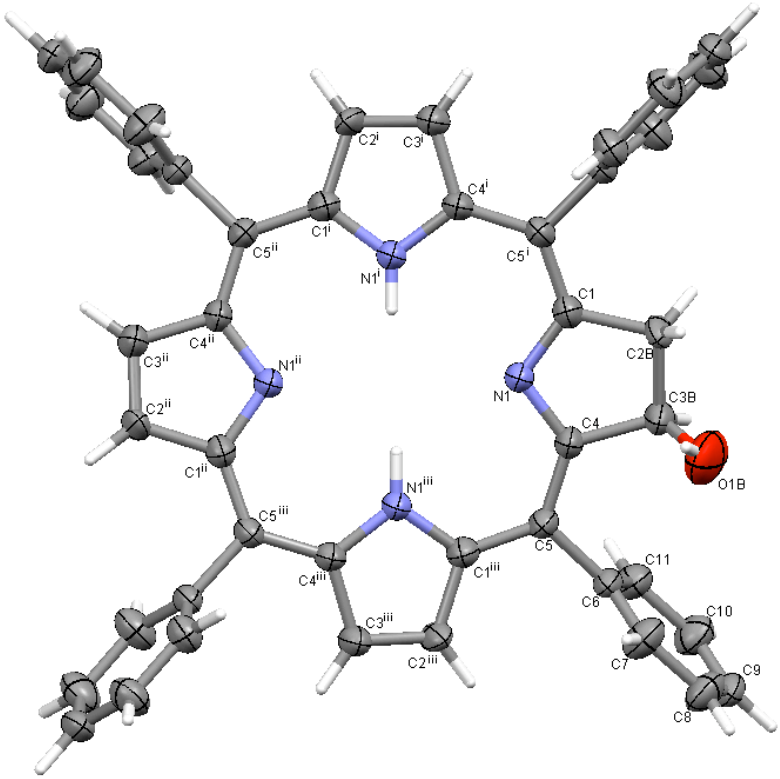

Figure ESI-89. ORTEP Representation of **11a**, top view, and numbering used. The molecule is located on and disordered around a crystallographic 4-fold axis (see Figure ESI-91), and only one set of disordered atoms representing one individual molecule is shown. Ellipsoids at 50% probability level. Symmetry operators: (i) y, -x-1, -z+2; (ii) -x, -y, z; (iii) -y+1, x, -z+2. Labels for the phenyl rings are only shown for the crystallographically independent unit.

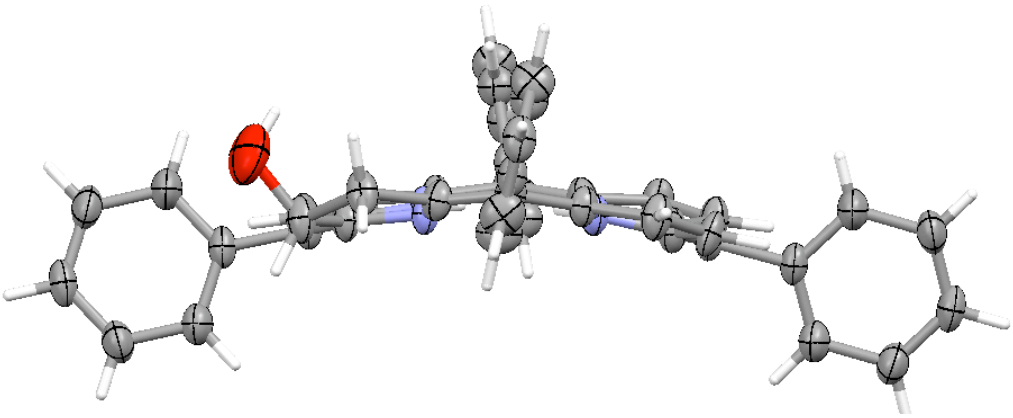

Figure ESI-90. ORTEP Representation of **11a**, side view. The molecule is located on and disordered around a crystallographic 4-fold axis and only one set of disordered atoms representing one individual molecule is shown. Ellipsoids at 50% probability level.

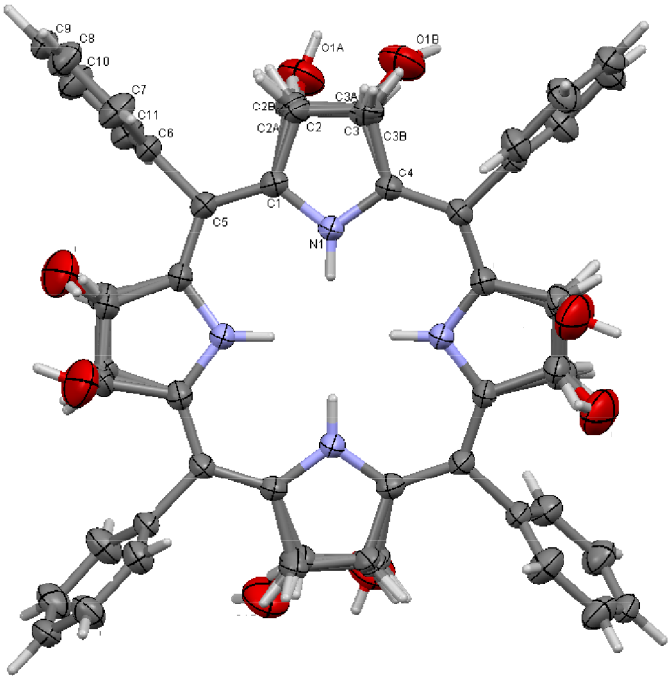

Figure ESI-91. ORTEP Representation of **11a**, also showing the disorder. The molecule is located on a crystallographic 4-fold axis. Ellipsoids at 50% probability level.

Note:
Friedel pairs were merged prior to refinement.
The molecule, while itself asymmetric, is located on a four fold axis and thus disordered. Three pyrrol and two differently oriented dihydropyrrol-ol are disordered with each other in a ratio of 6 to 0.55(1) to 0.45(1).
Bond distances within the minor dihydropyrrol-ol sections were restrained to be chemically meaningful. As reference were used the known values found in the related di-hydroxyl compound. sp^3-C-O distances were restrained to 1.41(2), sp^3-C-sp^3-C distances to 1.54(2) and sp^2-C-sp^3-C distances to 1.52(2) Å. Overlapping carbon atoms and the two oxygen atoms were constrained to have identical ADPs, and the overlapping C atoms were restrained to be approximately isotropic (within a standard deviation of 0.01 $Å^2$).

Table ESI-1. Comparison of the optical properties of a porphyrin and its corresponding benzylic alcohol derivative.

Porphyrin -CH_3/CH_2R	**λ_{max}/nm (ε/$M^{-1}\times cm^{-1}$), reference**	**Porphyrin – CH_2OH/CHOHR**	**λ_{max}/nm (ε/$M^{-1}\times cm^{-1}$), reference**
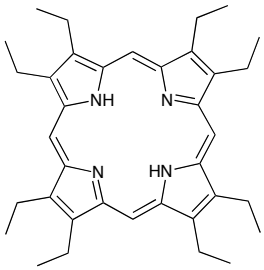	Solvent: $CHCl_3$ 399(177827), 498 (13489), 536 (9332), 567 (2344), 618 (4265) Higuchi, H.; Shinbo, M.; Usuki, Masanobu; Takeuchi, M.; Hasegawa, Y.; Tani, K.; Ojima, J. *Bull. Chem. Soc. Jpn.* **1999**, *72*, 1887-1898.	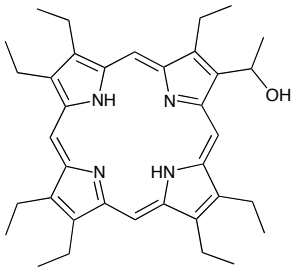	Solvent: CH_2Cl_2 400 (15910), 498 (15400), 534 (12700), 566 (9600), 620 (7200) Vicente, M. G. H.; Smith, K. M. *Tetrahedron* **1991**, *47*, 6887-6894.
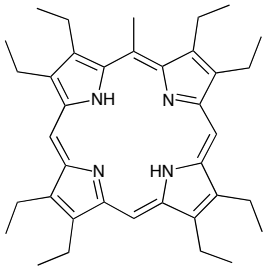	Solvent: CH_2Cl_2 408.2, 507.6, 540.5, 578.0, 628.9 Wu, G.-Z.; Gan, W.-X.; Leung, H.-K. *J. Chem. Soc. Faraday Trans.* **1991**, *87*(18), 2933-2937.	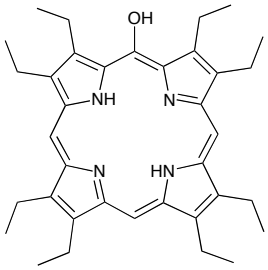	Solvent: CH_2Cl_2 401.6, 505.0, 540.5, 574.7, 628.9 Wu, G.-Z.; Gan, W.-X.; Leung, H.-K. *J. Chem. Soc. Faraday Trans.* **1991**, *87*(18), 2933-2937.
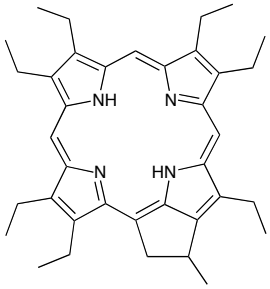	Solvent: $CHCl_3$ 403(239000), 503 (14600), 538 (5200), 566 (6500) Ponomarev, G. V.; Shul'ga, A. M. *Chem. Heterocycl.Compd.(Engl. Transl.)*, **1984**, *20(4)*, 383-388.	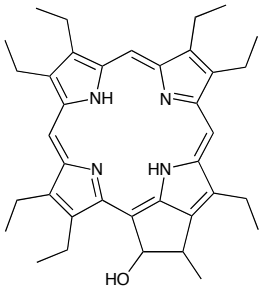	Solvent: $CHCl_3$ 402, 502 (14600), 537 (6000), 565 (6100), 618 (815) Ponomarev, G. V.; Shul'ga, A. M. *Chem. Heterocycl.Compd.(Engl. Transl.)*, **1984**, *20(4)*, 383-388.
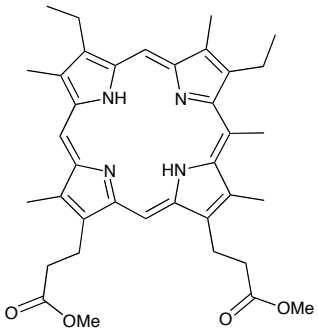	Solvent: CH_2Cl_2 390 (209300), 495 (12400), 528 (8400), 564 (5600), 617 (3900). Freeman, B. A.; Smith, K. M.; *Synth. Commun.* **1999**, *29(11)*, 1843-1856. Solvent: CH_2Cl_2 398 (102000), 498 (8400), 530 (6000), 566 (4100), 620 (2900)	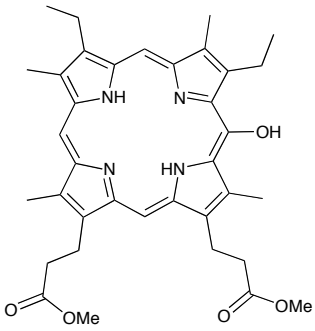	Solvent: CH_2Cl_2 406, 506, 542, 578, 628. Torpey, J. W.; de Montellano, P. R. O. *J. Org. Chem.* **1995**, *60(7)*, 2195-2199. Solvent: $CHCl_3$ 402 (186208), 499 (14454), 533 (8318), 568 (6761), 621.5 (4266).

	Lee, D. A.; Smith, K. M. *J. Chem. Soc. Perkin Trans. 1* **1997**, *8*, 1215-1228.		Chau, D. D.; Clezy, P. S.; Henderson, R. W.; Pham, H.-Ph.; Ravi, B. N. *Aust. J. Chem.* **1983**, 36(8), 1639-1648.
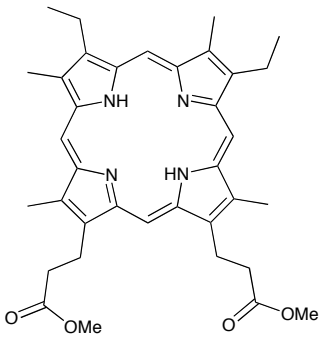	Solvent: $CHCl_3$ 400, 499, 533, 567, 594, 621 Kojo, S.; Sano, S. *J. Chem. Soc. Perkin Trans. 1* **1981**, 2864-2870.	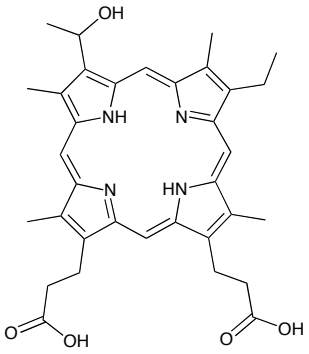	Solvent: $CHCl_3$ 402, 498, 533, 567 621 Mironov, A. F.; Nizhnik, A. N.; Deruzhenko, I. V.; Bonnett, R. *Tetrahedron Lett.* **1990**, *31(44)*, 6409-6412.
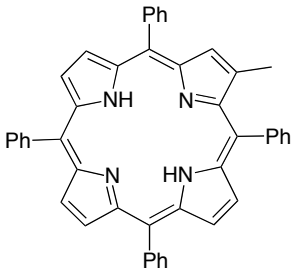	Solvent: CH_2Cl_2 417, 514, 546, 588, 644 Terazono, Yuichi; Dolphin, David; J. Org. Chem. 2003, 68(5), 1892-1900. 417 (407378), 519 (165958), 552 (47863), 591 (37153), 648 (29512) Crossley, M. J.; Harding, M. M.; Tansey, C. W.; J. *Org. Chem.* **1994**, *59(16)*, 4433-4437.	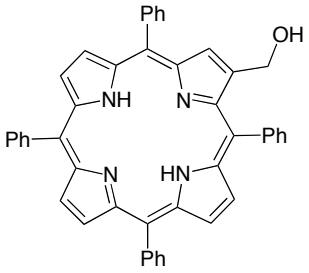	Solvent: $CHCl_3$ 420 (401000), 515 (18400), 548 (5900), 588 (5400), 642 (3400) Ponomarev, G. V.; Maravin, G. B. *Chem. Heterocycl. Compd. (Engl.Transl.)* **1982**, *(18)1*, 50-55.
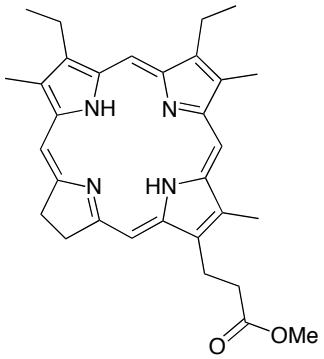	Solvent: CH_2Cl_2 λ_{max} (log ε): 388 (5.20), 496 (4.03), 522 (3.54), 544 (3.21), 594 (3.57), 618 (3.62), 648 (4.61) Burns, D. H.; Caldwell, T. M.; Burden, M. W.; *Tetrahedron Lett.* **1993**, *34*, 2883-2886.	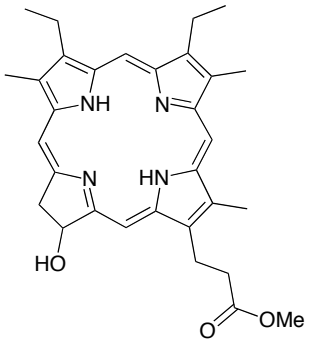	The UV–vis spectrum of chlorin **3a** shows a small (10 nm) hypsochromatic shift of the Q band relative to the corresponding chlorin. Burns, D. H.; Li, Y. H.; Shi, D. C.; Delaney, M. O.; *Chem. Commun.* **1998**, 1677-1678.